GEO 511: Master Thesis

Relating Forest Productivity to Environmental Conditions by Means of Multiple ALS-derived Variables

Benjamin Kellenberger
09-713-637

Supervisors:
Dr. Felix Morsdorf
Prof. Dr. Ross Purves

Faculty Representative:
Prof. Dr. Michael E. Schaepman

Remote Sensing Laboratories
Department of Geography
University of Zurich

September 22, 2014

Abstract

Forests play an essential role within carbon fluxes in the context of global warming, and a proper estimation of forests' productivity and their interaction with the environment is hence paramount. Research on how and to what degree forests interact with their environment has hitherto been carried out on a small number of trees and/or influencing variables as well as at one time event only.

This thesis attempted to overcome these gaps and tried to establish a link between growth of an entire forest and up to six environmental influences (altitude, terrain gradient, terrain aspect, potential solar radiation, TWI). Both forest growth and the influences were derived from two ALS acquisitions in 2002 and 2010 over the Ofenpass valley in the Swiss National Park. For the forest growth, a single tree identification algorithm has been used. Besides conventional OLS regression techniques, a spatially sensitive version called SLR has been used to assess regional differences in the growth response.

Although the results indicated weak to absent correlations, a number of properties and model guidelines could be found: results revealed a stronger correlation when the single tree identification was used instead of only CHM differences; solar radiation and TWI were the best tree growth predictors; regional differences were not significant enough to be caught up by the SLR. Most importantly, this study revealed that the derivation of regressors from topographic models alone is insufficient and that meteorological data and other parameters have to be included as well.

Contents

List of Figures

List of Tables

Abbreviations

AGL	**A**bove **G**round **L**evel
ALS	**A**irborne **L**aser **S**canning
CHM	**C**anopy **H**eight **M**odel
DBH	**D**iameter at **B**reast **H**eight
DSM	**D**igital **S**urface **M**odel
DTM	**D**igital **T**errain **M**odel
GPP	**G**ross **P**rimary **P**roduction
GPS	**G**lobal **P**ositioning **S**ystem
GWR	**G**eographically **W**eighted **R**egression
IMI	**I**ntegrated **M**oisture **I**ndex
INS	**I**nertial **N**avigation **S**ystem
LiDAR	**Li**ght **D**etection **A**nd **R**anging
NPP	**N**et **P**rimary **P**roductions
OLS	**O**rdinary **L**east **S**quares (Regression)
PAR	**P**hotosynthetically **A**ctive **R**adiation
PRF	**P**ulse **R**epetition **F**requency
SLR	**S**calable **L**ocal **R**egression
SNP	**S**wiss **N**ational **P**ark
TWI	**T**opographic **W**etness **I**ndex
VIF	**V**ariance **I**nflation **F**actor

Chapter 1

Introduction

1.1 Motivation

The influence of forests on the global carbon cycle has commonly been approved as a key component in investigations among ongoing climate change research and debates (Pan et al., 2011). Forests share the overarching property of being built up by large biomass quantities and hence provide an important terrestrial carbon reservoir (Reichstein et al., 2013). Furthermore, forests as part of a living ecosystem constantly grow, and recent studies hence assigned forested areas a particularly important role as global carbon *sinks* (Ciais et al., 2009, Erb et al., 2013, Ma et al., 2012, Nabuurs et al., 2003, Pan et al., 2011, Reichstein et al., 2013, Schimel, 2014). In turn, effects are also observable the other way round, as forests themselves appear to be influenced by changes in the global climate and carbon cycle shifts (Bonan, 2008, Ma et al., 2012, Pan et al., 2011). Consequently, embedding forests in the global climate change discourse requires a thorough understanding of ecological as well as biological processes present within them. More precisely, if environmental conditions are assumed to have an effect on an individual tree's growth, they indirectly alter forest productivity, and hence the capability of these biotopes to act as said carbon reservoirs and sinks. Therefore, describing and parameterizing environmental influences on tree growth is as important as approximating forest productivity itself. In a nutshell, this thesis seeks to provide an estimation and assessment of forest productivity on the basis of influences from the environment.

1.2 Organization of this thesis

This thesis is divided into six major chapters plus Appendix. The Introduction Chapter addresses topics related to state of the art and further gives an overview over potential conditions and factors ought to have an influence on tree growth. ALS sampling principles will be elaborated as well. In the Methods Section, the study area will be described briefly, and parameterizations of the influence factors as well as the single tree identification process based on ALS data shall take part. The Results Section gives an overview over the forest productivity estimation (both statistically and visually by usage of spatial maps). These results will then be brought to context and analyzed in the following Discussion, whose key statements finally leave room for Conclusion and Outlook Chapters giving a summary over the major findings respectively addressing further work to be done.

The Appendix is structured as follows: a first part contains more detailed results and images of the statistical analyses, while two succeeding parts list the MATLAB- and Python-code as written specifically for this thesis.

1.3 State of the Art and Problem Description

Hitherto, investigations and quantifications of ecological impacts on forest productivity have commonly been carried out on the basis of one factor at a time: Rossi et al. (2006) for instance examined the effect of available sunlight on growth, Lloyd and Fastie (2002) analyzed growths in regions of low air temperature, and Bigler et al. (2006) assessed the reactions of trees if confronted with water shortage. Further variables ought to have an effect on forest productivity are the tree's age due to consequent physiological issues (Koch et al., 2004), topographic parameters such as terrain gradient and aspect (Fekedulegn et al., 2002), and finally also short-term effects like changes in forest management (Erb et al., 2013) and occurrences of catastrophes like droughts or wildfires (Loudermilk et al., 2013). In addition, a few theses indeed examined the effect of multiple potential environmental influence factors on tree growth at once, but did so with a relatively small number of trees and for specific sites like urban areas (e.g. Iakovoglou et al. (2001)). Similar progress has been made in productivity estimation via related parameters such as Gross and Net Primary Production (GPP resp. NPP; Vicca et al. (2012)) for single trees,

carried out on the basis of tree rings (Babst et al., 2012) and (vegetation) indices sourced from optical remote sensing data (Beck et al., 2011, Schubert et al., 2012). All in all, the linkage between the environment and individual trees seems to have a strong fundament despite consistent remaining uncertainties as expectable within ecological investigations. However, analyses typically suffer from one or more issues:

- environmental influences are investigated only one at once,
- analyses are carried out on the basis of single trees rather than entire forests,
- data are acquired at one time event only.

As soon as forests are seen as part of a superimposed ecosystem involving a multitude of processes at once, these issues have to be accounted for. Especially in the context of climate *change*, momentary GPP and biomass estimations fail to provide a sufficient foundation for trend analyses and development monitoring purposes; they suffer from a "temporal scaling problem" (Morsdorf et al., in revision). As already shown, biomass estimations based on optical remote sensing products are indeed feasible, but lack the vertical dimension especially appreciable for tall-grown vegetation areas. However, estimations using the SAR approach still does not solve the Furthermore, productivity estimations require an integration over entire forest stands to reach an adequate statistical sample size and capture regional (instead of only individual) effects. Means of manual measurements, repeated over time, would be an unrealistically cumbersome task to achieve. Sample acquisition would thus not only incorporate a temporal, but also a spatial scaling problem. All in all, there is need for larger-scale, time-variant and multivariate ecological studies.

Fortunately, the development of new remote sensing technology provided an answer to such issues in the form of laser scanning. Sensors of this type have been developed for terrestrial, airborne as well as spaceborne use, but especially Airborne Laser Scanners (ALS) gained growing popularity in forest-related studies and are increasingly used for tasks such as tree height modeling (Chen et al., 2007). ALS systems overcome drawbacks of conventional optical remote sensing instruments by being able to sample not only large areas, but provide *vertical* measurements as well (Lefsky et al., 2002b). For said intentions, this property can be exploited in multiple ways: on the one hand, Lefsky

et al. (2002a) have shown that forest biomass can be estimated using tree height. With repeated ALS passes, estimations become not only tree heights, but height differences, which may be seen as directly related to forest productivity. On the other, many of the environmental influences on growth mentioned at the beginning of this Section can, to a certain extent, be derived from ALS acquisitions. Consequently, Airborne Laser Scanning plays a pivotal role in such analyses, and provides an expedient synthesis of ecological studies and state-of-the-art technology.

On the basis of these topics, the following research goals are to be covered in this thesis:

1. Establishing a link between environmental and tree-inherent influence factors on a tree's growth.
2. Applying this investigation not only on the basis of one factor, but multiple at a time
3. Extending analysis to entire forest stands instead of single trees only.
4. Investigating how well forest productivity and environmental influence factors can be parameterized by means of ALS-derived data alone. Particular focus is laid on a new technique to derive single trees based on the ALS point cloud (see Section 2.3).
5. As an additional property, the magnitude of growth response differences within the study area will be examined by means of specifically developed spatial statistical tools.

1.4 Tree Growth Influence Factors

1.4.1 Tree Age

The age of a tree has been reported to have an influence on the tree's growth rate in a variety of ways (Koch et al., 2004, Ryan and Yoder, 1997) and may be considered as one of the growth prediction candidates not directly related to environmental conditions. Tree age, and the history of its surrounding forest, can influence a tree's response to climate (Lloyd and Fastie, 2002). Trees were reported to have a reduced growth rate

with progressing age (Martínez-Vilalta et al., 2007), which also results in a maximally reachable tree height (Ryan and Yoder, 1997). Such maximum tree heights are to date hardly quantifiable due to poor understanding of the influences (Koch et al., 2004). The conventional approach to overcome this issue was to use Diameter at Breast Height (DBH) to estimate biomass (Whittaker et al., 1974). Nevertheless have foresters been using the correlation between maximum height of individual trees and growth rate of them in younger years to predict further growth (Ryan and Yoder, 1997). Furthermore, in the work of Avsar (2004) the relation between tree height and DBH has turned out to be reasonably strong, indicating that studies based on tree height might yield comparable results as if DBH was used. As for biological reasons, a common assumption holds an aggravated water transport through the tree liable for growth limitation due to a reduction of photosynthetic carbon gain (Koch et al., 2004, Ryan and Yoder, 1997). For instance, Hubbard et al. (1999) found that older (and indeed taller) individuals of the *Pinus ponderosa* species had a 44% lower hydraulic conductance as well as 63% lower water potential among one-year-old needles compared to younger siblings, thus probably indicating reduced photosynthesis rates. At the same time, the greater height of trees might favor the formation of embolisms, possibly due to freeze-thaw events (Mayr et al., 2003a), drought stress (Mayr et al., 2006), or other reasons. Therefore, if trees show signs of suffering from water shortage, it might not automatically be drought and lack of water supply from the environment causing it, but rather tree fitness emerging from the individual itself.

Kalliovirta and Tokola (2005) thoroughly assessed models for the prediction of stem diameter and tree age using mainly the tree's height and crown width on the basis of different tree species, one of which belonging to the Pine species (*Pinus sylvestris*). Despite their recommendation towards models using both the tree height and crown diameter as explanatory variables for estimation, they stated that tree age among coniferous species is mostly related with the tree's height.

All in all, older trees are likely to show a reduced metabolic rate and consequently less biomass production than young individuals (Gower et al., 1996). The inclusion of an age proxy thus may encompass a variety of causes for tree growth reduction at once. It is important to note, though, that these are mostly intrinsic to the tree itself and only partially controlled by environmental conditions (i.e. temperature and water stress). Such external stress factors also affect young trees and saplings and need to be included

separately. However, in case the hypothesis of a reduced growth rate with increasing tree height holds true, it should thus be possible to reverse the model and estimate an average growth rate based on a tree's age, possibly approximated using its current height.

1.4.2 Sunlight Exposure

Solar radiation is the primary supply of energy for life on the Earth's surface (Szargut, 2003, Wild et al., 2005). Estimations have been made that 99.8% of the energy at the Earth's surface is due to sunlight (Dickinson and Cheremisinoff (1980), in Kumar et al. (1997)). For logical reasons, solar radiation needs to be considered as a, if not the major driving factor determining the healthiness and growth capability of single trees, forest stands, yet entire ecosystems. Ecosystems are inter alia defined as "machines supplied with energy from an external source, usually the sun" (Monteith, 1972), underlining the prevalence of sunlight as an energy supplier. In ecosystems, the importance of the sun for trees manifests itself in a variety of processes that depend on the diurnal amount of electromagnetic radiation present, and this either directly by absorption of the shortwave electromagnetic radiation part of the spectrum, or indirectly re-emission as longwave radiation, and thus heat. Among plants, the most obvious process dependent on solar radiation, photosynthesis, depends on electromagnetic wavelengths between 400 and 700 (resp. 380 and 710) nm (Jacovides et al., 2003), which is thus called "Photosynthetically Active Radiation" (PAR; McCree (1981)). Plants are thus subject to a constant process of growing towards maximal utilization of available light while keeping structural stress at a minimal level (Hart et al., 2003). Other plant functions depend on this wavelength range as well, but a broader electromagnetic spectrum is required for all plant functions to work properly (Daubenmire (1974), in Kimmins (2004)). UV light does not play an essential role in plant physiology though (Kimmins, 2004). More precisely, excessive UV light had sometimes been seen as a major growth inhibitor for trees at high altitudes near the treeline, but this effect is highly contentious (Kimmins, 2004). Heat as another important consequence of incoming sunlight mainly originates from the interactions of the shortwave electromagnetic irradiance, which is being absorbed and emitted in longer wavelengths (thermal infrared). The amount of longwave (thermal) incoming radiation from the sun is more or less negigible. This is an essential property of the energy fluxes on the earth insofar as it simplifies the solar radiation budget calculation later on, since no longer wavelength radiation propagation paths need to be considered in the

model. What might need to be considered though is that solar radiation is subject to constant variation throughout the landscape, day, and, in advanced models, solar cycle and atmospheric composition. The landscape primarily alters solar radiation due to topography (especially slope and aspect (Kimmins, 2004, Kumar et al., 1997)), ground reflectance resp. albedo (Corripio, 2003) and position of patches neighboring the area of interest (Kumar et al., 1997). Also, in a very mountainous terrain, shading due to adjacent mountains and hills plays an essential role by attenuating the direct part of the solar irradiance (Hughes, 2000). Daily variation is given due to the number of sunshine hours (Ampratwum and Dorvlo, 1999) and position of the sun relative to the Earth's surface (solar altitude and azimuth angles (Corripio, 2003, Kumar et al., 1997)). Day length (and thus probably the amount of solar radiation in general) was found to be of special importance for tree growth and to be more important than temperature in the study of Rossi et al. (2006).

On clear days, about 5% of the radiation gets scattered in the atmosphere, and this fraction may rise over 17% on average days to 100% for completely overcast weather situations (Kimmins, 2004). Under cloudy conditions, plants thus mainly receive scattered sunlight and the effects affecting the direct radiation part (such as hill-shading) diminish. If the cloud cover for the investigated area and time period was at hand, a very precise solar radiation model would be computable. However, the consequences for further growth estimation or prediction models would probably be not measurable with such an increase in model accuracy. Moreover, it is likely for a study area of moderate size to be affected by clouds all the same throughout the field, making such efforts of exact budget calculation redundant.

The establishment and computation of a solar radiation budget model alone does not yet predict the way a tree resp. forest stand grows though; the relation between solar radiation and growth rate may in fact not be positive at all. For instance, Kimmins (2004) states that the *absence* of solar radiation has a higher effect on plant growth than adequate presence (or excessiveness) of it. More precisely, plants in dark areas feature more cell division, hence elongation processes, and a reduced leaf production, resulting in fast growth and tall but thin stems (which are so-called *etiolated* plants; Kimmins (2004)). One would expect that especially trees growing below a (dense) forest canopy become etiolated. However, etiolation is most obvious in herbaceous plants,

and completely absent in shade-tolerant species, such as pines as present in this thesis' investigated area (Kimmins, 2004).

With respect to such observations, the expected response of trees to sunlight suddenly becomes very vague. Processes such as photosynthesis are just too complex to be assumed to follow (daily) variation in incoming sunlight (Kimmins, 2004). Hence, the safest thoughts on the impact of solar radiation on plants may be that both entire absence and excess result in growth stagnation or even death of the individual. The effects of budgets between excess and absence may in turn not be as predictable. It may be that trees on south-facing slopes show rapid growth due to the great availability of solar radiation. At the same time, pines are light-demanding species (Kimmins, 2004), and especially plants growing in the shadowed north-facing slopes may try to reach more illuminated parts as quickly as possible and could thus grow taller than their conspecifics in more frequent sunlight. In the present thesis, analyses are thus carried out on an exploratory basis, making very limited assumptions.

1.4.3 Temperature

Among the possible abiotic factors inhibiting tree growth rate temperature has been one of the most investigated in the literature. Focus has usually been laid on influences of air temperature (e.g. Gamache and Payette (2004), Petit et al. (2011)). In fact, summer air temperature has typically been the most often identified factor functioning as a growth-limiting climatic variable (Briffa et al. (1995), Graumlich and Brubaker (1986), Jacoby et al. (1985), Norton (1984); all in Gamache and Payette (2004)), and this in various ways. For instance, significant correlations have been found between plant respiration respectively photosynthesis and temperature increases (Chapin et al., 1996). More importantly, the formation of wood (xylogenesis) in trees under cold annual air temperatures was found to be accelerated by warmer temperatures (Danby and Hik, 2007, Gorsuch and Oberbauer, 2002, Petit et al., 2011). Especially Petit et al. (2011) reported a significantly increased increment in shoot length of heated trees in comparison to the unheated control sample, and suspected xylogenesis, more precise cambial activity, to be the key process for the determination of growth limitation. However, at the same time trees with an increased growth rate in summer have been reported to be more susceptible to frost drought in winter (Danby and Hik, 2007, Gorsuch and Oberbauer,

2002). Growth inhibition due to temperature effects do not only apply for the winter season though: shoots are typically surrounded by a "hull" of warmer temperatures around the trees as long as they are not at the top of the tree crown. In this case, these shoots reach into the outer atmosphere with colder temperatures, resulting in a reduced growth rate of their tissues (Körner, 1998).

However, there have also been doubts recently on the linkage between increased air temperatures and higher growth rates (Lloyd and Fastie, 2002). Nevertheless, trees confronted with low mean annual temperatures typically show both a lower tree ring width and height growth rate (Gamache and Payette, 2004, Körner, 2003), and additionally, warmer temperature events in such environments may even alter a tree's morphological appearance, letting the tree erect into an upright form from a previous shrub-like shape (Devi et al., 2008). More generally, air temperatures are likely to influence a tree's structural growth, i.e. the "investment of photo-assimilates" (Körner and Paulsen, 2004). These effects become generally more distinct at the treeline (Birmann and Körner, 2009, Danby and Hik, 2007, Dullinger et al., 2004, Richardson and Friedland, 2007), which is called "climatic treeline" if a major influence of the temperature on it is assumed (Alvarez-Uria and Körner, 2007). Some studies calculated a generally applicable mean temperature at which the treeline occurs (Körner and Paulsen (2004) for instance suggested a mean temperature of 6.7 °C at which treelines are situated sans human influences). In association with global warming, treeline advances were especially coherent with temperature increases (Harsch et al., 2009). The present study's investigated area covers regions where upper treelines are present. However, individuals at the border are typically composed of *krummholz* and dwarf shrubs, sometimes even distorted growth forms (Smith et al., 2003) and hardly grow taller than a few meters. With the restrictions posed to the investigated trees, such individuals would possibly not even be recognized. Therefore, treeline effects are, if present, only marginal.

The soil temperature as a counterpart to air temperature also plays an important role in the health status and growth rate of trees. In fact, Alvarez-Uria and Körner (2007) consider soil temperature as a primary factor influencing plant growth in general. Consequences of cold soil temperatures are for instance reduced root diameters (Chapin (1974), in Alvarez-Uria and Körner (2007)), a resistance of trees to grow their roots into cold soils (Alvarez-Uria and Körner, 2007), and altered nutrient and water uptake (Vapaavuori et al., 1992). Soil temperature is often characterized by a delayed adaptation

to the air temperature above ground (Alvarez-Uria and Körner, 2007, Pregitzer et al., 2000), and thus "lags behind" it. Consequently, trees are typically confronted with low soil temperatures for a longer time than with low air temperatures, which further raises the stress potential.

Both soil and air temperatures have distinct effects and consequently affect different parts of the individual tree, and the effects have often been discussed resulting in contradictory results. For instance, Barber et al. (2000) and Lloyd and Fastie (2002) identified a diminishing effect of warmer air temperatures on tree ring width respectively tree growth in general. This stands in contrast to the common assumption of decreased air temperatures to inhibit tree growth, which was also stated by others (e.g. Petit et al. (2011) or Gamache and Payette (2004)). However, it is important to note in such a case that the eventual tree growth in height may not always be correlated to tree ring width, since the latter can also depend on stabilization requirements on steep mountainsides. Also, Lloyd and Fastie (2002) identified this negative correlation between air temperature and tree growth rate only in areas with less water availability. It is therefore conceivable for temperature changes to be accompanied by an altered water ability in the form of soil moisture (Koch et al., 2004, Lloyd and Fastie, 2002), which may therefore lead to an additionally increased growth inhibition for trees. This temperature-induced drought stress holds especially true for forests with a limited water supply and an increased air temperature (Lloyd and Fastie, 2002), resulting in reduced carbon uptake (Barber et al., 2000).

1.4.4 Altitude

The elevation of a tree above sea level is inherently linked to the often investigated (alpine) treeline (e.g. Däniker (1923), Körner (1998), Miehe and Miehe (1994), Tranquillini (1979), Wardle (1993); all in Körner and Paulsen (2004)). Alpine treelines share the characterization by a typically abrupt change (Birmann and Körner, 2009) from upright trees to shrubby forms (Körner and Paulsen, 2004), acting as a transition zone (ecotone) rather than a sharp line (Birmann and Körner, 2009, Dullinger et al., 2004). The causes for treelines are, despite numerous studies, not fully understood (Grace et al., 2002). The most often mentioned assumption of a growth limitation at high altitudes due to low temperatures (Becker and Bugmann, 2001, Kittel et al., 2000, Shi et al., 2008,

Shiyatov and Mazepa, 2007, Smith et al., 2003, Vaganov et al., 1999) underwent revisions and was found to be not as strong as previously thought (Grace et al., 2002). However, these doubts were often targeted towards e.g. a globally applicable temperature threshold value to explain treelines around the world (see e.g. Körner and Paulsen (2004)). If they hold true for investigations based on regionally scaled areas is to be investigated within the framework of this study.

1.4.5 Terrain Slope and Aspect

Slope or gradient is the maximum rate of change in height at a specific point from its neighbors (ESRI, 2011b); aspect denotes the direction of the slope (ESRI, 2011a). Both parameters serve as underlying variables within many topographic indices and other variables and are therefore often already included in analyses, even if indirectly. In the present study, terrain slope is an essential part of the solar radiation budget calculation (see Sections 1.4.2 and 2.5.1 for an elaboration). However, there is more to these properties in ecology, especially when it comes to environmental conditions for trees.

Fekedulegn et al. (2002) investigated the influence of terrain aspect (separated into northeast and southwest) on radial growth and found that three of four tree species showed significantly higher growth rates at northeastern compared to southwestern aspects. Consistent with the involvement of aspect in other ecological factors, the authors explained growth differences with variations of precipitation and drought, and also species-specific tolerances of and sensitivity to water shortage or moisture (for instance, yellow poplar was found to be the most sensitive to moisture (Fekedulegn et al., 2002)). Additionally, however, the authors concluded that drought alone cannot be made responsible for growth differences, underlining the investigated theory of a multidimensional growth influence model.

Similarly, also slope respectively the steepness of the terrain is a property that is found to be used in other variables, such as in water runoff modeling (see Sections 1.4.6 and 2.5.2). Consequently, the effects of slope alone on tree growth has rarely been investigated in the literature.

1.4.6 Drought

Water shortage is a phenomenon that often occurs together with increased temperatures (Barber et al., 2000, Mayr et al., 2006). Trees generally show the highest growth rate in moist soils (Ryan and Yoder, 1997), and a reduction in the water potential due to parched soils reduces the positive pressure (turgor) of plant cells (Koch et al., 2004). In summer, rising temperatures may thus not only cause drought stress, but also reduce the sensitivity of growth rate to temperature fluctuations (Barber et al. (2000), Lloyd and Fastie (2002); both in Gamache and Payette (2004)). Bigler et al. (2006) examined drought effects in the Swiss Valais region, which, just like the area examined in this study, is an inner-alpine dry valley (Rigling et al., 2002). The authors found that single drought years as well as continuous drought periods resulted in long-term negative effects on ring widths. In this area, drought could accordingly be a major reason for the decline of the Scots pine that was observed (Bigler et al., 2006). Drought is not only limited to warm summer temperatures though. As a special case, extremely low soil temperatures falling below the freezing point in winter prevent water uptake by the tree; together with the increased evapotranspiration due to still warm air temperatures, this effect is called frost drought (Mayr et al., 2006, 2002), or winter desiccation (Tranquillini, 1980). This effect gets amplified as soon as the tree crown stands out of the snow cover (Petit et al., 2011) and is exposed to high wind speeds (Mayr et al., 2002). Especially the unusually cold winters in Europe bringing along multiple freeze-thaw events thus induce severe drought stress to trees (Mayr et al., 2002). In fact, even if the water temperature is above the freezing point, trees may witness frost drought due to a higher viscosity of water at lower temperatures (Kimmins, 2004). Consequently, there is a higher risk of embolisms among trees suffering from frost resp. low temperature drought (Mayr et al., 2003b, 2002), eventually limiting growth or even leading to a tree's death (Koch et al., 2004). Embolisms particularly occur as soon as the water potential in conduits is lower than xylem-specific thresholds where air crosses cell borders (Mayr et al., 2006). In consensus with the altitude-temperature correlation, the embolism rate of trees at low elevation was indeed significantly lower than at higher levels in the study of Mayr et al. (2006), whereas embolism stress due to drought was an "important stress factor", at least for *Picea abies* (Mayr et al., 2006). Additionally, drought as a stress-inducing factor may indirectly cause the appearance of other harms to trees, which makes it therefore an exemplar for the decline-disease theory (see e.g. Suarez et al. (2004)). For instance, Mattson and Haack

(1987) (in Bigler et al. (2006)) reported drought combined with higher temperatures to promote insect outbreaks and phytopathogens. Similar consequences were described in Kimmins (2004). This makes sense as such climatic conditions favor insect development populations (Berryman (1989), in Bigler et al. (2006)).

1.5 Airborne Laser Scanning principles

1.5.1 ALS data acquisition

In order to establish an adequate statistical sample size, the above mentioned (bio-) physical factors, most interpolated and available over the entire study area rather than for single trees, must be assignable to as many trees as possible. This also means that all growth rates for each of these trees has to be known and measured during the same time period, which would be an unrealistically cumbersome task to achieve (Morsdorf et al., in revision). Furthermore, change detection additionally requires a sample integration over time, or in the present case of growth analyses over a defined time period, two discrete time measurements. A possible solution to this problem is to use height models derived by airborne laser scanners (Wehr and Lohr, 1999), recorded at multiple time stages. ALS systems have gained growing popularity in remote sensing and are increasingly used for tasks such as height modeling and forest-related studies (Chen et al., 2007). Essential properties of ALS for this study are the directly given height measurement for each sampled point as well as the possibility to discriminate between top of canopy and ground, and therefore the ability to derive tree heights from the datasets.

Included in an ALS are two major components: a LiDAR (Light Detection And Ranging) sensor measuring the actual returning laser beam as well as a positioning and orientation system, comprised by a Global Positioning System (GPS) and an Inertial Navigation System (INS). LiDAR scanners emit laser pulses of known wavelength and intensity (in the case of a full-waveform system; see below) or amplitude (discrete-return system) and measure the time until return, and therefore the distance between emitter and ground target. Each emitted pulse will then be scattered at different time stages from targets having different heights. Therefore, multiple signals (echoes) originating from one emitted laser pulse may be recorded. Consequently, depths in the field, eventually target heights, become measurable. The way these returning signals are measured and stored depends

on the LiDAR configuration or specification; in case only a small number of echoes are recorded, the LiDAR is termed a *discrete return* system, whereas sensors capturing all the backscattering signals belong to the *full-waveform* scanner family. Full-waveform systems allow for recording entire (vertical) transects of forests and other heterogeneous ground targets and therefore lead to a larger amount of retrievable information from the data (Heinzel and Koch, 2011), and thus an increased control of data interpretation by the user (Heinzel and Koch, 2011, Mallet and Bretar, 2009). However, analyses of full-waveform data are cumbersome and still a field of research (Heinzel and Koch, 2011), but there is great potential especially for forestry applications; full-waveform LiDAR systems have in fact been developed for this kind of targets (Mallet and Bretar, 2009). The present study's main input was limited to discrete return sensors and data though since tree heights and ground terrain data were sufficient for all further analyses.

1.5.2 LiDAR Error Sources

As mentioned above, descriptions of tree physiology parameters on a regional level would hardly be feasible without means like ALS measurements due to the extreme amount of field work required. However, ALS-based height samples do not come without drawbacks and it is important to treat ALS-sampled data with caution due to a multitude of potential error sources.

In theory, the most important error sources for ALS products are shown in Figure 1.1 and may be seen as a system encompassing the platform (ALS and carrier), the sampled objects resp. targets (ground, forest stands, other objects), and finally post-processing methods. Platform-related error sources comprise e.g. the beam divergence angle, the positioning of the platform, the pulse repetition frequency (PRF; Hopkinson (2007)) and, to some extent, the flight planning (scan patterns) (Andersen et al., 2006). The LiDAR footprint size further affects the accuracy of the estimated tree height, and the footprint size in turn is dependent not only on the hardware configuration but also on the flying altitude of the ALS platform in a geometrical way (Morsdorf et al., 2006). Target-related error sources that add up are effects such as reflectance in the sampling wavelength of the LiDAR, phenology (leaf-on versus leaf-off states of plants), and slope of the terrain (Andersen et al., 2006). Post-processing of raw ALS point clouds, such as the interpolation into a raster, always includes systematic deviations and simplifications (for instance,

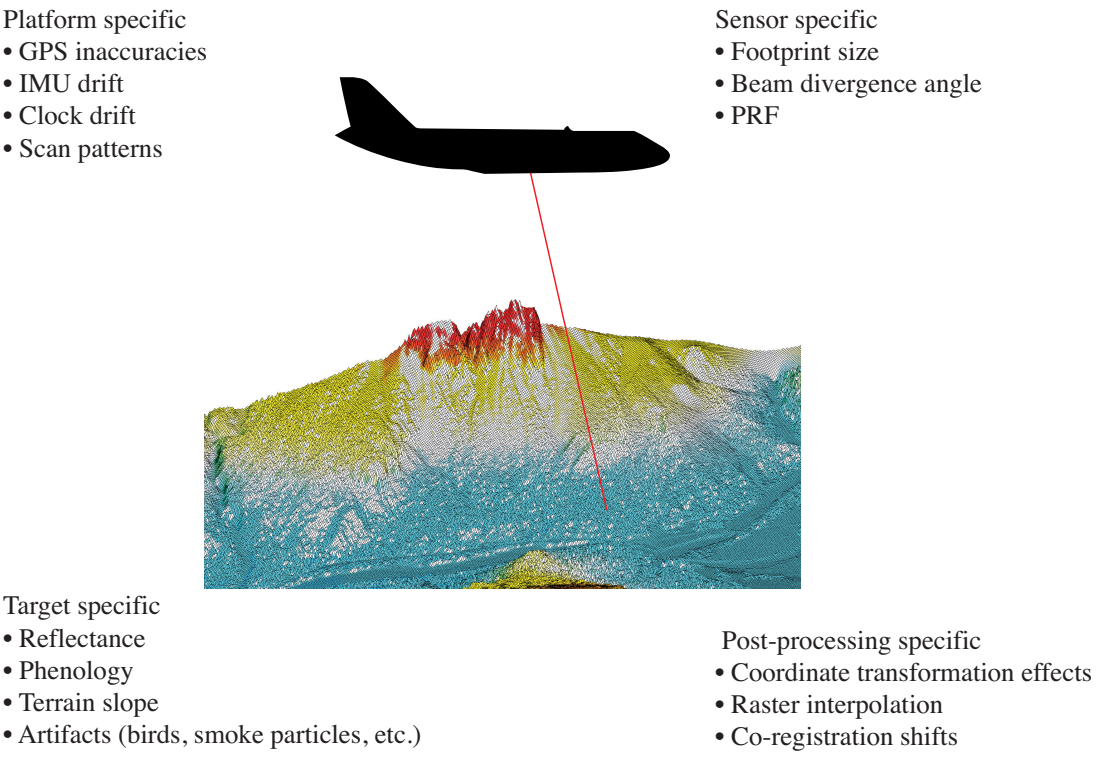

FIGURE 1.1: The most important error sources for ALS-derived height models.

a raster cell might contain an average height value of all raw points from the ALS point cloud that lie within its boundaries, and thus represents a simplification of the original data). In the present thesis, post-processing steps are expected to superimpose platform- and sensor-related error sources and cause the largest tree height estimation biases. In combination, these error sources may lead to significantly under- or overestimated height measurements of trees and therefore also to false alarms in the single-tree identification process.

1.6 Hypotheses

As stated above, previous studies have found correlations between growth inhibition or promotion and various environmental influences among different tree species and populations. However, in most cases, the limited sample size due to the required efforts for analyses prevented the studies from being able to provide a result that is valid in a holistic sense, and able to explain growth patterns for entire forest stands. With the advancing technology and refinement of methods due to Airborne Laser Scanners (ALS), such processes might to some extent be reproducible not only for individual trees, but also for

their surrounding neighbors and a tree population as a whole. In addition, by including several influences at once, a single model of tree growth and hence forest productivity assessment and even prediction approaches practicability. This thesis therefore seeks to provide explanation for tree growth rates over an entire valley in the Swiss National Park. Since trees in this study are abstracted and measured using multi-temporal ALS measurements, and since virtually all of the investigated influences are derived from digital height models (DHM), the methods used here and insights gained from the estimation processes may be transferable to other test sites.

A further topic which will be addressed below deals with spatial autocorrelation and methods to include this property (see Section 2.6.3 for further explanations). Especially due to the diverse study area, showing ecologically distinct spatial regions, spatial regression models are expected to be advantageous over regular Ordinary Least Squares (OLS) counterparts. Therefore, an inter-comparison between two regression techniques (spatial/non-spatial) will be carried out with the tree growth model and influence factors described above.

Based on this background, the following hypotheses are to be covered in this study:

1. A tree's growth rate depends on a set of distinct physical and biophysical influences, including the tree's age, the amount of potential solar radiation, temperature, steepness and exposition of the ground, and water availability.

2. Spatial differences and effects in tree growth (spatial autocorrelation) can be properly identified, measured, and accounted for in a multivariate ecological regression model.

Chapter 2

Material & Methods

2.1 Study Area

The introduced causes potentially affecting tree growth are expected to be most evident under the absence of any human-induced interaction such as woodcutting or artificial fires. The choice of a study area where human interference has been absent for a long time is therefore crucial. This study examines the described effects within the Ofenpass valley situated in the Swiss National Park (SNP), whose forests have not been managed since the park establishment in 1914 (Verrelst et al., 2010). The only expectable human interactions are due to touristic activities (although paths are not to be abandoned by law), as well as a road situated on the northern slope of the valley. The Ofenpass valley is comparable to the Valais for its location amid the inner Alps and its dryness (see e.g. Rigling et al. (2002) or Bigler et al. (2006)), with a mean annual precipitation of 900 to 1100 mm (Schaepman et al. (2004)). The valley's altitudes range from 1500m a.s.l. and reaches up to 1900m in the eastern part, while surrounding mountain ridges and peaks reach up to 3000m (Morsdorf et al., 2004).

Vegetation in the Ofenpass valley is characterized by alpine forest stands, dominated by mountain pine (*Pinus montana* ssp. arborea) and stone pine (*Pinus cembra*) species (Morsdorf et al., 2004). On the northern slope, more than a fifth of the upright trees are dead (Morsdorf et al., 2005), which has mainly been caused by root rot fungi Dobbertin et al. (2001). The investigated study area will cover the entire Ofenpass valley as shown in Figure 2.2. A sample view of the forested Ofenpass valley is given in Figure 2.1.

FIGURE 2.1: Overview of the Ofenpass valley near Stabelchod in the SNP.

2.2 LiDAR Data

The ALS sampled data originates from two helicopter-based flight campaigns date to 2002 and 2010. The covered area in the 2002 dataset was slightly smaller in size ($14km^2$) compared to the 2010 data and was entirely encompassed by the latter and was therefore decisive for the study area. Two different ALS instruments were used (Toposys Falcon II in the 2002 dataset and Riegl LMS Q 560 in 2010), and height and surface models were computed by Toposys using their proprietary TopPit software. 2.1 lists the most important sensor specifications of the two instruments.

2.3 LiDAR Single Tree Detection

The processing sequence of the LiDAR point cloud datasets in this study is described in detail in Morsdorf et al. (in revision) and is based on Morsdorf et al. (2004). In short, data was pre-processed in the steps listed as follows:

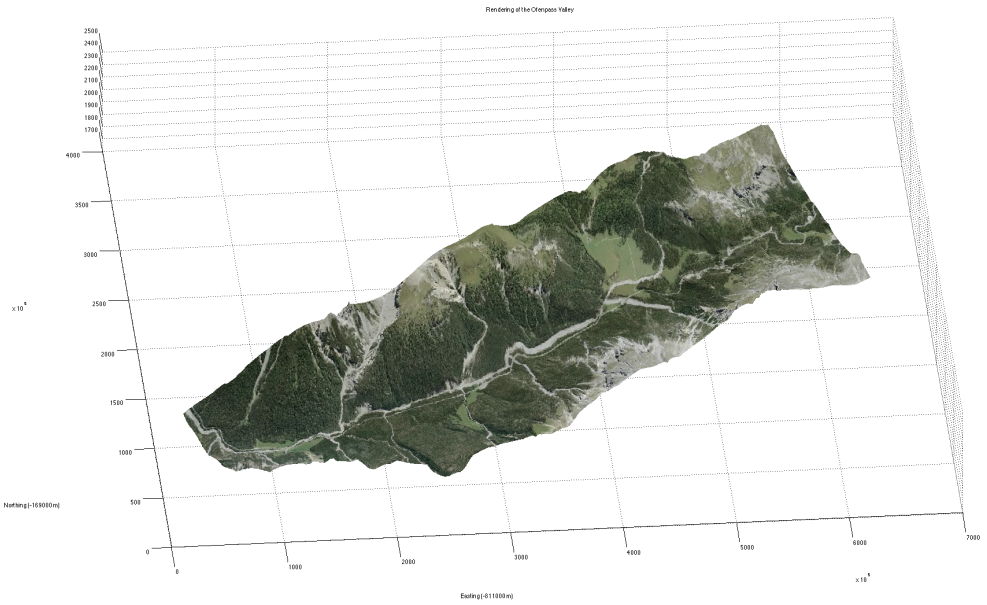

FIGURE 2.2: Rendering of the study area (Ofenpass valley) with an overlay texture[1].

	Unit	2002	2010
Instrument		Toposys Falcon II	Riegl LMS Q 560
Beam deflection		Fiber array	Rotating mirror
PRF	$[kHz]$	83	70
Echo detection mode		first, last	up to 7*
Nominal flying altitude AGL	$[m]$	500	700
Max. Scan Angle	$[°]$	$\pm$7.3 (fixed)	$\pm$15
Wavelength	$[nm]$	1560	1550
Pulse duration	$[ns]$	5	4
Beam divergence	$[mrad]$	1	≤ 0.5
Avg. echo density	$[1/m^2]$	38.1	27.4
Time of acquisition		October 2002	September 2010

TABLE 2.1: Specifications of the two used ALS datasets. *The full-waveform supported by the LMS Q 560 was recorded, but only discrete returns were used in this study, extracted during post-processing.

1. Identification of local height maxima in the CHM. These local maxima are assumed to represent measurement returns from tree tops.

2. Clustering of the point cloud by means of approximating a 3D Gaussian fit curve to the local maxima (mean) as well as tree height and crown diameter (curve standard deviation).

3. Matching of trees from the two datasets, which is based on a tree's location in the x and y domain (the presumed tree height is unusable since the actual height might

be significantly different due to the time gap between the two datasets. Moreover, the actual increase representing tree growth is of main interest in this case). The matching algorithm makes use of a nearest neighbor search.

The single tree identification resulted in a total of 408'915 objects for the 2002 dataset and in 1'216'936 objects for 2010. The total number of matched pairs between the two datasets were 403'624 objects. Table 3.1 lists further statistical information for the identifications. It is important to note that despite positive results for successful tree identification in Morsdorf et al. (2004), misclassifications and false alarms do happen, and they occur in a multitude of ways: for instance, it may well be that heights get overestimated due to birds, smoke particles or other objects large enough to generate a return for the LiDAR. Such errors are typically easy to identify in extreme overestimations as in the 2002 dataset, where the maximum height clearly exceeds any realistic value. However, as soon as e.g. birds flying just above the canopy are erroneously recorded, an accurate identification and elimination may not be feasible anymore. In order to limit such systematic errors as good as possible beforehand, the maximum sensible tree height was assumed to be at most 40m and the identified objects constrained to lie below this value.

Secondly, the tree matching step revealed that some trees featured a height decline over the eight years instead of a growth. Also, some seemed to have reached a stagnation in growth and seemed to have more or less the same height in both 2002 and 2010. Trees that have stagnated or lost height are depicted as green respectively red dots in Figure 2.3. Obvious explanations, besides a mismatching or displacement in the algorithm, are avalanches, blowdowns or other causes resulting in a tree's death and eventual fall-down. Consequently, all trees with theoretical negative growth rates have been excluded from further analyses as well.

Thirdly, some identified objects in the field may have had a height comparable to (young) trees, but were in fact other species, boulders, or comparable. Based on the formulation of Körner (1998), who defined a tree as having a height of at least three meters, all objects below this threshold were omitted in the analyses. This also coincides with the findings of Kalliovirta and Tokola (2005) who found young trees below the three meter mark to not respond well to their age prediction models.

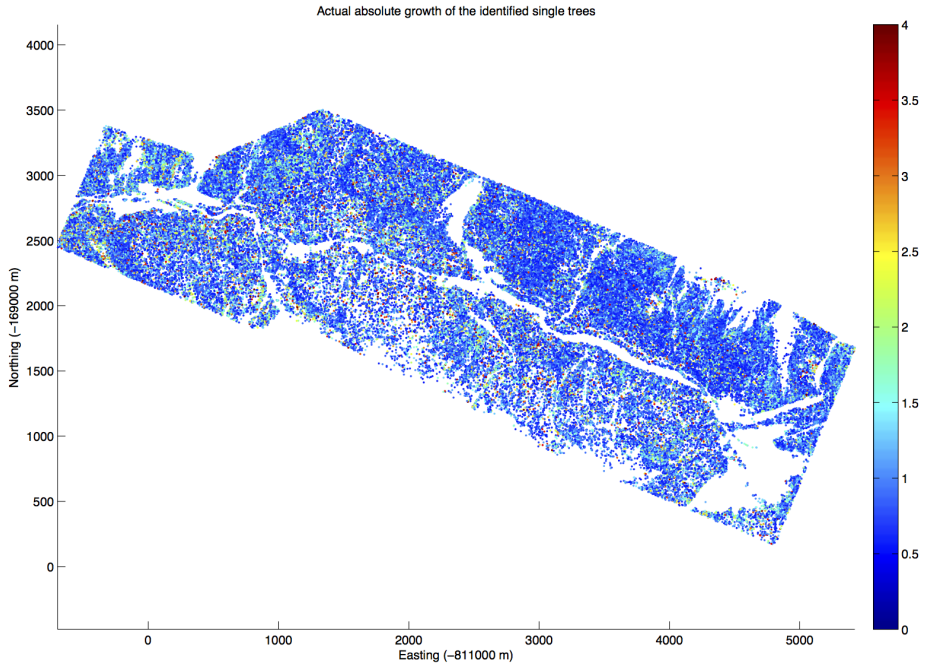

FIGURE 2.3: Height difference of the identified single trees between 2002 and 2010.

2.4 Raster Data Preparation

Besides the single tree identification, also rasterized datasets of the sampled surface and ground were derived from the LiDAR point cloud. As discussed in Section 1.5.2, ALS sampled data may be prone to increased noise originating from a number of different error sources, and thus deviations in tree height estimation. This logically was also the case in the present study's datasets. The usage of the rasterized canopy height model omitted the step of identifying single trees and hence helped reducing the number of error sources and total amount of error present. In order to get rid of objects other than trees as good as possible and reduce the influence of young trees where only vague growth signals are visible, the rasterized data were limited the same way as the single trees identified to the tree height and growth range described in 2.3.

The consideration of the rasterized CHM mainly leads to a reduction of methodological errors. However, the problems of platform-related error sources continue to exist also within this dataset. These errors are of geometrical or physical origin and may thus not be eliminable. In order to at least reduce their impact on the data, the CHM differences dataset has been smoothed with an average kernel of 10x10 pixels (5x5m).

2.5 Environmental Influence Variables Approximation

For a number of environmental influence factors, calculation is either straight-forward or not required at all. This is the case in the tree's age, which is approximated with the initial tree height in 2002 in a linear relationship, as well as the altitude, which is derived from the DTM. The rest of the factors and their approximations will be addressed below. All in all, the following influences and their parameterizations will be included as explanatory factors in further analyses:

- Tree age: tree height
- Sunlight exposure: solar radiation budget
- Temperature: altitude [m]
- Slope
- Aspect
- Water availability/drought: Topographic Wetness Index (TWI)

These variables and the relations between them are further shown in a flow chart in Figure 2.4.

2.5.1 Sunlight Exposure

There have been a number of studies addressing the calculation of the solar radiation budget values for surfaces (e.g. Corripio (2003), Kumar et al. (1997)). In conventional cases, a pixel-wise exact value of total solar radiation, integrated over one year, may be required for further calculations. Also, depending on the number of modeled (atmospheric) paths of radiation as well as wavelengths (shortwave, longwave), the calculation may become too expensive to accomplish. The objective of this study deviates from such problems insofar as it only requires relative radiation differences between (forest) patches of the study area, which therefore does not only reduce the required accuracy level of the radiation budget calculation, but also dramatically simplifies its execution. It is easily assumable that meteorological conditions and changes have a more or less equal impact over the entire study area and in sum affect all trees evenly. Moreover, too

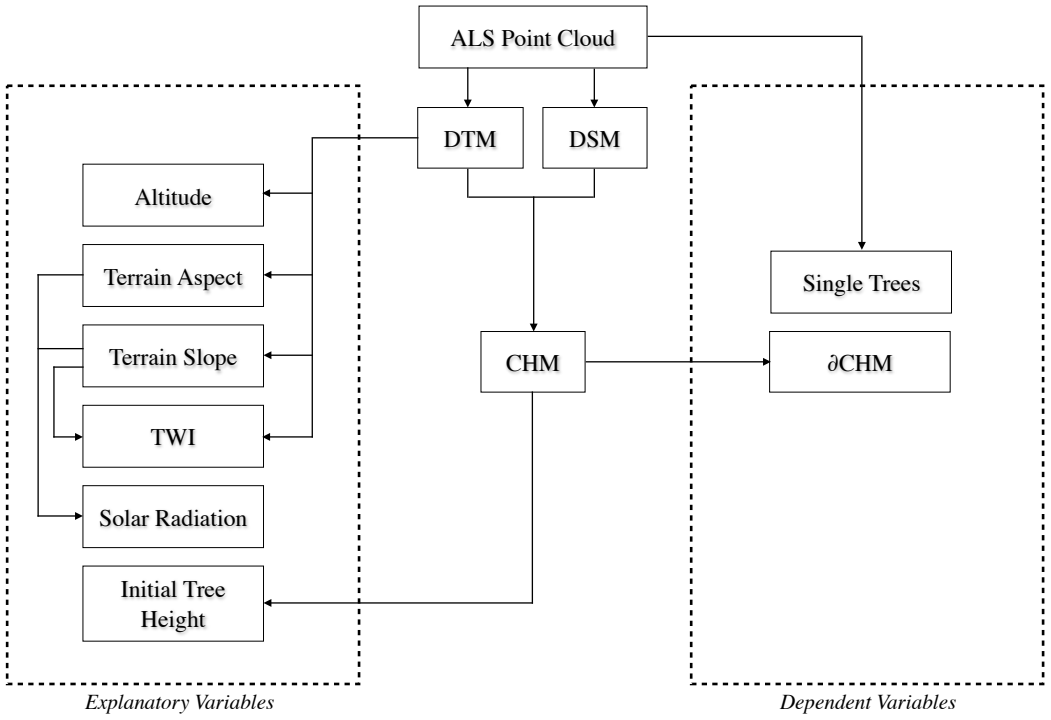

FIGURE 2.4: Flow chart showing the dependence of the variables used in the statistical model, with differentiation of explanatory (environmental influences) and dependent (forest growth) variables. See Section 2.6 for further details.

complex atmospheric paths such as multiple light scattering from neighboring areas do not need to be calculated as they may be assumed to either appear uniformly over the entire scene, or else to be too marginal to alter the resulting solar radiation significantly. Finally, since we do not need to know the exact budget, an integration over one year is not necessary; instead it may be sufficient to know the radiation of the days having the shortest respectively the longest day length, covering the entire variation of both number of sunshine hours and solar elevation angle. For the northern hemisphere, the summer solstice occurs on June 21 and the Winter solstice around December 21, which correspond to the day numbers 172 resp. 355, assuming no leap-year.

Eventually, most solar radiation differences between the trees are to be found due to the incidence angle of the (direct) solar radiation path on the earth's surface (Kumar et al., 1997), and also the amount of shading present during the day originating from obscuring escarpments. In addition, the investigated study area features a very rugged terrain, which, depending on the solar altitude and azimuth angles, casts a significant amount of shadow on certain areas, therefore blocking at least the directly transmitted part of solar

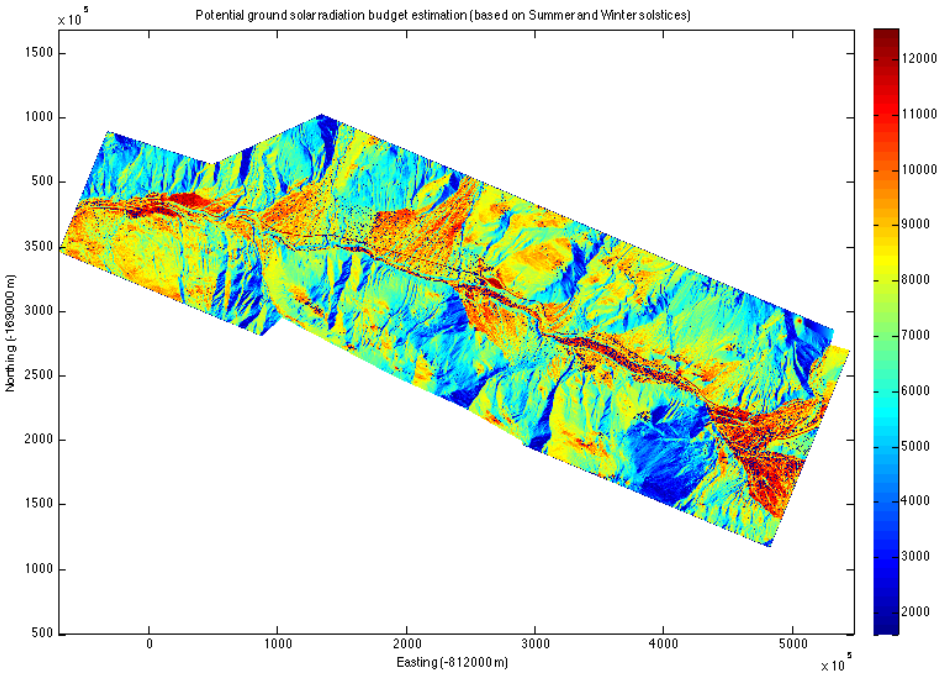

FIGURE 2.5: Potential ground solar radiation budget over study area (Summer and Winter solstices, one hour temporal sampling resolution), including relief shading effects.

irradiation (Chalkias, 2004). The amount of hillshading in the scene largely depends on the solar position and was thus required to be repeatedly calculated for each radiation integration time step. Hillshading was calculated using ESRI's algorithm (ESRI, 2014b), and standardized to a range of [0, 1] for an easier calculation of direct shortwave radiation attenuation.

The solar radiation for the Summer and Winter solstices was calculated following Kumar et al. (1997) with a temporal integration interval of one hour. This model estimates per-pixel values of incoming shortwave radiation on direct or diffuse (scattered by the atmosphere) paths and also considers slope, aspect, and also neighboring surfaces (Kumar et al., 1997).

2.5.2 Water Availability

A thorough assessment of the causes and potential influences of tree growth inhibition due to water stress would not be feasible for such a large number of trees as present in the study area. It is also questionable whether an investigation of factors such as hydraulic

efficiency of every tree in detail would be sensible, keeping in mind that the total number of growth-promoting or inhibiting influences is high. Therefore, analyses were reduced to the potential water availability for each tree's ground based on the height model. A common approach including the terrain characteristics at each point is the Topographic Wetness Index (TWI; Sørensen et al. (2006)), which is described in Equation 2.1:

$$TWI \; = \; \ln\left(\frac{c}{\tan\left(\beta\right)}\right) \tag{2.1}$$

where c is the specific upstream catchment area of each investigated patch and β denotes the topographic gradient at the same location. The catchment area in turn is calculated through the process of flow accumulation, where the total upslope area draining into this one patch is calculated (Schwanghart and Kuhn, 2010). Patches draining into others were retrieved using the D8 algorithm (Fairchild and Leymarie, 1991), which, for each grid cell, evaluates the height difference to its eight neighbors and chooses the neighbor with the largest difference as the drainage cell (Martz and Gabrecht, 1998). Despite its popularity, the usage of the D8 algorithm has often been regarded as being critical as it cannot handle flat topographic areas (Jones, 2002). In the present study, however, the mountainous terrain hardly features any flat areas, and the usage of the D8 algorithm was therefore assumed to be accurate enough.

2.5.3 Gradient and Aspect

The calculation of terrain gradient and aspect is relatively straight-forward and has been done using MATLAB's Terrain Data Analysis toolbox[2]. The resulting maps are shown in Figures 2.7 and 2.8 respectively.

2.6 Statistical Model

2.6.1 General Considerations

The relation of spatial data to approximated natural influences is inherently prone to a number of delicate statistical issues which mandatorily need to be considered during

[2]http://www.mathworks.ch/ch/help/map/ref/gradientm.html

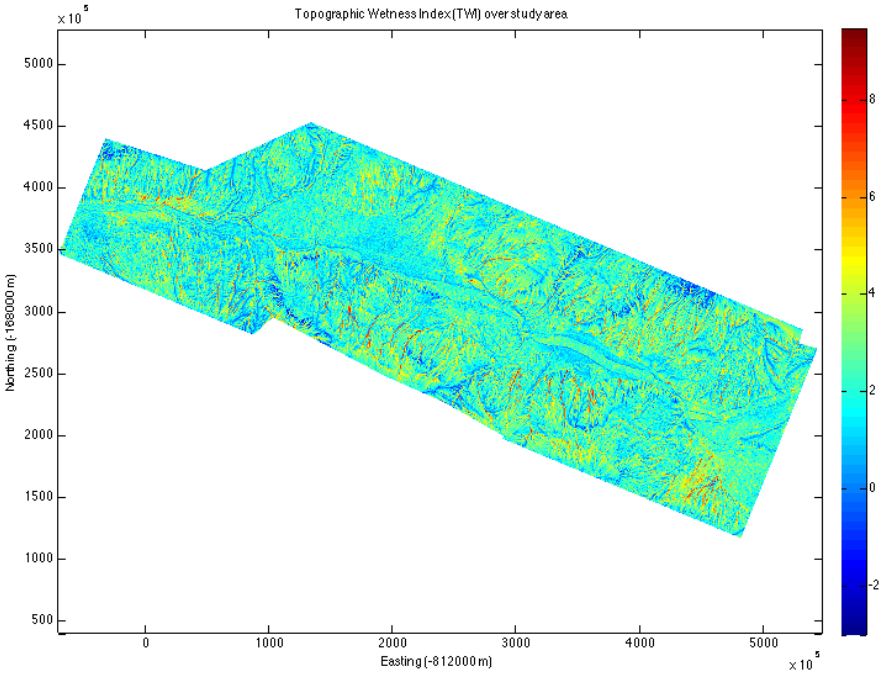

FIGURE 2.6: Result of the Topographic Wetness Index (TWI) calculation over the study area.

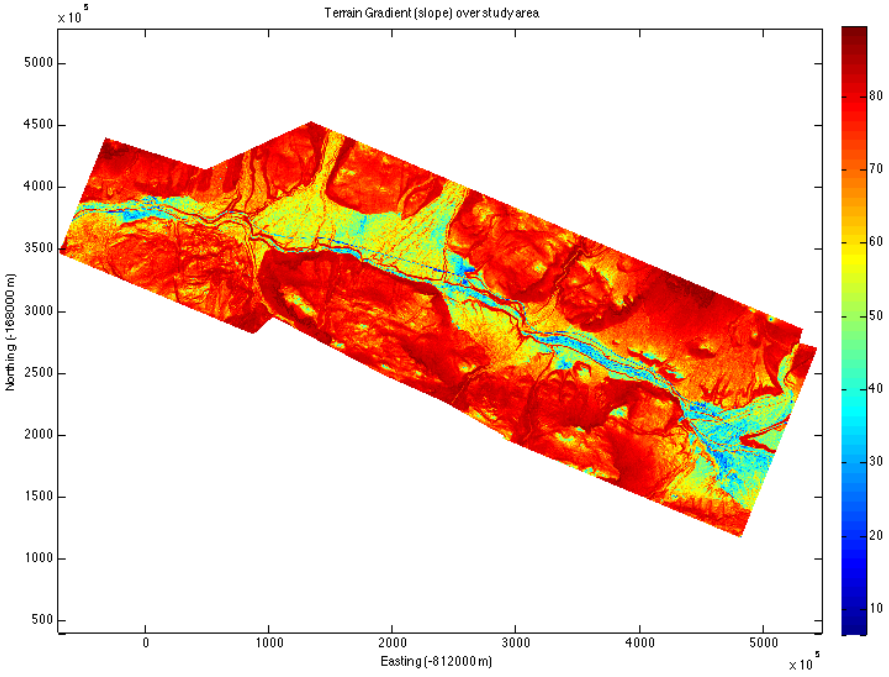

FIGURE 2.7: Terrain gradient over study area, smoothed using a square moving average kernel (5x5m). Values are given in degrees.

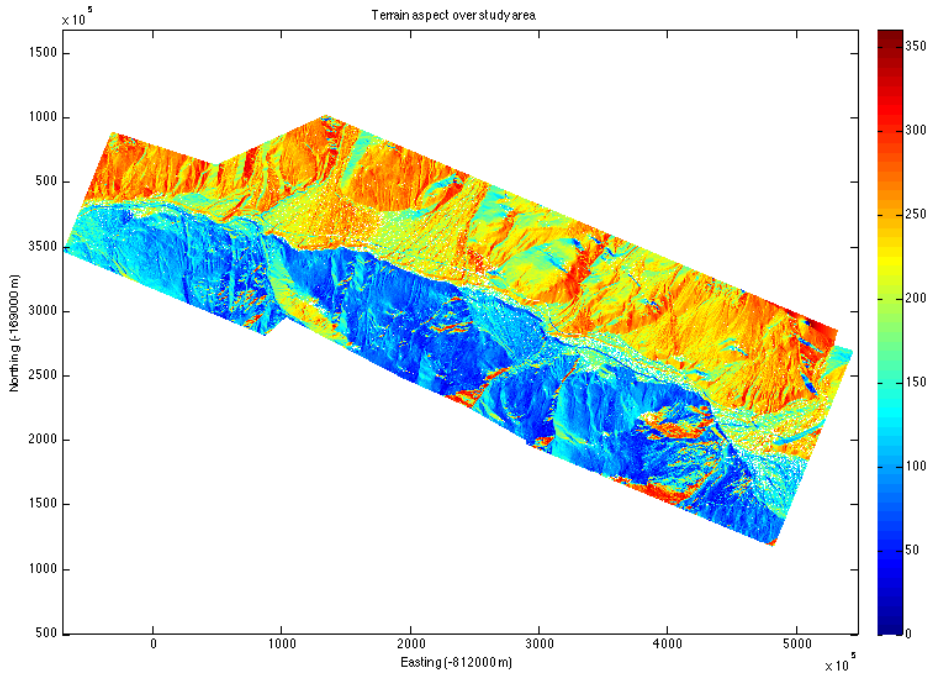

FIGURE 2.8: Terrain aspect over study area, smoothed using a square moving average kernel (5x5m). Values are given in degrees.

the establishment of a model. Therefore, a careful assessment of statistical preconditions and well-considered choice of model is paramount. In this thesis, central focus is laid on *geo*statistical models as well as their performance in comparison to regular estimation models such as the Ordinary Least Squares (OLS) regression technique.

Model-wise, regular multiple OLS regressions are thus applied as a first step in order to retrieve a general estimation for fitting quality. Subsequently, spatial regression models will be calculated to address the common problems occurring when dealing with spatial data as described below. These statistical regression models include the location of the samples in their calculation to address problems like spatial autocorrelation as well as spatial nonstationarity. Section 2.6.3 will address these issues in detail and give an overview over the applicable techniques in this model. Finally, a comparison of the model outcomes (predictions and residuals) may provide valuable information on the difference in accuracy between ordinary statistical techniques and their counterpart spatial estimators.

The analyses will be carried out based on the two underlying dataset types (variables based on the interpolated raster datasets respectively the derived single trees). In all

models, differences in tree height between 2002 and 2010 will be used as the dependents, and the environmental influences described above as the explanatory variables. Furthermore, the division between northern and southern slopes' trees will be included nonetheless to be able to differentiate data between the different micro-climates prevalent in the two slopes' regions. Since the height increments of trees relative to their "initial" height in 2002 are of interest as well, these models will be repeated to conform with this idea (in this case, the tree height as an estimation for tree age consequently will not be considered). The significance level (α) for all tests will be set to 0.05.

2.6.2 Statistical Preconditions

A variety of tests to assess the statistical preconditions will be run to verify the accurateness of prediction. The generally proposed statistical regression techniques also used in this case are based on the OLS regression. Therefore, even if it may not be mandatory, it is desirable for the standard regression technique to be parametric as well for best comparability. The residuals of all models will thus be tested for Normal distribution and, if necessary, required transformations may be applied to account for any deviations. Normal distribution will be tested qualitatively by examination of histograms and Quantile-Quantile- (Q-Q-) plots, and, moreover, by using Kolmogorov-Smirnov- (K.-S.-) tests.

Furthermore, multivariate linear regression models require the explanatory variables not to show correlation within each other, which is generally known under the term "multicollinearity". This effect may cause severe errors and misleading results in statistical analyses and is by some seen as a "threat" and a "symptom of poor experimental design" (Farrar and Glauber, 1967). In the present case, Multicollinearity may indeed be expected due to relations between some of the input variables (the solar radiation budget as modeled here for instance depends on, and thus may correlate with, the slope of the terrain). Technically spoken, it is of course reasonable to suspect an inappropriate experimental design behind such analyses. However, it also becomes clear that if environmental variables shall be derived almost entirely from topography, such design problems become unavoidable. With respect to this issue, a careful surveillance of multicollinearity

effects and, if necessary, measures to avoid them are crucial. One way to measure multicollinearity involves the examination of the Variance Inflation Factors (VIFs) between each independent variable:

$$VIF = \frac{1}{1 - R_i^2} \tag{2.2}$$

R_{ij}^2 denotes the coefficient of determination between the independent variables i and j. Variables showing VIFs above a certain threshold are usually omitted from statistical analyses (threshold values between 5 and 10 have usually been proposed (Neter et al., 1989)).

Further tests to be performed involve an estimation for homoscedasticity and first-order autocorrelation. Homoscedasticity is a desirable requirement for a statistical model and denotes the homogeneity of variance along the entire range of the dependent variable. In the case of heteroscedasticity, the variance does not remain equal, which violates the variance homogeneity assumption of the (multivariate) OLS model. Heteroscedasticity may well be expectable in the applied dataset already due to the declining variance with increasing tree growth values. Analysis of heteroscedasticity will be done using the Breusch-Pagan test as well as standardized residual plots.

Finally, autocorrelation in general refers to a common problem in general statistics where an outcome signal shows a (linear) relationship with itself. In regression analyses, residuals showing autocorrelation violate the assumption of uncorrelated error terms. The most common test to detect autocorrelation, the Durbin-Watson test, will also be applied in this study.

2.6.3 Spatial Peculiarities

Traditional statistical analyses have been extensively used in scientific theses and are well-established means of correlation indication. This study includes a few dependent and a number of independent variables and hence seems to be an ideal candidate for such tests. There is, however, a central property within all variables, that basically turn every test upside down that is to be used: their spatial nature.

Following Tobler's first law of geography ("everything is related to everything else, but near things are more related than distant things"; Tobler (1970)), geostatistical studies have often focused on *spatial autocorrelation* as a central property in spatial datasets. Spatial autocorrelation involves random variables whose values, within a certain distance between each other, are either more similar (positive autocorrelation) or more diverse (negative autocorrelation) than would be expected without the spatial property (Legendre, 1993). Visually spoken, spatial data showing spatial autocorrelation are often clustered together and show patchiness (Legendre, 1993). The most incisive consequence of spatial autocorrelation on statistical analyses is that a global model suddenly fails to explain variance among samples that, within their locality, behave differently than the rest of the data. Therefore, there is need for a specialized regression model that accounts for spatial autocorrelation, also including spatial versions of the preconditions tests explained above.

The most common example for a spatial regression model is the *Geographically Weighted Regression* (GWR), which has originally been described by Brunsdon et al. (1998). GWR accounts for such variations with location (spatial nonstationarity; (Brunsdon et al., 1998, Chen et al., 2012)) by incorporating a local neighborhood function with a given radius (Brunsdon et al., 1998), and tries to give a local model estimate depending on this neighborhood (ESRI, 2014a). The underlying principle of GWR is explained in Brunsdon et al. (1998). In the present study, GWR thus turns out to be favorable due to two reasons: *(i.)* both tree growth rates are very likely to show (positive) spatial autocorrelations due to similar conditions approximated by the independent factors, and *(ii.)* there may be effects within factors, such as an increased solar radiation also raising temperature and lowering soil moisture content, which need to be accounted for. Spatial autocorrelation is therefore assumed to be of special importance in this thesis' analyses, because both the tree growths as well as the explanatory variables are expected to be similar in certain regions.

The vast amount of data in this study, however, massively restricts the application of GWR despite fast systems and large amounts of RAM available. In order to avoid such calculation problems, Pozdnoukhov and Kaiser (2011) have proposed a spatial regression technique providing comparable results to GWR, but considering the property of scalability. The authors thus named their method the *Scalable Local Regression* (SLR). SLR establishes a number of regression models with a spatial center that include all points

within the specified locality radius (hereby denoted as kernel size) and predicts each point by inclusion of a weight dependent on its distance to the kernel center (Pozdnoukhov and Kaiser, 2011). Once all models are established, the final prediction of a point is a sum of each model it lies in; the SLR hence works on a streaming principle (Pozdnoukhov and Kaiser, 2011). There are a number of optional properties applicable within the model like a local (machine-) learning method ("receptive field weighted regression"; Schaal and Atkeson (1998), in Pozdnoukhov and Kaiser (2011)), which are turned off in this study to get a local counterpart as close as possible to the global regular OLS. Analyses were performed using the open source distribution of SLR provided by the authors[3].

[3] http://ncg.nuim.ie/i2maps/

Chapter 3

Results & Interpretation

This thesis' aim to examine the relation between ALS-derived influence factors and tree growth has been targeted by means of multiple regressions. Unlike previous studies, analyses included more than one potential influencing parameter at once, and was further carried out on the basis of large forested areas instead of a low number of trees. Therefore, it should eventually be possible to provide answers on how well the research goals described in Section 1.3 have been reached. Regressions have further been tested not only on the ALS-derived single trees, but also on the mere CHM differences, and any improvements within the regression results might shed light on whether the single tree identification process improves the result or not.

This Chapter is divided into three major parts. A first Section lists descriptive statistical parameters of the investigated datasets (CHM height differences and ALS-derived single tree growths) and thus provides a glimpse on the statistical distribution of the tree growths within eight years. The next Section addresses statistical preconditions that have to be met for the regular OLS multivariate regression models. A third major Section finally provides regression results (both for the OLS and SLR models).

3.1 Descriptive Statistics of the Dependent Variables

Table 3.1 shows the most common descriptive statistical parameters of the analyzed datasets. Minimum and maximum values correspond to the restrictions placed upon potential samples (tree growths $\in [0.5, 4]m$) and are only listed for completeness.

		% samples	# samples	Min	Max	Mean	Median	SD
Single Trees	abs.	26.54	107′125	0.50	4.00	1.13	0.91	0.66
	rel.	26.54	107′125	0.02	1.32	0.15	0.11	0.13
δ CHM	abs.	4.70	3′915′393	0.50	4.00	1.36	1.12	0.77
	rel.	7.64	6′360′328	0.00	4.0	0.24	0.14	0.33

TABLE 3.1: Most common descriptive statistics for the investigated datasets (absolute and relative height differences of the CHM models as well as the identified single trees). In row are the percentage of examined data points relative to the total number, their absolute number, minimal and maximal value of the samples, the mean and median values of the samples, and finally also the standard deviation of the samples.

The statistics reveal that the single tree derivation process combined a very high number of ALS sampling points to a single tree, which makes sense regarding the point density of these instruments and the diameter a tree reaches on average, especially in an old-grown forest. Slightly more than 50% of all pixels of the interpolated CHM raster within the study area were assumed to be trees. Furthermore, mean and median growth values suggest that trees grew only little.

3.2 Statistical Preconditions of the OLS Regression Models

A number of tests have been performed prior to or after the respective OLS regressions in order to assess statistical meaningfulness of each model. These included a check for normal distribution using histograms, Q-Q-plots and K.S.-tests, an assessment of multicollinearity by means of VIF scores, a check for autocorrelation by application of a D.W.-test, and finally a visual inspection of the standardized residuals to retrieve potential heteroscedasticity effects.

Both the histograms and Q-Q-plots as shown in Figure A.1 indicate no normal distribution in all test cases. This corresponds to the results of the K.S.-tests listed in Table 3.3, whose p values indicate a rejection of the null hypothesis ("residuals are normally distributed at the 0.05 level").

Data have further been tested for multicollinearity (i.e. the correlation between the explanatory variables) by means of the Condition Index (CI), VIF and variance decomposition proportions as outlined in Belsley et al. (2004) and Friendly and Kwan (2009).

Table 3.2 contains the VIF scores for each independent variable set used in all OLS regression models. Since all VIFs lie below the proposed thresholds of 5 and 10, it can

Variable	Altitude	Sol.Rad.	Gradient	Aspect	TWI	Height 2002
δ CHM, abs.	1.2	1.4	1.4	1.2	1.0	1.2
δ CHM, rel.	1.1	1.3	1.4	1.0	1.0	-
Single, abs.	1.1	1.6	1.0	1.1	1.4	1.2
Single, rel.	1.0	1.4	1.0	1.1	1.4	-

TABLE 3.2: Variance Inflation Factors (VIFs) for all four explanatory variable sets as used in the OLS regression models (CHM differences and single trees; absolute and relative). Tree height in 2002 was not part of the explanatory variables in the relative cases as it is already contained in the dependent variable. Since all VIFs lie below 5, no multicollinearity is to be expected on a global scale.

be assumed that multicollinearity among the explanatory variables is not to be expected on a global scale.

The p values of the D.W.-tests on autocorrelation are listed in Table 3.3 as well. p values for the D.W.-tests are less than 0.05 in all cases as well, hence indicating that also autocorrelation is present within all four models.

Model	data	K.S.	Durbin-Watson
δ CHM	abs.	0.00*	0.00*
	rel.	0.00*	0.00*
Single Trees	abs.	0.00*	0.00*
	rel.	0.00*	0.00*

TABLE 3.3: Resulting p values from the K.S.- (Kolmogorov-Smirnov-) and D.W.- (Durbin-Watson-) tests based on the residuals from the OLS models. The tests showed that there is a high chance for all four residuals sets to suffer from autocorrelation and residuals not being normally distributed.
* K.S.-test p values are significant at the 0.05 level

Finally, Figure A.3 depicts scatter plots of standardized predictions versus standardized residuals as emerged from the OLS calculations. In case of (required) homoscedasticity, the residuals would be scattered among the prediction axis in a homogeneous way. Since this is not the case in all OLS models, it has to be assumed that this precondition is not fulfilled as well.

3.3 Regression Results

3.3.1 OLS Estimations

In an initial step, regular OLS models have been carried out on the basis of both the CHM as well as identified single trees, both for absolute and relative height differences.

This resulted in four models for whose the most important model statistics are listed in Table 3.4. These statistics include coefficients of determination (R^2) for the general OLS estimates and also statistical parameters of the additionally carried out ANOVA on the independent variables against zero (F-statistics value and p value). The null hypothesis for the ANOVA states that all regression coefficients are equal to zero (no environmental variable has an influence on the height differences).

Model	data	R^2	F	p
δ CHM	abs.	0.11	70114.33*	0.00
	rel.	0.01	8283.61*	0.00
Single Trees	abs.	0.03	613.13*	0.00
	rel.	0.04	924.27*	0.00

TABLE 3.4: OLS regression statistics for both the CHM differences as well as single tree growth models (absolute and relative), listing in row the coefficients of determination, the F test statistics for the ANOVA, and also their respective p values.
* Coefficients are significantly different from zero at the 0.05 level

The R^2 values of all four OLS regressions indicate a very weak goodness of fit for the estimation and hence a high number of outliers and insufficient predictions. The F values resulting from the ANOVA in turn are very high. Consequently, the p values for all four models are zero, indicating that the null hypothesis for the ANOVA can be rejected at the 0.05 level.

Furthermore, with focus on spatial distributions, both the OLS predictions and residuals are depicted in their spatial context in Figures 3.1 and 3.2, respectively Figures 3.3 and 3.3 for the CHM differences, and A.4, A.5 and A.6, A.7 for the single tree growths. Residual statistics are given in Table 3.5.

Model	data	min $\mid r \mid$	max $\mid r \mid$	mean	median	std	RMSE
δ CHM	abs.	0.00	5.21	0.00	0.18	0.72	2.00
	rel.	0.00	3.83	0.00	0.09	0.32	0.69
Single Trees	abs.	0.00	3.09	0.00	0.20	0.65	1.72
	rel.	0.00	1.17	0.00	0.04	0.13	0.31

TABLE 3.5: Descriptive parameters for the OLS regression residuals. Listed in order are the minimal and maximal values of the absolute residuals as well as the mean, median, standard deviation and RMSE of the residuals (non-absolute). RMSE scores are given as unstandardized values and should only be compared within the regression models' dependent variable type (absolute respectively relative tree growth).

As can be seen in the maps (Figures 3.1 and 3.2), growth on the north-facing slope of the study area has been predicted to be greater in the absolute CHM difference model (yellowish areas). For the CHM dataset, this corresponds fairly well to the ALS height

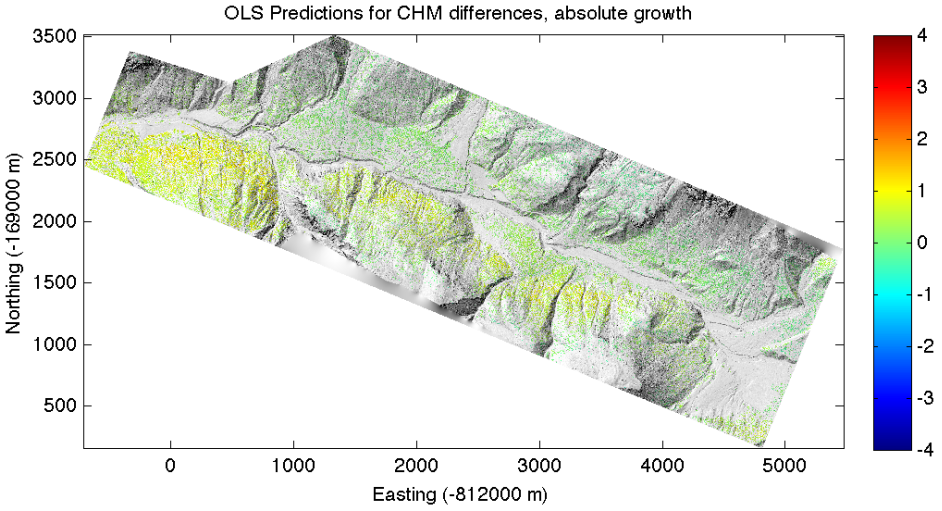

FIGURE 3.1: Prediction map depicting the OLS result based on absolute CHM differences.

differences, and thus the independent variable. The residuals, however, nevertheless indicate that the OLS estimation for this dataset has some flaws. This is especially visible statistically: absolute CHM height differences estimated by OLS show an RMSE of over two meters, which is far more than the average growth signal of $0.91m$ (median). The relative CHM differences as predicted with OLS share similar issues: while the predictions for the southern part of the study area came out higher than for the other slope, the actual signal shows no differences between these two parts. Consequently, also the relative CHM difference residuals resulted in a rather high RMSE, with most trees having been over-, and a small part underestimated, the latter severely though (see the residuals Histogram in Figure A.2, top right).

The absolute single tree predictions by the OLS method appear to be relatively constant, with little variation over the study area. On the north-facing slope (southern part of the study area), tree growth predictions are partially slightly lower than their surroundings, but indifferent from the south-facing slope. The residuals in turn show a particularity

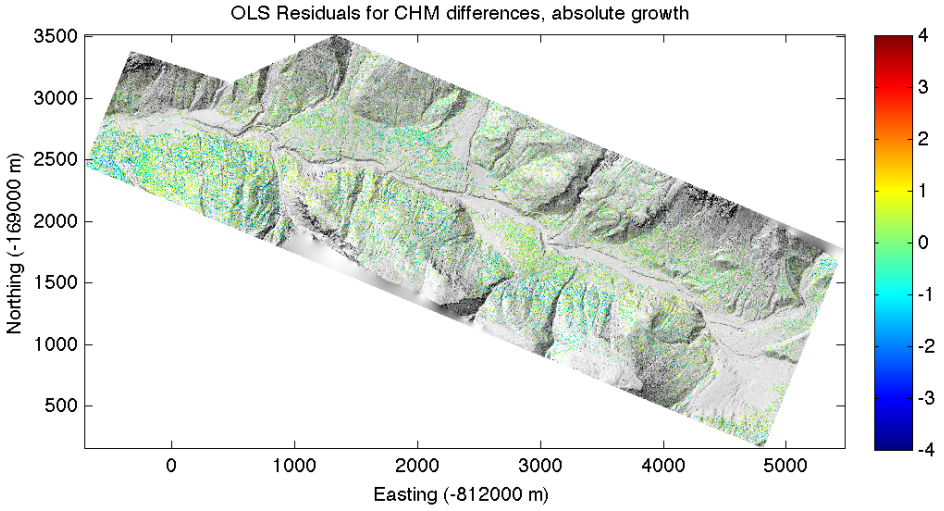

FIGURE 3.2: Residuals map depicting the OLS result based on absolute CHM differences.

that is, albeit to a lower degree, also visible in the CHM models: a high number of single samples or small groups scattered throughout the entire study area that got massively underestimated (visible as blue spots in Figure A.5). Furthermore, the RMSE is slightly lower than in the CHM differences model, but still higher than the average growth signal.

In the relative single tree growth case, spatial prediction patterns are comparable to the absolute OLS single tree prediction model. The residuals, however, seem to contain less outliers (underestimations) than in the absolute case, which is visible both in the spatial distribution and the residuals histogram (Figures A.7 and A.1 respectively). Also, the relative OLS predictions' RMSE sees a much higher improvement compared to the CHM model than in the absolute case. All in all, the OLS models so far might lead to the assumption that the single tree model, based on relative growth estimations, provides the statistically best solution.

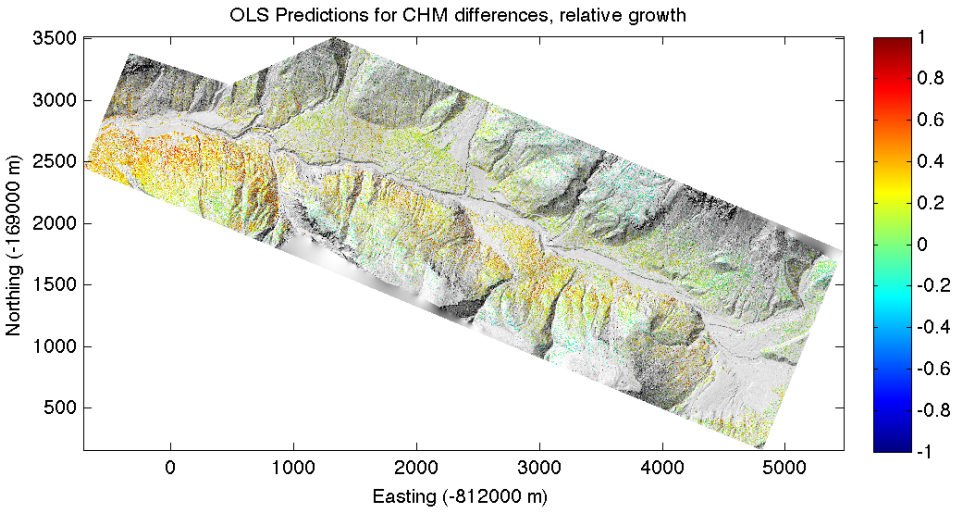

FIGURE 3.3: Prediction map for the OLS regression based on relative CHM differences.

3.3.2 SLR Estimations

In addition to the global OLS models, also SLR predictions have been carried out in order to assess potential spatial nonstationarity effects. In a first run, SLR models have been run with similar configurations as in the OLS case (the same variables), but only on the single trees dataset and with three different locality sizes (local inclusion radii of 1km, 500m, and 250m). The resulting prediction and residual maps are shown in Figure A.8 for the absolute, and Figure A.9 for the relative case, respectively.

At a first glance, all six SLR models seem to have produced very exaggerated predictions, with high sensitivities to some of the predictor variables. In the 1km case, growth was especially underestimated at places where solar radiation budget estimations were low. This can be seen in Figure A.8, top left in the northwestern and southeastern part of the valley. Consequently, the majority of samples show strong negative residuals (Figure A.8, top right). The 500m and 250m models share these properties, but feature additional effects in the form of large hotspots of underestimation (500m model case; westernmost

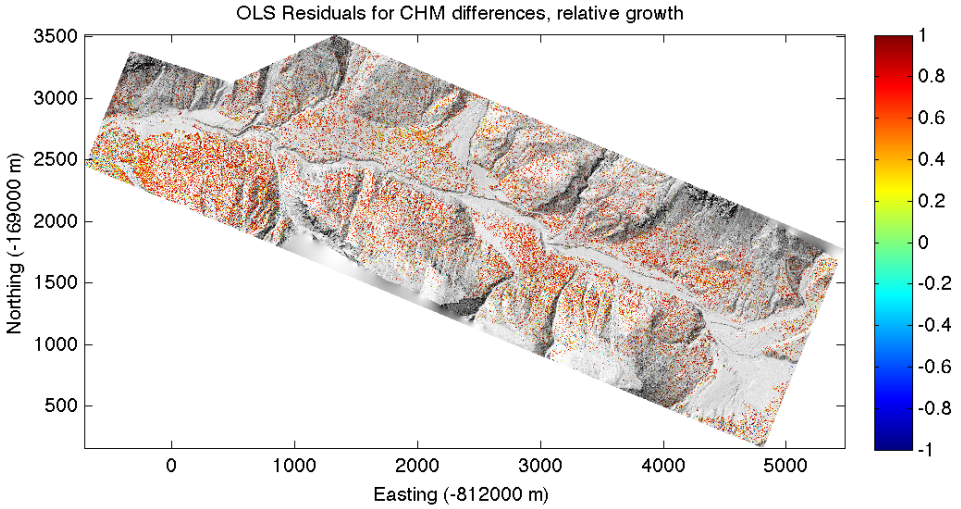

FIGURE 3.4: Residuals map for the OLS regression based on relative CHM differences.

part of the study area), respectively underestimation (250m case; central part of the valley). An assumption may be that these flaws are due to the smaller locality size of these two models, as they are not visible in any of the input variables.

The relative SLR estimations share the same underlying features and issues, but with different origins: instead of solar radiation, the altitude of each sample tree seems to be the main driving factor leading to a relative growth overestimation towards the mountain ridges as well as to an underestimation within the valley bottom. The 1km model contains a strong underestimation in the mid-western part of the valley, while this part has been massively overestimated in the 250m model. The relative 500m model, however, did not result in an underestimation unlike in the absolute case, but still suffered from the altitude-related bias effect. This model also featured the lowest RMSE of all relative SLR models, although this score was still above the one if estimations were retrieved using the OLS approach.

All in all, the spatial patterns, residual histograms and RMSE scores of all six SLR estimations showed that one or two input variables had a too strong effect on the predictions

outcome. As all SLR models gave out VIFs above 10 for most of the sample points, and with respect to the fact that some of the input variables were inter alia calculated using each other, it was standing to reason that strong multicollinearity effects were indeed responsible for the biased SLR predictions. Therefore, the statistically most accurate model (relative growths, 500m kernel size) was re-run without altitude, aspect and gradient, hereby denoted as "SLR revised". For comparison reasons, also the relative single tree growth OLS model underwent a revision and was carried out with solar radiation and TWI as the only predictors ("OLS revised"). Solar Radiation and TWI only share terrain gradient as a direct common variable, but also involve further calculations and were thus expected to cause less collinearity effects. The results of both the revised SLR and OLS model are listed and depicted in Table 3.6 and Figures 3.5 to 3.8 respectively.

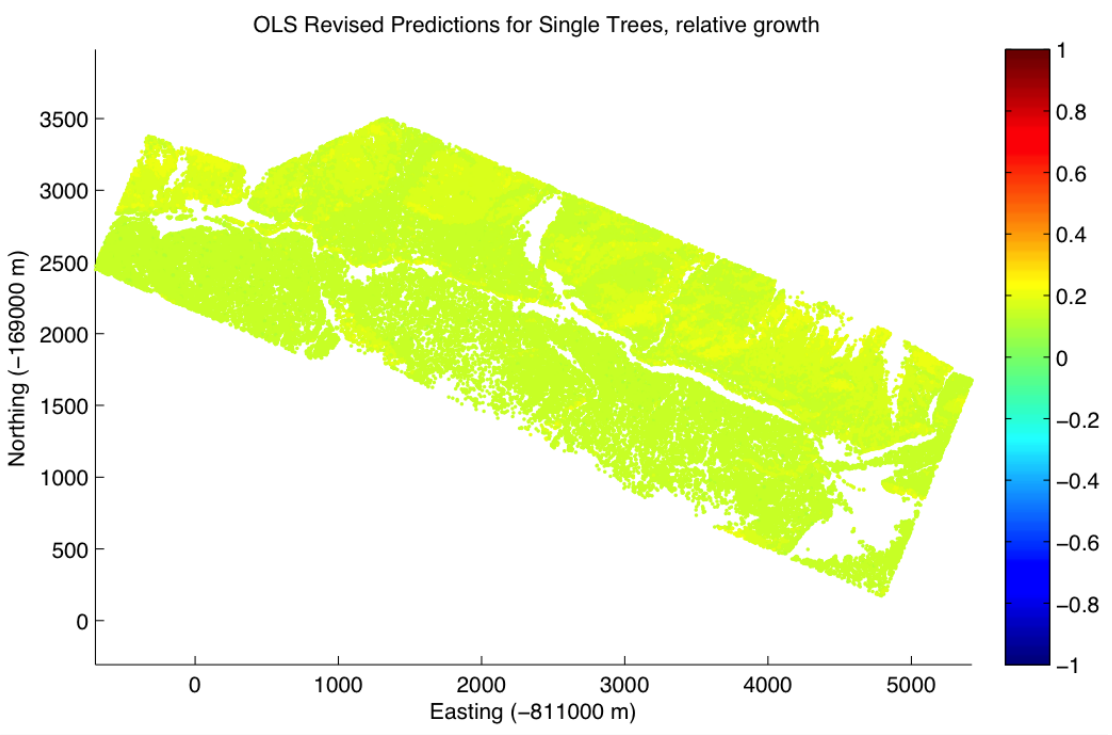

FIGURE 3.5: Prediction map of the revised OLS model on relative single tree growths.

With terrain gradient, aspect as well as altitude removed from the explanatory variable pool, also the SLR model provided more credible predictions. Compared to all other relative models, the revised SLR model's residuals resulted in the lowest RMSE score. There still remain a few areas where relative growth was underestimated though; particularly in the (south-) eastern part of the Ofenpass valley. Once more, these patterns of underestimation seem to correspond with low solar radiation budget calculations as

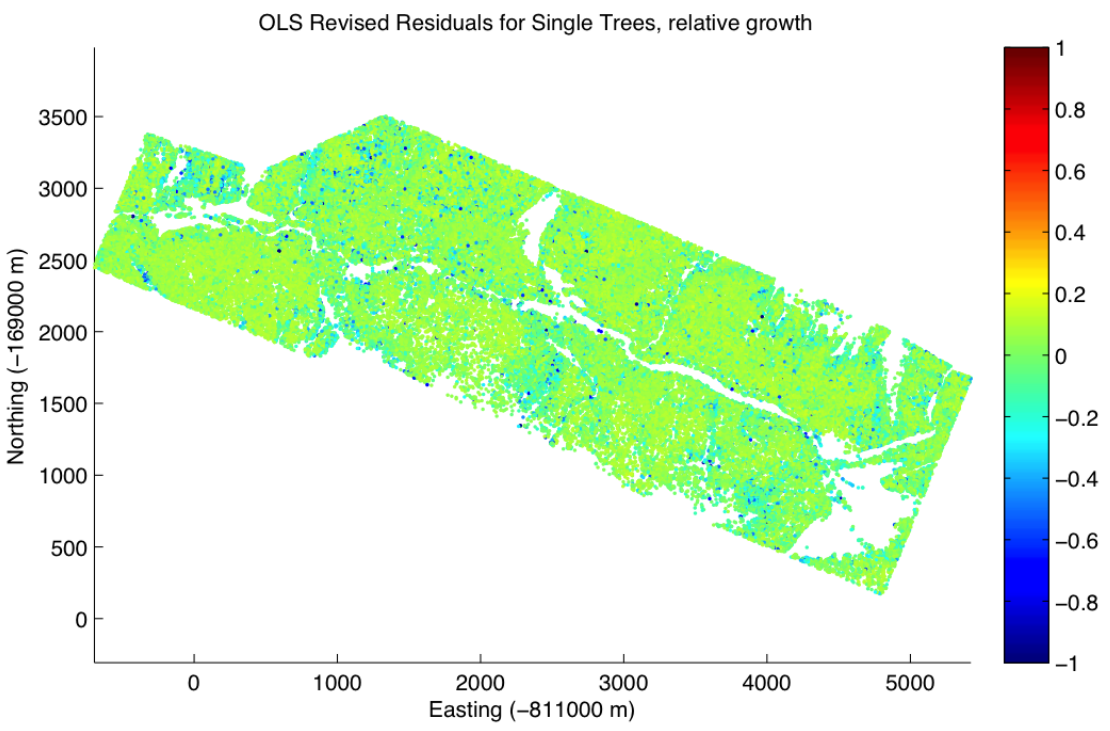

FIGURE 3.6: Residuals map of the revised OLS model on relative single tree growths.

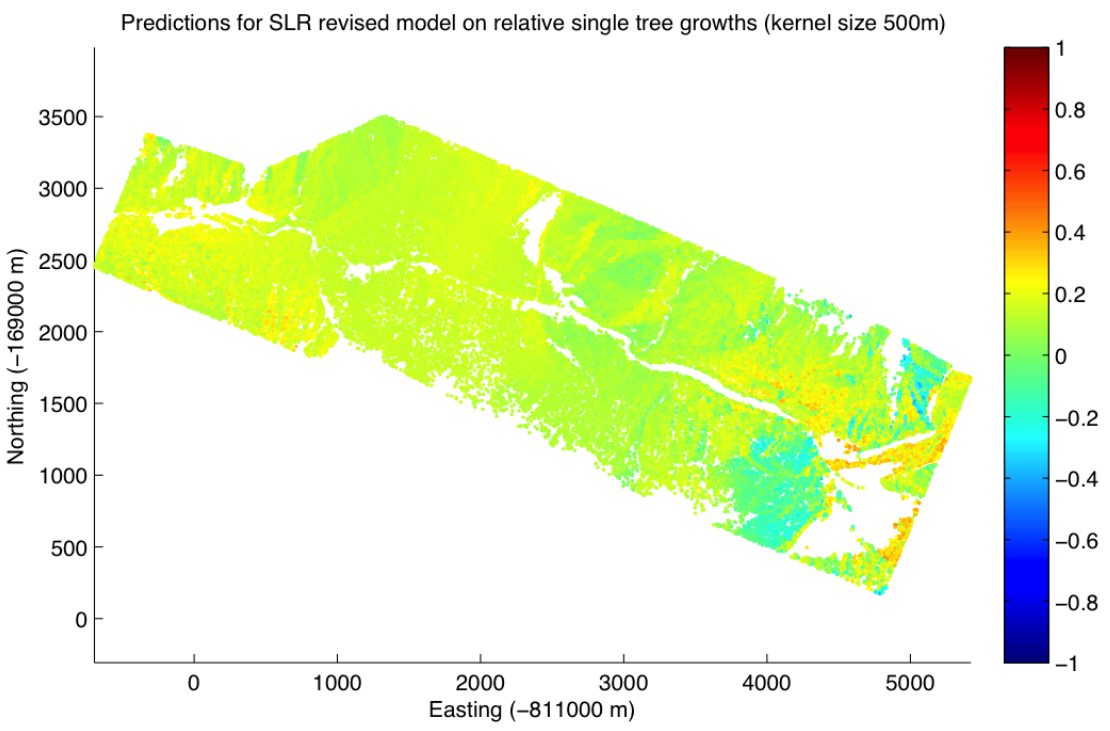

FIGURE 3.7: Prediction map of the revised SLR model on relative single tree growths.

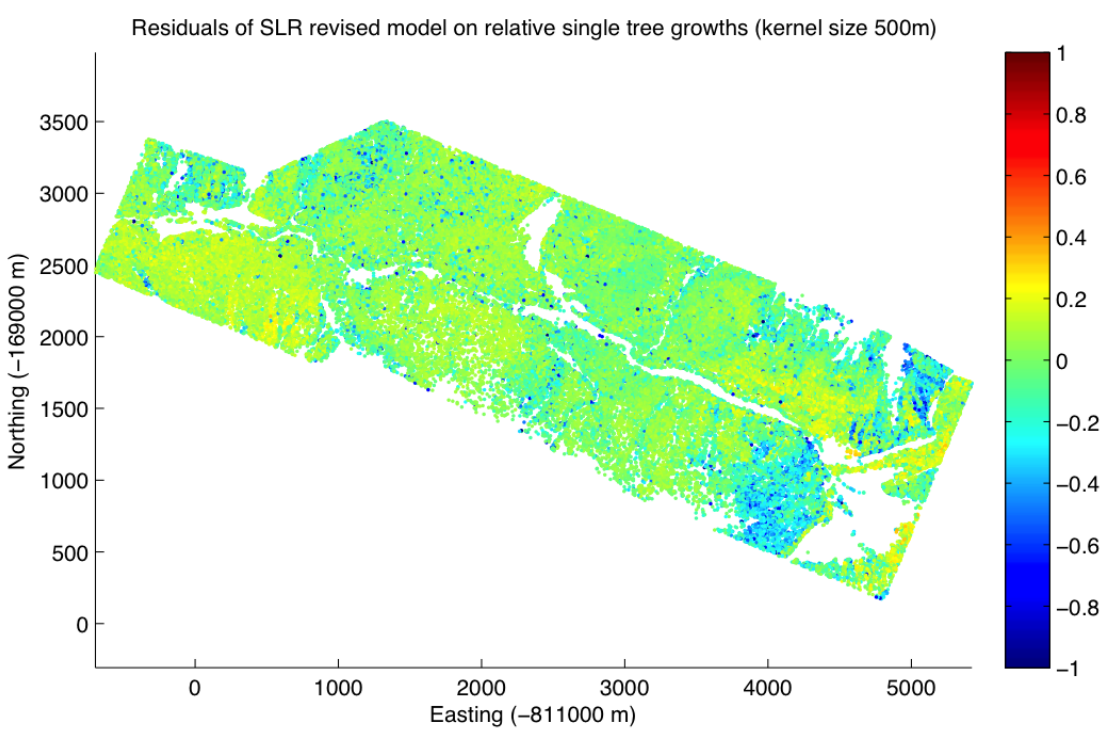

FIGURE 3.8: Residuals map of the revised SLR model on relative single tree growths.

Model	min $\mid r \mid$	max $\mid r \mid$	mean	median	std	R^2	RMSE
OLS revised	0.00	1.17	0.00	0.05	0.13	0.02	0.31
SLR revised	0.00	1.36	-0.03	0.02	0.16	-	0.16

TABLE 3.6: Parameters of the revised OLS and SLR regressions on relative single tree growths (kernel size of the SLR model was 500m). Given in order are the minimum and maximum values of the absolute residuals as well as the mean, median and standard deviation of the residuals (sans absolute value), the coefficient of determination of the revised OLS model, and lastly the RMSE of the residuals. R^2 values cannot be given for the SLR model due to its way of functioning.

seen in Figure 2.5. Other than that, the spatial patterns are comparable to those of the revised OLS model, including the single outliers scattered throughout the study area (rendered as blue spots). In the OLS case, predictions and hence also residuals did not differ much from the original relative single tree case.

Chapter 4

Discussion

This thesis related forest productivity to environmental influences. Research questions to be answered could be classified into two major categories: on the one hand, this thesis attempted to relate environmental influences to tree growths. Unlike previous studies, analyses were carried out with more than one influence factor at once, and on the basis of entire forest stands rather than a few single trees. On the other, further assessments covered the feasibility to derive the influencing parameters from ALS data alone. In addition, also forest productivity as the dependent variable was estimated from ALS data by means of a state-of-the-art single tree identification method. Statistical relations were examined using multivariate OLS regression techniques as well as methods incorporating distances between sample trees to account for spatial nonstationarity.

This Chapter broadens the context of the outcome of this study and answers the research questions summarized above. Firstly, error sources and uncertainties related to the used ALS products and methods will be addressed. This topic is followed by a discussion about the actual estimation results and model properties. Findings are then brought to context and summarized in a synthesis at the end of this Chapter.

4.1 ALS Uncertainties

The total number of potential error sources from the raw ALS data acquisition principle is comparably large as outlined in Section 1.5.2. There, error sources were classified into platform-, sensor-, target-, and post-processing-specific errors. With respect to the

effort spent to identify single trees within the LiDAR point cloud, it is likely for target- and processing-related errors to account for most of the uncertainty in tree and tree height retrieval. Gaveau and Hill (2003) investigated the accuracy of vegetation height estimation based on ALS data and have found a general negative bias of around 1.27m within trees. As it turned out they found that this effect seemed to be caused by not only an insufficient sampling density of (small footprint-) LiDAR systems, but also by lack of density within the tree crown itself, allowing the laser pulse to penetrate through the treetop to a certain extent before being reflected. Morsdorf et al. (2004) used a single tree detection method similar to the one applied in this thesis and found trees to indeed be underestimated as well. In the work of Morsdorf et al. (in revision), where the same method was used, the underestimation resulted in around 0.27m and 0.49m for two examined datasets.

Since this study examined coherences on the basis of multi-temporal data, there was one processing step possibly accounting for the most severe error source: the matching of the identified single trees. Within the time span of eight years, trees might have changed in shape as well as in size and height, and some might have needed to grow at an angle due to landslides. Furthermore, the Ofenpass valley is characterized by a comparably high tree density, which additionally complicates the matching step. Therefore, the height error due to mismatching might be as large as the tree heights themselves. With respect to the average growth of around 0.9m in the Ofenpass valley, there hence is a high risk that the height estimation errors alone are higher than the actual growth signal, and that ecological studies in slowly growing forests based on (multi-temporal) ALS acquisitions might not yet yield good results.

4.2 Regression Results

Growth predictions as provided by the initial OLS and SLR models resulted in an overall rather heterogeneous outcome, as can be seen in the predictions and residuals maps (see Chapter A). Especially the initial SLR models produced extreme predictions, which however improved within the revised SLR model. Despite heterogeneity, all regression models shared a number of generally observable properties. For instance, neither an SLR nor a OLS estimation provided a solution showing strong linear relationships on a global scale. In all OLS cases, coefficients of determination turned out to be very low (global R^2

values cannot be given for SLR models due to their way of functioning). Furthermore, a number of statistical preconditions for multiple linear regressions were not met:

- In the OLS case, residuals were not normally distributed, and heteroscedasticity was likely to be present among them
- In the SLR analyses, local VIFs indicated very strong multicollinearity among the independent variables

Residuals not being Normal distributed may have been caused by the restrictions applied to trees as described in Section 2.3. For instance, the removal of trees having an absolute "negative growth" assigned artificially shifted the expected growth range towards values greater than zero. The unrestricted dataset indeed contained a high number of trees with negative growth, probably due to alignment errors, tree blowdowns and other causes. The global average of absolute growths of trees based on this restricted dataset were around 0.9 m (median), being just slightly above the lower limit of the allowed growth range of 0.5 to 4 m. Consequently, with a global OLS estimation, residuals turned out to be negatively skewed (see Figure A.1), with the majority being slightly overestimated. However, as the main focus of this thesis was laid on forest *productivity* and not on tree mortality, the restriction to only positive height differences is thus reasonable.

As briefly addressed in the Results Chapter, the problem of multicollinearity posed severe restrictions especially on the SLR models. In their local models, VIFs were mostly above 10 and thus indicated present to strong local multicollinearity, at least in a statistical sense. While conventional statistical models suffer from multicollinearity if a number of predictor variables somehow show a certain correlation between each other, the problem turned out to be much worse in the present case. Some variables were not only statistically, but also mathematically related to each other. Therefore, an inclusion of all intended environmental variables caused an overreaction of the respective SLR models. In the OLS case, the effects were weaker probably since the multivariate least squares regression technique simply allows for certain variables not to be included at all (regression coefficients will be zero in this case).

These implications hence required removal of those variables leading to uncertain estimations. As can be seen in the initial relative SLR models in Chapter A, altitude has

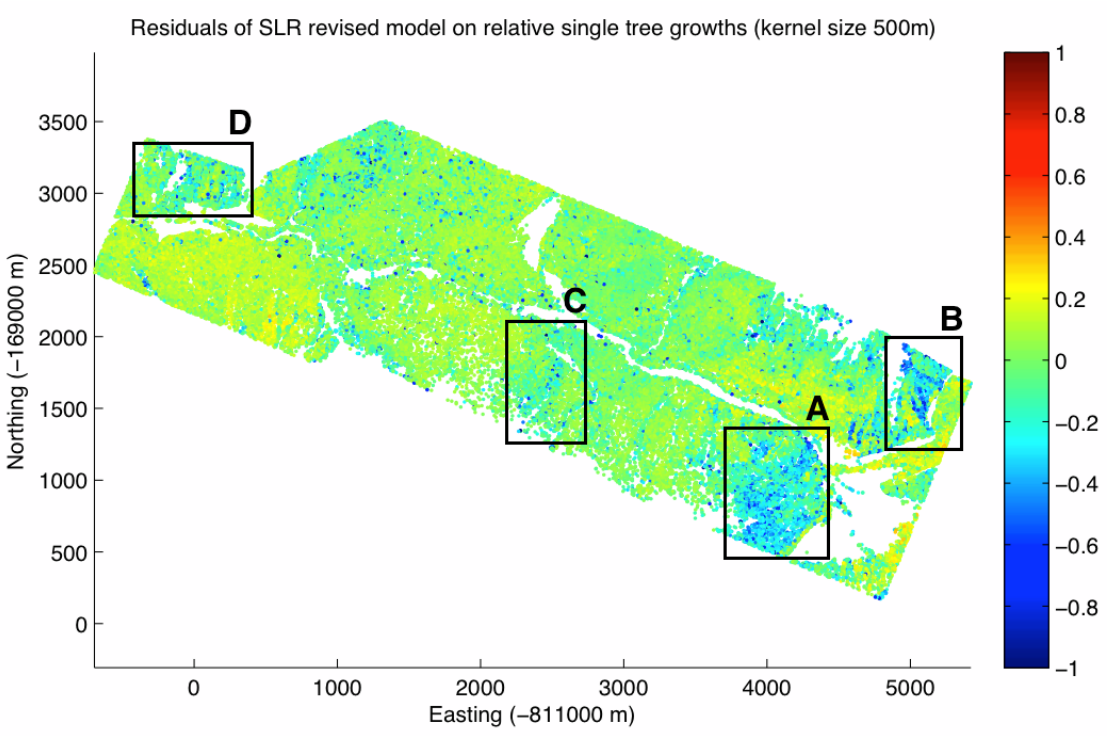

FIGURE 4.1: Areas containing particular residual patterns of the revised SLR model.

been the main driver for a bias within the residuals. Altitude was originally intended to represent an approximation of air temperature. The fact that an omission of it resulted in a strongly improved model (see Figure 3.8) is in agreement with Paulsen et al. (2000), who also found that tree growth did not change gradually towards the treeline, and hence higher altitudes. Their findings that tree growth did change in an abrupt manner could not be reproduced in this thesis though. All in all, even if the results did not give hints on whether temperature had or had no effect on the growth of trees, it revealed that an approximation of air temperature using altitude is not satisfactory, and that the raw, untransformed altitude alone certainly had no influence on growth. Trees in the study area were distributed at heights between 1765 and 2386m. This range of 621m has probably been too small to result in significantly different air temperatures.

Terrain gradient and aspect were further removed as they mainly caused (multi-) collinearity effects. This comes with no surprise due to the multiple inclusion of both of them in solar radiation and TWI. Potential solar radiation varies with the sun inclination angle on the surface, and is thus directly dependent on terrain gradient as well as aspect (Corripio, 2003). TWI witnessed similar problems due to its inclusion of terrain gradient (Sørensen et al., 2006). Fekedulegn et al. (2002) being one of the few papers explicitly

examining the effect of terrain aspect on tree growth also did so mainly in combination with drought stress and precipitation. Consequently, it might well be that their findings could have been reproduced with solar radiation instead of terrain aspect.

This leads to an issue which is directly related to proper variable selection and avoidance of multiple definitions: the inclusion of influence factors parameterized in a way that only a fraction of what they actually encompass is contained in the model. This effect is more relevant within a part of the investigated factors than within others. Potential ground solar radiation, for instance, is a more or less known relationship between solar irradiance, atmospherical conditions and the overall geometric constellation of the Earth and sun. Even if the application of a potentially more advanced model raised the accuracy of the retrieved solar radiation budget, it would not have made such a strong difference on the growth prediction outcome. However, this is also due to the small study area size of 14km^2, and is to be re-addressed when analyses are carried out at larger scales: if, for instance, the study area is massively expanded, effects such as cloud cover become more prevalent.

Other parameterizations were much more prone to the effect that only parts of the intended influences were considered. The most prominent example for this can be found within water availability: TWI only includes relative estimations of water running downhill from a contributing upslope area (Sørensen et al., 2006), with equal amounts of water available at the top of the hills for each part of the study area. Other effects, such as water loss due to evapotranspiration or soil infiltration, or additional water gain originating from mountain streams, lakes, increased local precipitation and other sources, are completely absent. Some of these effects are—once more—already contained in other variables, such as evapotranspiration being directly related to solar radiation. Others can be included by using compound indices. Iverson et al. (1997) for instance developed the "Integrated Moisture Index" (IMI), which includes soil water holding capacity, hillshading and curvature in addition to flow accumulation estimations, and combines them using a weighting scheme. Even if it was tested only in relatively arid regions, the IMI or a comparable compound index might lead to improved growth predictions in the alpine Ofenpass valley as well.

It becomes evident that a proper definition and choice of explanatory variables is one of the most crucial part of an analysis as carried out here. A deficient implementation

of environmental influences otherwise leads to high estimation errors, visible in the high RMSE values of the initial models, and also to an increased uncertainty in the accurateness of the statistical model itself. Also, with respect to the fact that both the revised OLS and SLR models provided similar results in the end, it may be said that the parameterization of environmental influences requires even more focus than the actual regression technique itself. This statement, however, might only be valid to a certain extent, and probably depends on the distribution of the data: in the present study, spatial autocorrelation which SLR should account for was indeed to be expected, but tree growths did not form spatially distinct regions that would have resulted in definable patterns. Instead, tree growth differences occurred at a much smaller scale: for instance, the underestimated trees scattered throughout the study area (blue spots) did not form larger patches. Therefore, even the SLR model regarding such spatial effects could not provide a solution to estimate these trees, simply because the inclusion radii down to 250m were still too high. Any attempts to construct models small enough in space would possibly have led to a statistical insignificance as they would eventually only have included one or a handful of samples. A possibly much better solution would have been to seek for further potential environmental properties ought to have an effect on tree growth.

One such factor suspected to have an influence is competition between trees: those trees not surrounded by others within a certain distance probably had a better starting position for developing and growing tall. A number of different competition indices have been established so far. Rivas et al. (2005) compared a number of different competition indices (distance-independent as well as dependent), with various competitor selection methods for the distance-sensitive indices. Interestingly, they found that for their examined species (*Pinus cooperi* Blanco), the best distance-independent index provided a similarly high accurateness as the corresponding best distance-dependent index. Some of the indices rely on further tree structural properties like crown diameter or diameter at breast height (DBH). A number of studies have already shown that all of these parameters are indeed derivable from ALS-sampled data (e.g. Huang et al. (2011), Popescu et al. (2003), Yao et al. (2012)). Therefore, an inclusion of a means for competition might substantially increase the regression model accuracy, but comes at a cost of further error sources and uncertainty; additional work might be required to identify the best competition index for the investigated study area.

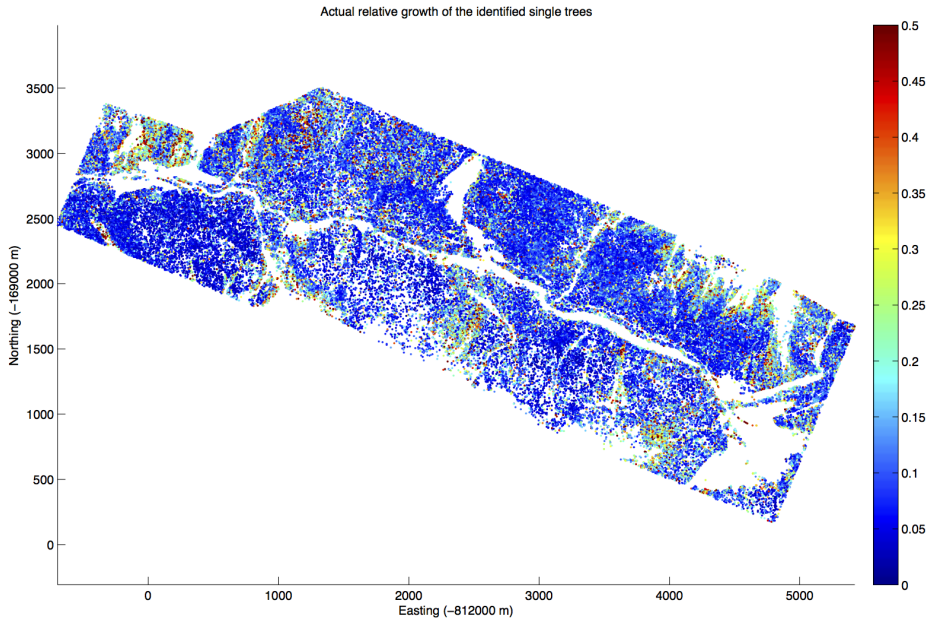

FIGURE 4.2: Growth of the identified single trees relative to their initial height as retrieved from the ALS data.

The results as retrieved within the context of this study did not provide a statistically strong relationship between influences of the environment and tree growths. However, especially the revised SLR model nevertheless showed a few findings: (i.) the effect of altitude seems to be vanishingly low, and (ii.) solar radiation might indeed have an influence, but any lack of high sunlight exposure does not lead to growth inhibition among trees. This can be seen in the easternmost parts of the study area, where trees are situated on particularly shadowed slopes, but still have not grown less than their neighbors that are more exposed to sunlight (areas A and B in Figure 4.1). Other areas, such as the center of the southern slope in the valley (area C; Figure 4.1) or the north-westernmost part of the study area (area D in Figure 4.1), have been underestimated by both the OLS and SLR models. The actual relative tree growths in Figure 4.2 show that these areas indeed encompass mainly trees with higher relative growths than their surroundings. This effect, visible in both areas C and D, is either due to small initial tree sizes in 2002, or due to indeed high growth during the eight years from 2002 to 2010 (see the turquoise to red trees in Figure 4.3). Since these regional patterns cannot be seen in the explanatory variables, both the OLS and SLR models consequently failed to predict accurate relative growths for the trees within them. The actual causes for these patterns

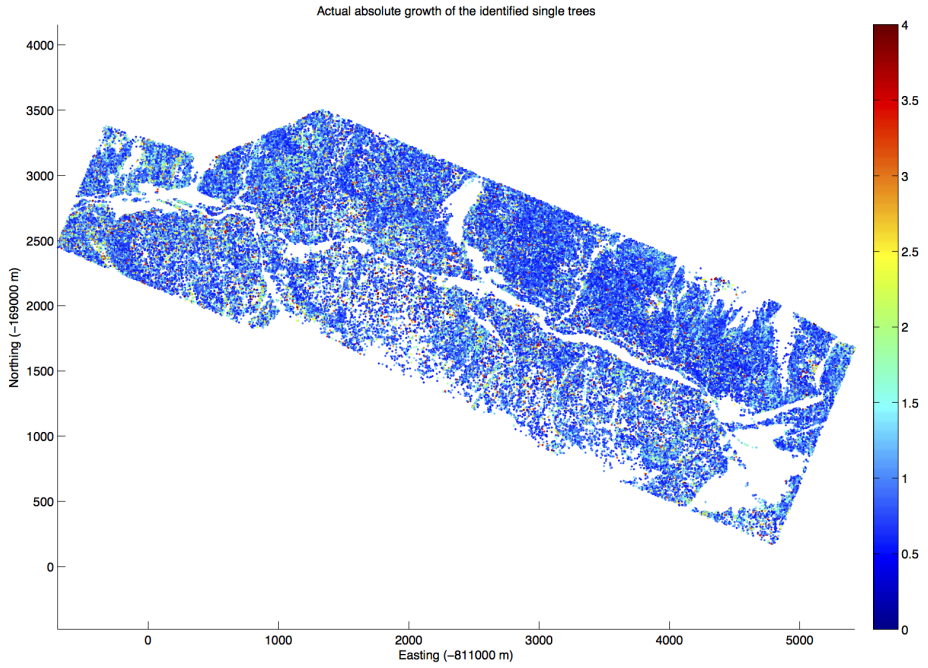

FIGURE 4.3: Absolute growth values of the identified single trees as retrieved from the ALS data.

remain unknown, although a possible explanation might be that these were simply other species, and hence these effects might could have been explained by inclusion of tree species classification as an additional variable.

4.3 Concluding Insights

Eventually, there remain three major issues which have led to the vagueness of the results as they are:

- Some of the included environmental influences were parameterized in a way that only a small part of their impacts on tree growth could be accounted for (e.g. water availability parameterized using TWI)
- Other potential influences were completely absent (e.g. competition, meteorological factors)

- Trees all in all showed a relatively small growth signal, and the ALS data post-processing until the retrieval of single trees resulted in an overly increased noise floor

Consequently, the growth prediction model as present in this case may not be able to work properly at any comparable test site. The findings nevertheless exemplify a number of peculiarities and guidelines for further improved models:

- The RMSE scores of all OLS models suggest that the identification of potential single trees from ALS-derived height measurements is beneficial.
- Multicollinearity can pose a severe problem when working with ecological data insofar as the explanatory variables have a physical impact on each other. Therefore, in order to avoid multiple variable inclusions, appropriate dimension reduction techniques or either a reduction of the number of variables become unavoidable.
- In contrast to this statement, however, solar radiation and TWI alone do not seem to explain enough variance within growth of trees. Other and more causal effects might be required in a model to provide better explanations, and hence predictions, of growth and growth differences.
- Directly related to the lack of explained variance is the finding that ALS-derived parameters alone seem to be insufficient for a proper identification of environmental influences on tree growth. Especially the usage of weather data like temperature and precipitation is expected to raise accuracy remarkably. The present thesis' investigated study area was of too small size to feature distinct meteorological, let alone climatic differences in space. An enlargement of the study area would hence be beneficial for the inclusion of weather data, as they are more likely to produce regional differences. This would also correspond to the aim to predict forest productivity in the context of larger-scale up to global processes.
- Models accounting for spatial nonstationarity and/or spatial autocorrelation are only of relevance as soon as regional effects are clearly visible at least on a certain scale. As soon as differences become too local, improvements in residual errors should not be expected anymore.

Chapter 5

Conclusion

This thesis aimed towards explaining tree growth on the basis of ecological influences. Unlike previous studies, analyses were carried out not only on a small number of trees but for entire forest stands, and not only with one or two predictor variables, but with six at once. Tree height was estimated on the basis of two ALS acquisitions taking place in 2002 and 2010, with a single tree identification procedure as described in Morsdorf et al. (in revision). In addition, also CHM differences were analyzed to examine the benefit of the single tree identification process.

The investigated ecological influence factors comprised solar radiation, altitude, initial tree height in 2002, terrain gradient, terrain aspect, and TWI. All of these variables were parameterized based solely on the same ALS datasets. Relations were examined by means of multivariate OLS regressions on the one hand, and a counterpart additionally addressing spatial relatedness, the SLR.

In a first run, tree growth had been estimated with all of the aforementioned influence factors as explanatory variables. Due to statistical preconditions not met, particularly owing to explanatory variables being correlated to each other, analyses had to be re-run with only solar radiation and TWI. This improved predictions especially in the SLR case, while the OLS results remained relatively similar.

The regression results showed that neither the multivariate OLS nor the SLR models were able to provide an overall trustworthy prediction (R^2 values for the OLS model ranged between 0.01 and 0.11; RMSE scores of the residuals lied between 1.72 and 2m for the absolute tree growth, and between 0.16 and 0.69 for the tree growth relative to the initial

tree height). Residual patterns nevertheless gave certain clues about the predictors' influence: solar radiation does not seem to be the limiting factor for tree growth, and TWI does at least explain parts of the variation. Other findings were more method- and model-specific: RMSE scores improved when analyzing single trees identified within the LiDAR point cloud rather than CHM height differences. Furthermore, a mere parameterization of predictors on the basis of terrain data alone has been found to be insufficient for ecological applications. Therefore, other data sources such as weather data might lead to improved results and hence are unavoidable. This also accounts for predictors not included in this study, such as tree competition, insect outbreaks, soil properties and other potential influences on tree growth.

Eventually, despite weak correlations in the statistical models, it becomes evident that multivariate analyses are essential within ecological studies. Especially when assessing the estimation of forest productivity, the dependence of more than one influence factor at once remains a key topic to be investigated. Furthermore, by regarding interactions and dynamics on a regional scale rather than locally for single trees, analyses correspond more to the aim of quantifying forest productivity in the context of the global carbon cycle. An extension of study areas to even larger scales may hence be appreciable, and spatial differences might then be better coverable by means of SLR and/or other spatially sensitive methods. To do so, however, requires the availability of more input data as well as a stronger tree growth signal, which can partially be achieved by improving the ALS single tree identification process on the one hand, and by using data with higher sampling density and longer time gaps between acquisition dates (and hence higher tree growths) on the other.

Chapter 6

Outlook

Multivariate, larger-scale ecological studies will continue gaining importance and are particularly expected to become a central part of analyses on global warming and global carbon fluxes. The interactions between forests and their environment are, on one side not yet fully understood, and on the other hardly quantifiable to date. This thesis sought to overcome this latter issue and attempted assessing forest productivity with environmental conditions.

The outcome of this study revealed a number of key aspects to be considered in further analyses, leaving room for further studies with improved conditions and methods. On the one hand, analyses in this study have shown that a restriction to topographic variables alone is insufficient for ecological parameter modeling. Further theses hence may also include other measurement series as predictors, such as weather data. On the other, there is room for improvement in terms of the single tree identification method from ALS data: in this study, the tree height estimation error turned out to be too large mainly due to the tree identification process and overshadowed any actual growth signal. Hence, retrying this study in a forest with taller growth rates, or else over a larger time period than eight years, might reduce this problem by an increased growth signal. Furthermore, however, improvements to the single tree identification from ALS data are unavoidable especially in the case of slowly growing forests, and are indeed on the way (Morsdorf et al., in revision).

Finally, repeating multivariate forest productivity estimations in a significantly larger test site might yield interesting results on larger-scale interactions between forests and

their environment as well as on differences between contiguous forest stands. In contrast to this study with a single enclosed valley, spatially sensitive statistical models such as the SLR are expected to be particularly powerful on multiple forests on larger areas.

Appendix A

Additional Figures

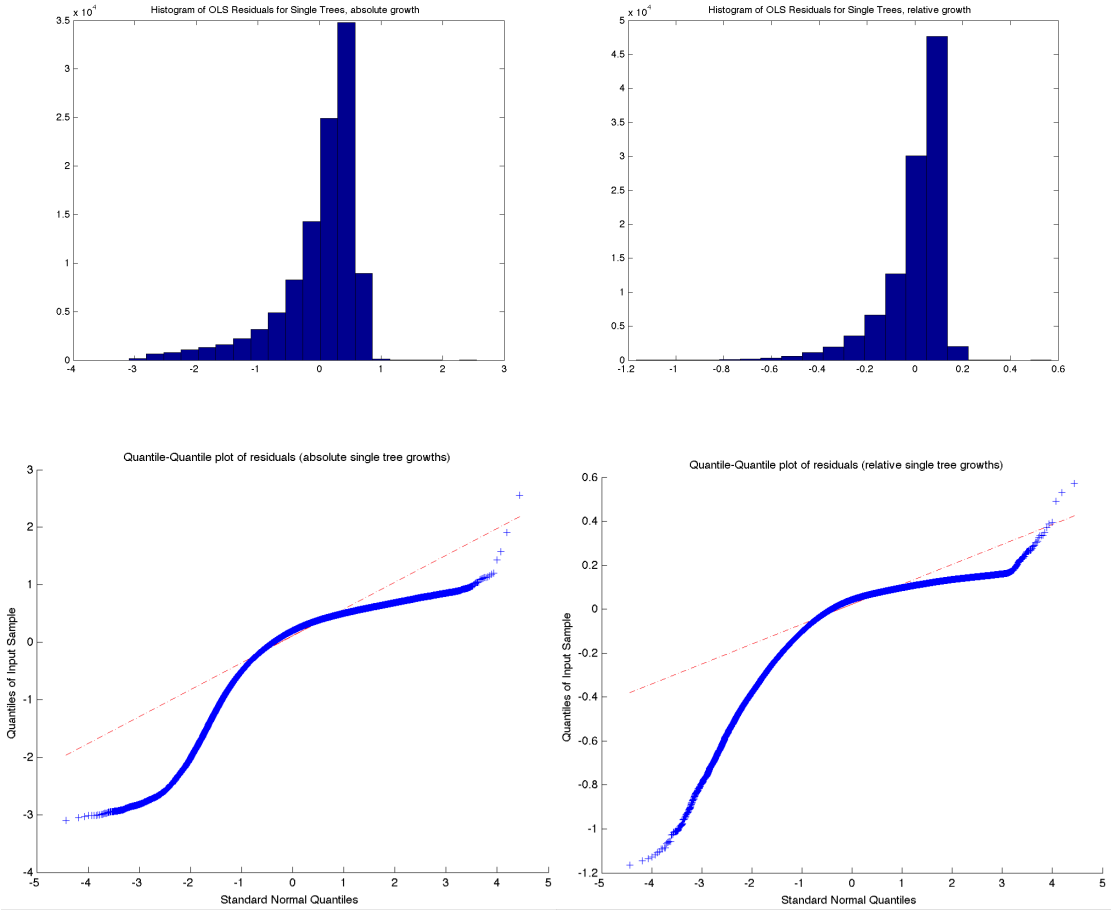

FIGURE A.1: Histograms (top) and Quantile-Quantile- (bottom) plots for the residuals emerging from the OLS regressions based on the identified single trees (absolute: left, relative: right).

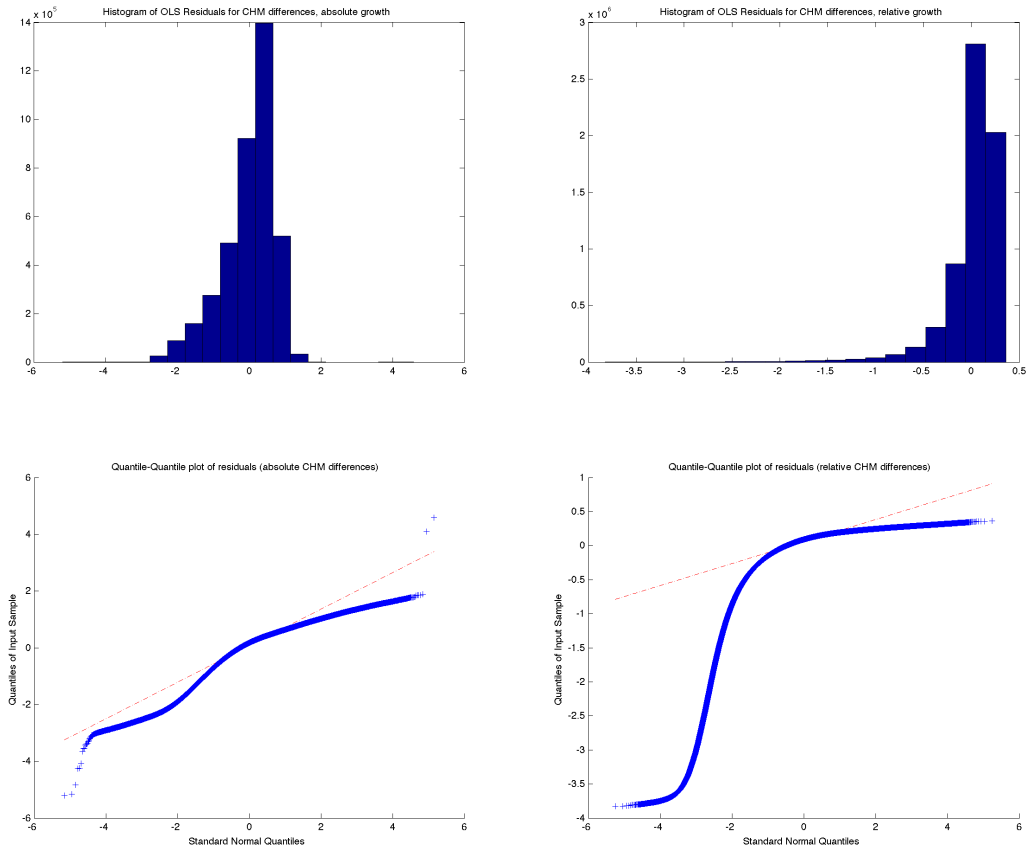

FIGURE A.2: Histograms (top) and Quantile-Quantile- (bottom) plots for the residuals emerging from the OLS regressions based on CHM differences (absolute: left, relative: right).

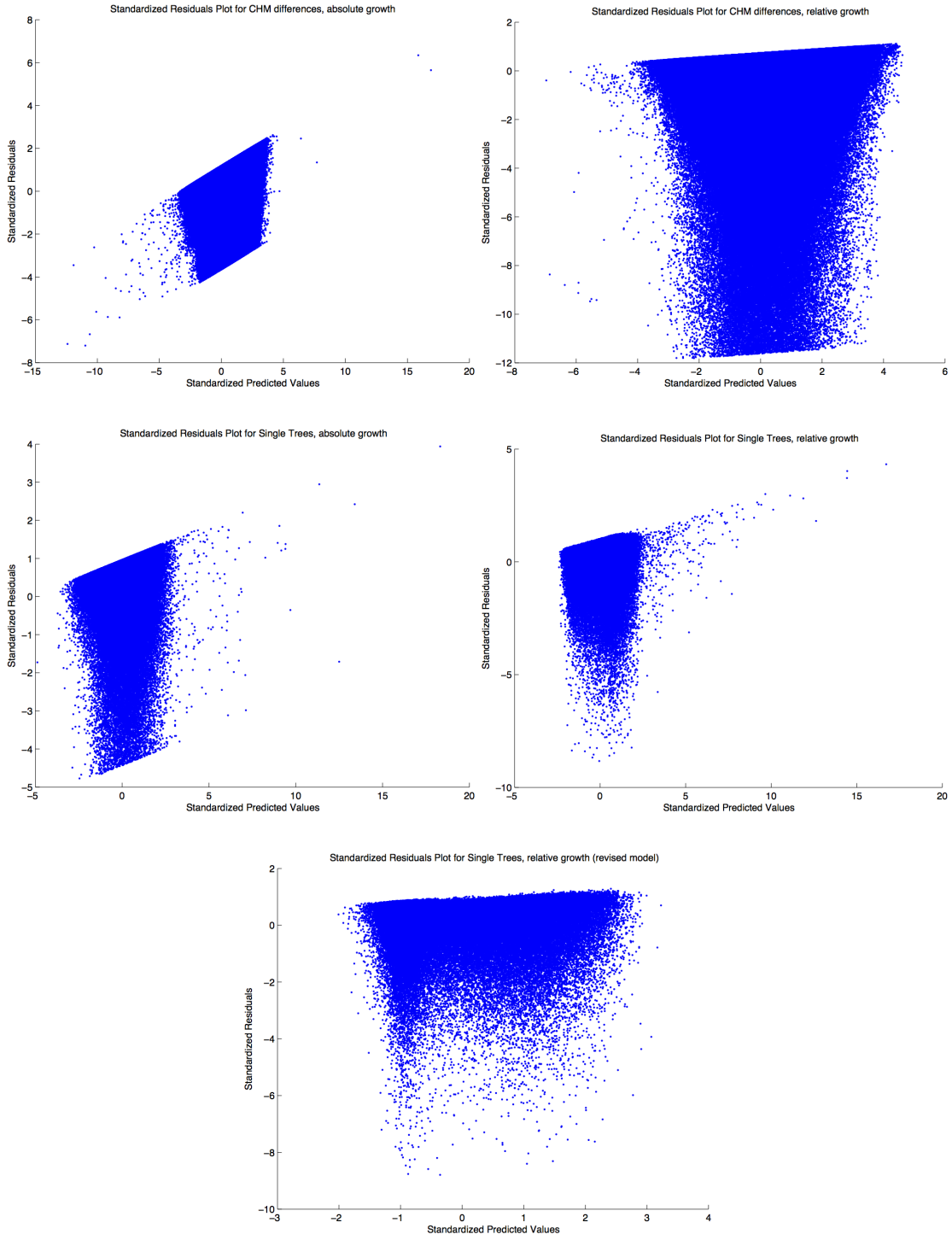

FIGURE A.3: Plots showing standardized predictions versus standardized residuals as an indication for heteroscedasticity. Plots are given for the OLS CHM differences (absolute and relative; top row), for the OLS single tree growths (ditto; middle row) as well as for the revised OLS model on single tree growths (bottom). As patterns are visible in all five plots, there are high chances that all models suffer from heteroscedasticity.

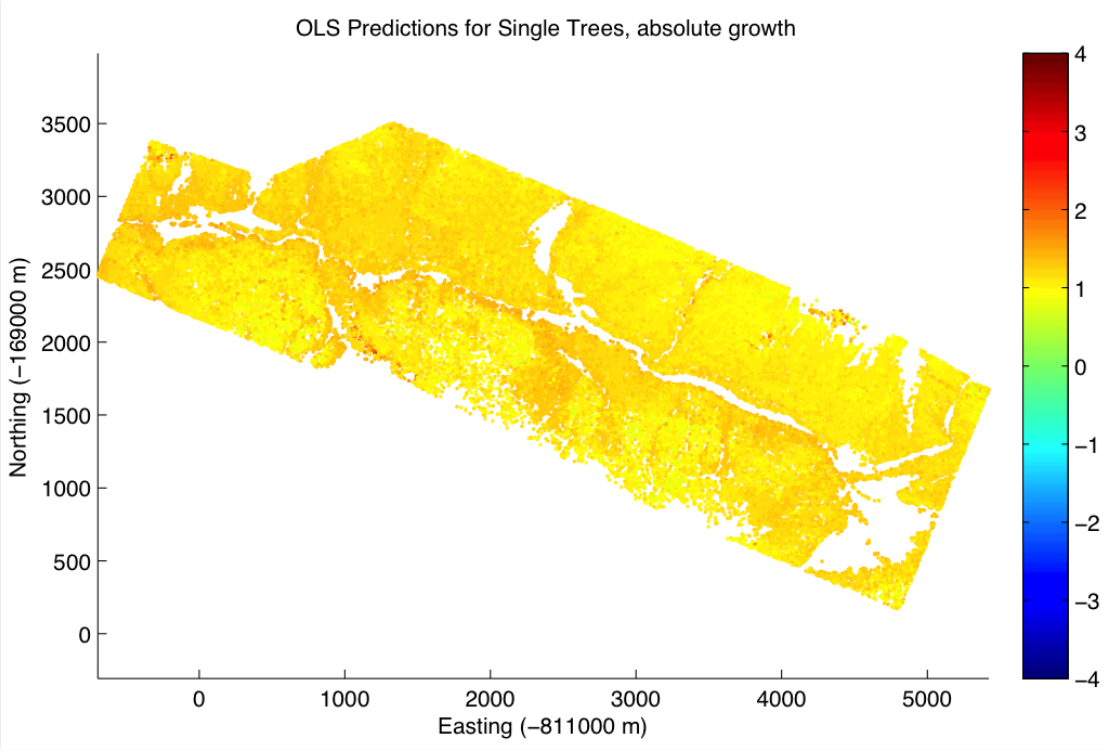

FIGURE A.4: Spatial distribution of OLS predictions on the basis of absolute single tree growths.

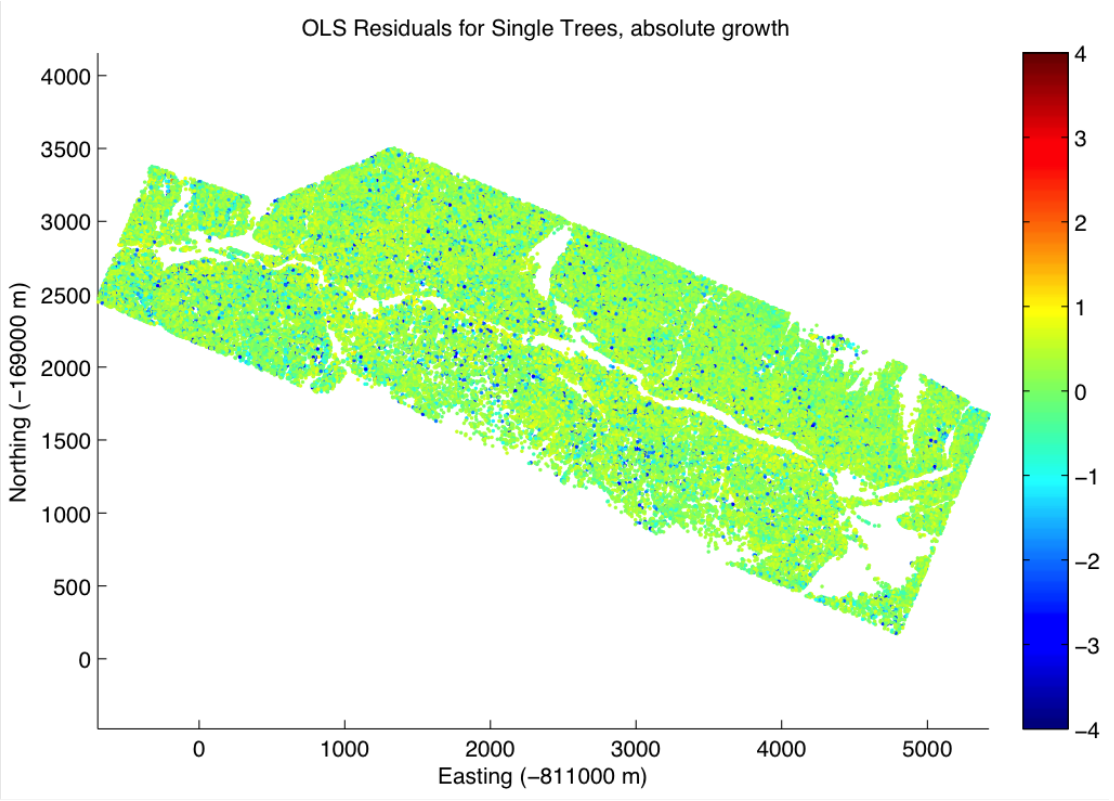

FIGURE A.5: Spatial distribution of OLS residuals on the basis of absolute single tree growths.

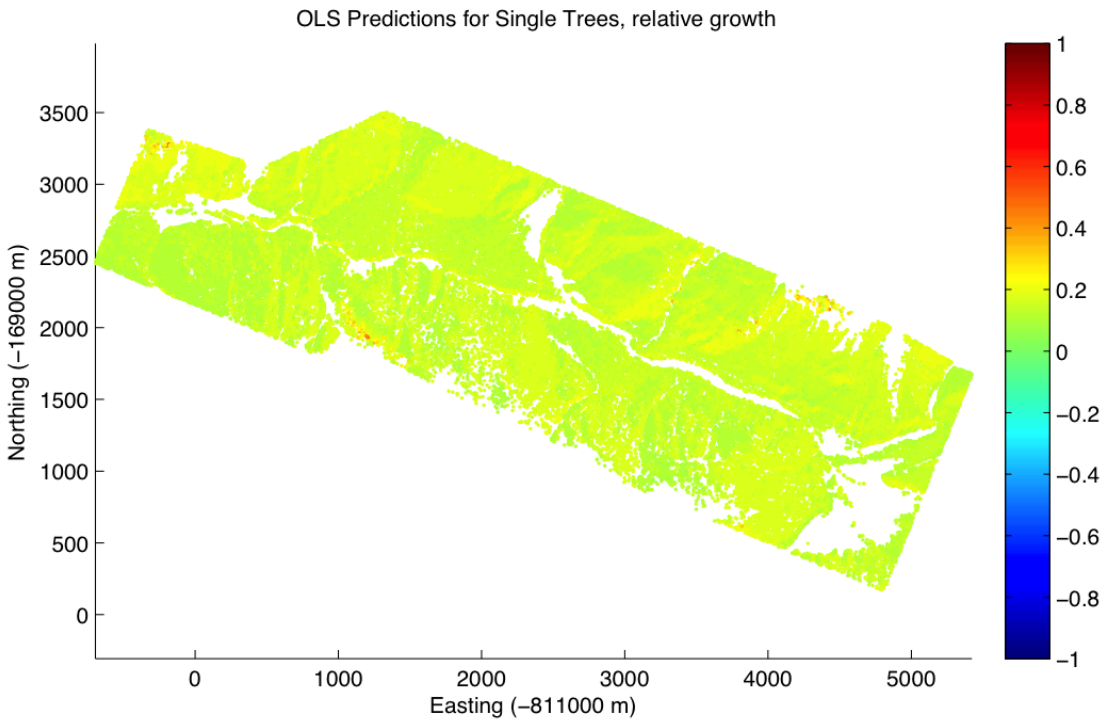

FIGURE A.6: Spatial distribution of OLS predictions on the basis of relative single tree growths.

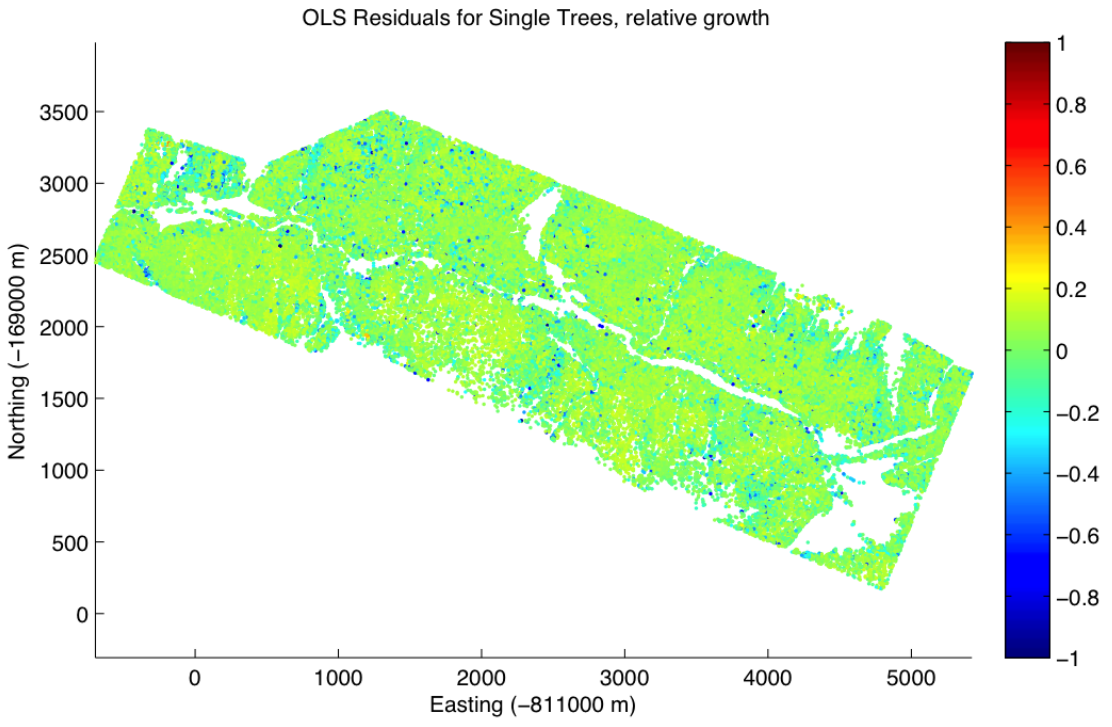

FIGURE A.7: Spatial distribution of OLS residuals on the basis of relative single tree growths.

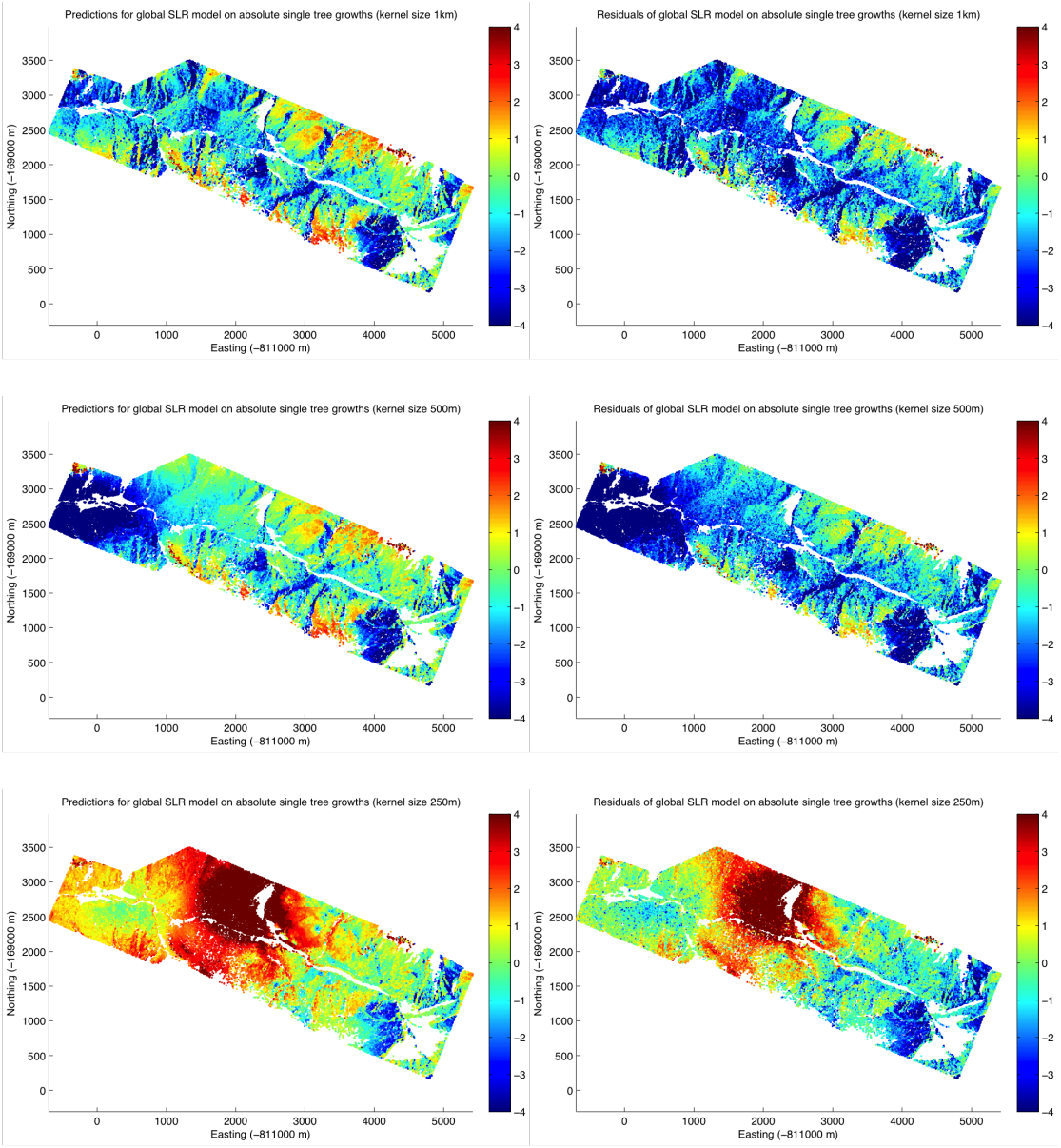

FIGURE A.8: Predictions (left) and residuals (right) of the SLR models based on absolute tree growths. Kernel sizes were 1km (top), 500m (middle) and 250m (bottom).

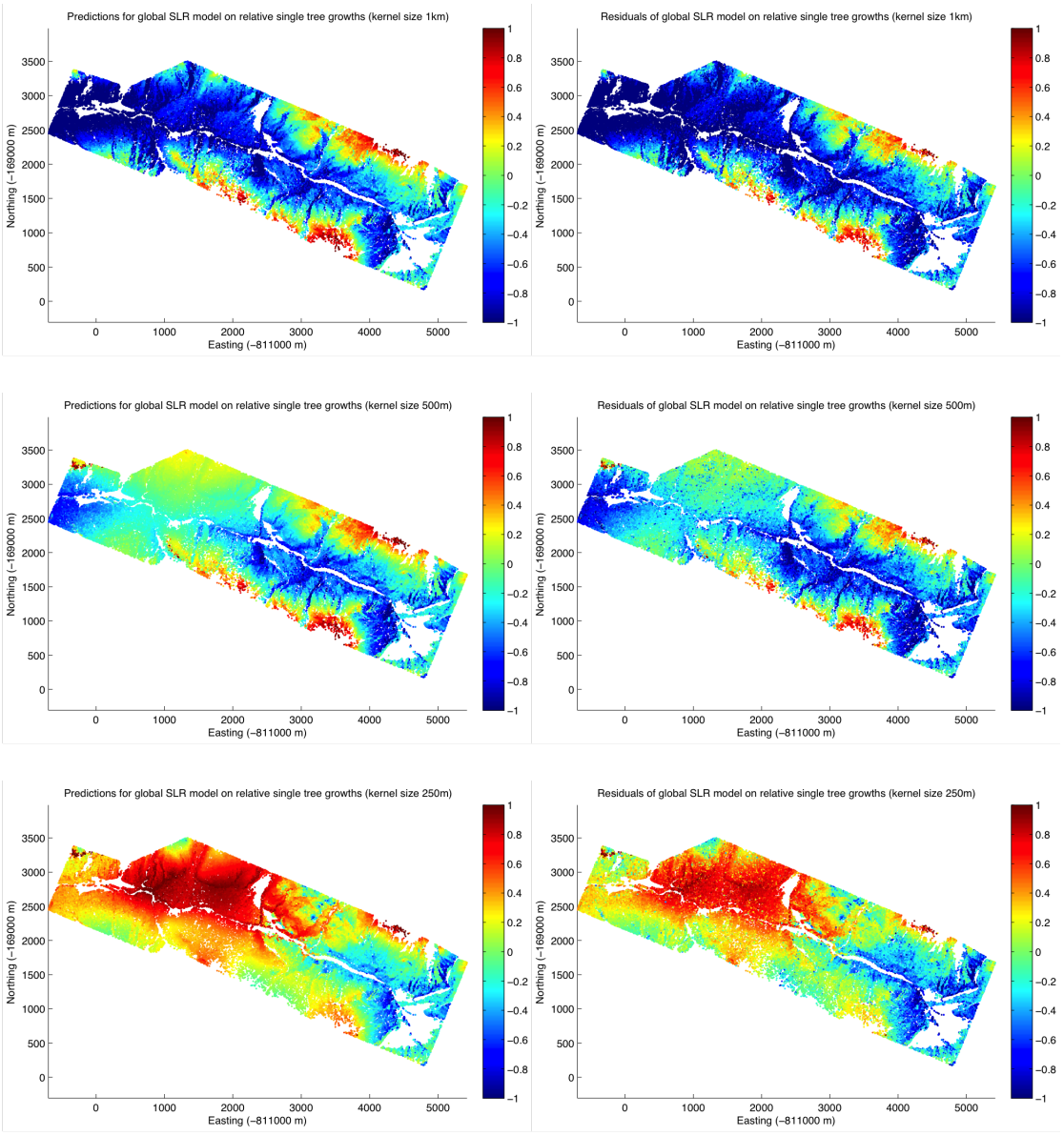

FIGURE A.9: Predictions (left) and residuals (right) of the SLR models based on relative tree growths. Kernel sizes were 1km (top), 500m (middle) and 250m (bottom).

Appendix B

MATLAB Scripts

B.1 Main Workflow

The code below denotes the main workflow as done in MATLAB based on the initially available data. Used custom functions are appended in the next Section.

```
%%%%%%%%%%%%%%%%%%%%%%%%%%%%%%%%%%%%%%%%%%%%%%%%%%%%%%%%%%%%%%%%%%%%%%%%%%%%%%%%
%%%%                                                                          %%%%
%%%%  $$$$$$$$$$$$....=7$$$$$$$$$$$$.............................  %%%%
%%%%  $$$777777$$$$=.:$$$$7777777$$$,.............................  %%%%
%%%%  $$$........$$$.$$$.........$$$,.............................  %%%%
%%%%  $$$.......=$$$..$$$$,......$$$,.............................  %%%%
%%%%  $$$.=7$$$$$$$....$$$$$$....$$$,.............................  %%%%
%%%%  $$$.$$$$$$$~.......+$$$$$..$$$,.............................  %%%%
%%%%  $$$...7$$$$$......... $$$$.$$$,.............................  %%%%
%%%%  $$$.....,$$$$$$........$$$.$$$,.............................  %%%%
%%%%  $$$........?$$$$$I....7$$$.+$$$,.............................  %%%%
%%%%  $$$.......... I$$$$$$$$$$...I$$$$$$$$$$$$...................  %%%%
%%%%  $$..............7$$$$$,......:7$$$$$$$7.....................  %%%%
%%%%  ..............................................................  %%%%
%%%%  measurements | products | policy                              %%%%
%%%%                                                                %%%%
%%%%%%%%%%%%%%%%%%%%%%%%%%%%%%%%%%%%%%%%%%%%%%%%%%%%%%%%%%%%%%%%%%%%%%%%%%%%%%%%
```

```
%%%%%%%%%%%%%%%%%%%%%%%%%%%%%%%%%%%%%%%%%%%%%%%%%%%%%%%%%%%%%%%%%%%%%%%%%%%%
%%%%
%%%% Main Workflow
%%%%
%%%% 2013–2014 Benjamin Kellenberger
%%%% RSL @ UZH
%%%%
%%%%
%%%% For custom functions, see further sections of the thesis' appendix.
%%%%
%%%% For Bibliography Sources and other References, refer to the
%%%% References Section in this thesis.
%%%%
%%%%%%%%%%%%%%%%%%%%%%%%%%%%%%%%%%%%%%%%%%%%%%%%%%%%%%%%%%%%%%%%%%%%%%%%%%%%

% ---------------------------------------------------------------------------
% 1. Variable Preparation
% ---------------------------------------------------------------------------

%% Constants
ks = 10;    % Kernel Size for smoothing filter

% Allowed height of "trees"
minAbsH = 3;
maxAbsH = 40;

% Min and max CHM differences
minAbsDCHM = 0.5;
maxAbsDCHM = 4;
minRelDCHM = 0;
maxRelDCHM = 4;

% ---------------------------------------------------------------------------
```

```
51 % ------------------------------------------------------------------------
52
53 %% Delta CHM
54 load ras.mat;
55
56 % Interpolate to 0.5m cell size
57 [dtm02, x, y, X, Y] = resizeMatrix(ras.dtm02, ras.x, ras.y, ...
58     ras.X, ras.Y, 2.*length(ras.x), 2.*length(ras.y));
59 dtm10 = resizeMatrix(ras.dtm10, ras.x, ras.y, ras.X, ras.Y, ...
60     2.*length(ras.x), 2.*length(ras.y));
61 dsm02 = resizeMatrix(ras.dsm02, ras.x, ras.y, ras.X, ras.Y, ...
62     2.*length(ras.x), 2.*length(ras.y));
63 dsm10 = resizeMatrix(ras.dsm10, ras.x, ras.y, ras.X, ras.Y, ...
64     2.*length(ras.x), 2.*length(ras.y));
65
66 % Calculate CHM and Delta CHM
67 chm02 = dsm02 - dtm02;
68 chm10 = dsm10 - dtm10;
69
70 dchm = chm10 - chm02;
71
72 % Save
73 dtm = struct('x', x, 'y', y, 'X', X, 'Y', Y, 'z', dtm10);
74 save('dtm.mat', 'dtm');
75
76 chm = struct('chm02', chm02, 'chm10', chm10);
77 save('chm.mat', 'chm');
78
79 save('dchm.mat', 'dchm');
80
81 % ------------------------------------------------------------------------
82
83 %% Mask
```

```
load mask.mat;

% Contents of File "mask.mat":
% – "mask": the original mask created using inpolygon and the trees as
%   well as poly2mask
% – "newmask": a manually modified version of "mask", removing
%   additionally unwanted regions

% ————————————————————————————————————————————————————————————

%% Environmental Influences

% Gradient & Aspect
[lat, lon] = ch1903ToWgs84(X, Y);
[asp, grad] = gradientm(lat, lon, dtm.z);
asp = asp .* pi ./ 180; % convert to radians
grad = grad .* pi ./ 180;
grad_smoothed = smoothenMatrix(grad, [ks ks], 'average');
asp_smoothed = smoothenMatrix(asp, [ks ks], 'average');


% Solar Radiation
sr = solrad(dtm.z, lat, 0.5, 0.2);  % Assuming a global reflectance
                                    % of 0.2. 0.5 = cell size [m]
sr_s = smoothenMatrix(sr, [ks ks], 'average');


% TWI
dtmGRID = GRIDobj(dtm.x, dtm.y, dtm.z); % Making use of the TopoToolbox
                                        % by Schwanghart & Kuhn, 2010
flowDir = FLOWobj(dtmGRID); % D8 Algorithm
fa = flowacc(flowDir); % Calculation of Flow Accumulation
fa(newmask == 0) = NaN;
```

```
fa_smoothed = smoothenMatrix(flipud(fa.Z), [ks ks], 'average');
twi = real(log(fa_smoothed ./ tan(grad_smoothed)));

clear fa fa_smoothed dtmGRID flowDir;


% Altitude
z_s = smoothenMatrix(dtm.z, [ks ks], 'average');


% Tree height
h_s = smoothenMatrix(chm.chm02, [ks ks], 'average');

% ------------------------------------------------------------------------

%% Apply Restrictions & Retrieve logicals

% Absolute
dchm_smooth = smoothenMatrix(dchm, [ks ks], 'average');
dchm_smooth(newmask == 0) = NaN;
dchm_smooth(dchm_smooth < minAbsDCHM) = NaN;
dchm_smooth(dchm_smooth > maxAbsDCHM) = NaN;
dchm_smooth(chm.chm02 > maxAbsH) = NaN;
dchm_smooth(chm.chm10 > maxAbsH) = NaN;
dchm_smooth(chm.chm02 < minAbsH) = NaN;
dchm_smooth(chm.chm10 < minAbsH) = NaN;

ii = ~isnan(dchm_smooth);

% Relative
dchm_rel = dchm ./ chm.chm02;
dchm_rel = smoothenMatrix(dchm_rel,[ks ks], 'average');
dchm_rel(newmask == 0) = NaN;
```

```
150 dchm_rel(dchm_rel < minRelDCHM) = NaN;
151 dchm_rel(dchm_rel > maxRelDCHM) = NaN;
152 dchm_rel(chm.chm02 > maxAbsH) = NaN;
153 dchm_rel(chm.chm10 > maxAbsH) = NaN;
154 dchm_rel(chm.chm02 < minAbsH) = NaN;
155 dchm_rel(chm.chm10 < minAbsH) = NaN;
156
157 temp = dchm_smooth >= 0.5 & dchm_smooth <= 4;
158 dchm_rel(~temp) = NaN;
159 clear temp;
160 % The above step is important because it only makes sense to restrict
161 % the *absolute* height differences to [0.5,4] m.
162
163 jj = ~isnan(dchm_rel);
164
165
166 % Logicals further restricted to independents
167 kk = ii & ~isnan(grad_smoothed) & ~isnan(h_s) & ~isnan(sr_s) & ...
168     ~isnan(z_s) & ~isnan(twi) & ~isnan(asp); % Absolute
169 ll = jj & ~isnan(grad_smoothed) & ~isnan(h_s) & ~isnan(sr_s) & ...
170     ~isnan(z_s) & ~isnan(twi) & ~isnan(asp); % Relative
171
172
173 save('regressionInput.mat','dchm_smooth','dchm_rel','asp', ...
174     'grad_smoothed','twi','sr_s','z_s','h_s','dtm');
175 save('logicals_dchm.mat','ii','jj','kk','ll');
176
177
178 % ------------------------------------------------------------------------
179 % ------------------------------------------------------------------------
180
181 %% Single Trees
182 load alltrees.mat;
```

```
% File contains structure "alltrees", which already consists of matched
% trees and their heights in 2002 ("h") and 2010 ("alsh")

alltrees.deltaH = alltrees.alsh - alltrees.h; % Abs. height increase
alltrees.dHrel = alltrees.deltaH ./ alltrees.h; % Rel. height increase

% Variable assignments
alltrees.grad_smoothed = getNearest(x, y, alltrees, grad_smoothed);
alltrees.asp_smoothed = getNearest(x, y, alltrees, asp);
alltrees.twi = getNearest(x, y, alltrees, twi);
alltrees.sr_s = getNearest(x, y, alltrees, sr_s);

alltrees.newmask = getNearest(x, y, alltrees, newmask);
% The above step is necessary since the manual creation of "newmask" led
% to a minor tree number decrease


% Logicals
ii_s = alltrees.newmask == 1 & ...
    alltrees.deltaH >= minAbsDCHM & alltrees.deltaH <= maxAbsDCHM & ...
    alltrees.h >= minAbsH & alltrees.h <= maxAbsH & ...
    alltrees.alsh >= minAbsH & alltrees.alsh <= maxAbsH;    % Absolute

jj_s = alltrees.newmask == 1 & ...
    alltrees.dHrel >= minRelDCHM & alltrees.dHrel <= maxRelDCHM & ...
    alltrees.h >= minAbsH & alltrees.h <= maxAbsH & ...
    alltrees.alsh >= minAbsH & alltrees.alsh <= maxAbsH;   % Relative


temp = alltrees.deltaH >= 0.5 & alltrees.deltaH <= 4; %see above

jj_s(~temp) = 0;
clear temp;
```

```
216
217
218 % Further restrictions (as above)
219 kk_s = ii_s & ~isnan(alltrees.grad_smoothed) & ~isnan(alltrees.h) & ...
220     ~isnan(alltrees.sr_s) & ~isnan(alltrees.twi) & ~isnan(alltrees.asp);
221
222 ll_s = jj_s & ~isnan(alltrees.grad_smoothed) & ~isnan(alltrees.h) & ...
223     ~isnan(alltrees.sr_s) & ~isnan(alltrees.twi) & ~isnan(alltrees.asp);
224
225
226 save('trees.mat', 'alltrees');
227 save('logicals_single.mat','ii_s','jj_s','kk_s','ll_s');
228
229 % ------------------------------------------------------------------------
230 % ------------------------------------------------------------------------
231
232 %% Save Data for SLR
233
234 % For the SLR invocation procedure, please refer to the remainder of the
235 % Appendix.
236
237 % indexing coordinates:
238 [y x] = size(X);
239 scaleFactor = y/x;
240
241 XC_s = scaledata(alltrees.x,0,1);
242 YC_s = scaledata(alltrees.y,0,scaleFactor);
243 % Function "scaledata" by Aniruddha Kembhavi
244 % http://www.mathworks.ch/matlabcentral/fileexchange/15561-data-scaling/
      content/scaledata.m
245 % Accessed 18.08.2014
246
247 % Absolute
```

```
slrSingleAbs = [XC_s(kk_s), YC_s(kk_s), ...
    alltrees.deltaH(kk_s), alltrees.grad_smoothed(kk_s), ...
    alltrees.asp(kk_s), alltrees.twi(kk_s), alltrees.sr_s(kk_s), ...
    alltrees.z(kk_s), alltrees.h(kk_s)];
dlmwrite('slr_global_abs_single.csv',slrSingleAbs,'delimiter',' ');
clear slrSingleAbs;


% Relative
slrSingleRel = [XC_s(ll_s), YC_s(ll_s), ...
    alltrees.dHrel(ll_s), alltrees.grad_smoothed(ll_s), ...
    alltrees.asp(ll_s), alltrees.twi(ll_s), ...
    alltrees.sr_s(ll_s), alltrees.z(ll_s)];
dlmwrite('slr_global_rel_single.csv',slrSingleRel,'delimiter',' ');
clear slrSingleRel;

%% ------------------------------------------------------------------------
% 2. Descriptive Statistics
%% ------------------------------------------------------------------------

%% dCHM

% Absolute
disp('Percentage, absolute, dCHM:');
disp(num2str(sum(logical(kk(:))) ./ length(kk(:)) .* 100));

disp('Num samples, absolute, dCHM:');
disp(num2str(sum(logical(kk(:)))));

disp('Min, absolute, dCHM:');
disp(num2str(min(dchm_smooth(kk(:)))));

disp('Max, absolute, dCHM:');
```

```
281 disp(num2str(max(dchm_smooth(kk(:)))));
282
283 disp('Mean, absolute, dCHM:');
284 disp(num2str(mean(dchm_smooth(kk(:)))));
285
286 disp('Median, absolute, dCHM:');
287 disp(num2str(median(dchm_smooth(kk(:)))));
288
289 disp('StdDev, absolute, dCHM:');
290 disp(num2str(std(dchm_smooth(kk(:)))));
291
292 % Relative
293 disp('Percentage, relative, dCHM:');
294 disp(num2str(sum(logical(ll(:))) ./ length(ll(:)) .* 100));
295
296 disp('Num samples, relative, dCHM:');
297 disp(num2str(sum(logical(ll(:)))));
298
299 disp('Min, relative, dCHM:');
300 disp(num2str(min(dchm_rel(ll(:)))));
301
302 disp('Max, relative, dCHM:');
303 disp(num2str(max(dchm_rel(ll(:)))));
304
305 disp('Mean, relative, dCHM:');
306 disp(num2str(mean(dchm_rel(ll(:)))));
307
308 disp('Median, relative, dCHM:');
309 disp(num2str(median(dchm_rel(ll(:)))));
310
311 disp('StdDev, relative, dCHM:');
312 disp(num2str(std(dchm_rel(ll(:)))));
313
```

```
%% Single Trees

% Absolute
disp('Percentage, absolute, single trees:');
disp(num2str(sum(logical(kk_s(:))) ./ length(kk_s(:)) .* 100));

disp('Num samples, absolute, single trees:');
disp(num2str(sum(logical(kk_s(:)))));

disp('Min, absolute, single trees:');
disp(num2str(min(alltrees.deltaH(kk_s(:)))));

disp('Max, absolute, single trees:');
disp(num2str(max(alltrees.deltaH(kk_s(:)))));

disp('Mean, absolute, single trees:');
disp(num2str(mean(alltrees.deltaH(kk_s(:)))));

disp('Median, absolute, single trees:');
disp(num2str(median(alltrees.deltaH(kk_s(:)))));

disp('StdDev, absolute, single trees:');
disp(num2str(std(alltrees.deltaH(kk_s(:)))));

% Relative
disp('Percentage, relative, single trees:');
disp(num2str(sum(logical(ll_s(:))) ./ length(ll_s(:)) .* 100));

disp('Num samples, relative, single trees:');
disp(num2str(sum(logical(ll_s(:)))));

disp('Min, relative, single trees:');
disp(num2str(min(alltrees.dHrel(ll_s(:)))));
```

```
347
348 disp('Max, relative, single trees:');
349 disp(num2str(max(alltrees.dHrel(ll_s(:)))));
350
351 disp('Mean, relative, single trees:');
352 disp(num2str(mean(alltrees.dHrel(ll_s(:)))));
353
354 disp('Median, relative, single trees:');
355 disp(num2str(median(alltrees.dHrel(ll_s(:)))));
356
357 disp('StdDev, relative, single trees:');
358 disp(num2str(std(alltrees.dHrel(ll_s(:)))));
359
360 clear;
361
362 %% ------------------------------------------------------------------------
363 % 3. OLS Regressions
364 %% ------------------------------------------------------------------------
365
366 % Note that most of the statistics are retrieved, but never read out
367 % and possibly overwritten by subsequent models. In order to see the
368 % values, just call the variables in the right position.
369
370 %% Constants
371 doStandardize = 0;  % Originally intended for better comparison between
372                     % absolute and relative models; now not used anymore
373 outputFormatDCHM = '-dpng';
374 outputFormatSingle = '-depsc';
375
376 if doStandardize
377     colorRangeAbs = [-1 1];
378 else
379     colorRangeAbs = [-4 4];
```

```
380 end;
381
382 dtm_grid = GRIDobj(dtm.x, dtm.y, dtm.z);
383
384 % Load in required datasets
385 load regressionInput;
386 load logicals_dchm;
387
388 % ------------------------------------------------------------------------
389 % ------------------------------------------------------------------------
390
391 %% DCHM, Absolute
392 X = cat(3, ones(size(dchm_smooth,1), size(dchm_smooth,2)), ...
393     asp, sr_s, h_s, z_s, grad_smoothed, twi);
394 Y = dchm_smooth;
395
396 [~, ~, stats, residStats, predictions_dchm_abs, residuals_dchm_abs] ...
397     = linReg(doStandardize,kk,Y,X);
398
399 pred_dchm_abs_grid = GRIDobj(dtm.x, dtm.y, predictions_dchm_abs);
400 resid_dchm_abs_grid = GRIDobj(dtm.x, dtm.y, residuals_dchm_abs);
401
402 pred_glob = figure;
403 imageschs(dtm_grid, pred_dchm_abs_grid, 'caxis', colorRangeAbs, ...
404     'colorbar', true);
405 set(pred_glob,'Position',[0 0 900 600]);
406 swisstick;
407
408 if doStandardize
409     title('OLS Predictions for CHM differences, absolute growth - std');
410     print(pred_glob,'ols_dchm_abs_pred_std',outputFormatDCHM);
411 else
412     title('OLS Predictions for CHM differences, absolute growth');
```

```
413     print(pred_glob,'ols_dchm_abs_pred',outputFormatDCHM);
414 end;
415 %close(pred_glob);
416 
417 % Residual maps
418 res_glob = figure;
419 imageschs(dtm_grid, resid_dchm_abs_grid, 'caxis', colorRangeAbs, ...
420     'colorbar', true);
421 set(res_glob,'Position',[0 0 900 600]);
422 swisstick;
423 if doStandardize
424     title('OLS Residuals for CHM differences, absolute growth - std');
425     print(res_glob,'ols_dchm_abs_resid_std',outputFormatDCHM);
426 else
427     title('OLS Residuals for CHM differences, absolute growth');
428     print(res_glob,'ols_dchm_abs_resid',outputFormatDCHM);
429 end;
430 %close(res_glob);
431 
432 % Residual histogram
433 res_hist = figure;
434 hist(residuals_dchm_abs(kk), 20);
435 set(res_hist,'Position',[0 0 900 600]);
436 if doStandardize
437     title('Histogram of OLS Residuals for CHM differences, absolute growth
      - standardized');
438     print(res_hist,'hist_ols_dchm_abs_resid_std',outputFormatDCHM);
439 else
440     title('Histogram of OLS Residuals for CHM differences, absolute growth
     ');
441     print(res_hist,'hist_ols_dchm_abs_resid',outputFormatDCHM);
442 end;
443 %close(res_hist);
```

```
444
445 % Normal distribution test
446 if doStandardize
447     [h,p,ksstat,cv] = normDistTest(residuals_dchm_abs(kk), ...
448         'absolute CHM differences (standardized) ', ...
449         'Predicted growths (standardized)', 'normDist_abs_dchm_std', ...
450         outputFormatDCHM);
451 else
452     [h,p,ksstat,cv] = normDistTest(residuals_dchm_abs(kk), ...
453         'absolute CHM differences', 'Predicted growths', ...
454         'normDist_abs_dchm', outputFormatDCHM);
455 end;
456
457 % Homoscedasticity test
458 pred_std = standardize(predictions_dchm_abs(kk));
459 res_std = standardize(residuals_dchm_abs(kk));
460 homosc = figure;
461 scatter(pred_std, res_std, '.b');
462 title('Standardized Residuals Plot for CHM differences, absolute growth');
463 xlabel('Standardized Predicted Values');
464 ylabel('Standardized Residuals');
465 print(homosc, 'resplot_ols_dchm_abs', '-depsc');
466
467 %--------------------------------------------------------------------------
468
469 %% DCHM, Relative
470 X = cat(3, ones(size(dchm_rel,1), size(dchm_rel,2)), asp, ...
471     sr_s, z_s, grad_smoothed, twi);
472 Y = dchm_rel;
473
474 [~, ~, stats, residStats, predictions_dchm_rel, residuals_dchm_rel] ...
475     = linReg(doStandardize,ll,Y,X);
476
```

```
pred_dchm_rel_grid = GRIDobj(dtm.x, dtm.y, predictions_dchm_rel);
resid_dchm_rel_grid = GRIDobj(dtm.x, dtm.y, residuals_dchm_rel);

pred_glob = figure;
imageschs(dtm_grid, pred_dchm_rel_grid, 'caxis', [-1 1], ...
    'colorbar', true);
set(pred_glob,'Position',[0 0 900 600]);
swisstick;
if doStandardize
    title('OLS Predictions for CHM differences, relative growth - std');
    print(pred_glob,'ols_dchm_rel_pred_std',outputFormatDCHM);
else
    title('OLS Predictions for CHM differences, relative growth');
    print(pred_glob,'ols_dchm_rel_pred',outputFormatDCHM);
end;
%close(pred_glob);

% Residual maps
res_glob = figure;
imageschs(dtm_grid, resid_dchm_rel_grid, 'caxis', [-1 1], ...
    'colorbar', true);
set(res_glob,'Position',[0 0 900 600]);
swisstick;
axis equal;
if doStandardize
    title('OLS Residuals for CHM differences, relative growth - std');
    print(res_glob,'ols_dchm_rel_resid_std',outputFormatDCHM);
else
    title('OLS Residuals for CHM differences, relative growth');
    print(res_glob,'ols_dchm_rel_resid',outputFormatDCHM);
end;
%close(res_glob);

```

```
510 % Residual histogram
511 res_hist = figure;
512 hist(residuals_dchm_rel(ll), 20);
513 set(res_hist,'Position',[0 0 900 600]);
514 if doStandardize
515     title('Histogram of OLS Residuals for CHM differences, relative growth
        - standardized');
516     print(res_hist,'hist_ols_dchm_rel_resid_std',outputFormatDCHM);
517 else
518     title('Histogram of OLS Residuals for CHM differences, relative growth
        ');
519     print(res_hist,'hist_ols_dchm_rel_resid',outputFormatDCHM);
520 end;
521 %close(res_hist);
522
523 % Normal distribution test
524 if doStandardize
525     [h,p,ksstat,cv] = normDistTest(residuals_dchm_rel(ll), ...
526         'relative CHM differences (standardized)', ...
527         'Predicted growths (standardized)', 'normDist_rel_dchm_std', ...
528         outputFormatDCHM);
529 else
530     [h,p,ksstat,cv] = normDistTest(residuals_dchm_rel(ll), ...
531         'relative CHM differences', 'Predicted growths', ...
532         'normDist_rel_dchm', outputFormatDCHM);
533 end;
534
535 % Homoscedasticity test
536 pred_std = standardize(predictions_dchm_rel(ll));
537 res_std = standardize(residuals_dchm_rel(ll));
538 homosc = figure;
539 scatter(pred_std, res_std, '.b');
540 title('Standardized Residuals Plot for CHM differences, relative growth');
```

```
541 xlabel('Standardized Predicted Values');
542 ylabel('Standardized Residuals');
543 print(homosc, 'resplot_ols_dchm_rel', '-depsc');
544
545 clear;
546
547 % ------------------------------------------------------------------------
548 % ------------------------------------------------------------------------
549
550 load trees;
551 load logicals_single;
552
553
554 %% Single Trees, Absolute
555 X = [ones(length(alltrees.deltaH),1), alltrees.asp, alltrees.sr_s, ...
556     alltrees.h, alltrees.z, alltrees.grad_smoothed, alltrees.twi];
557 Y = alltrees.deltaH;
558
559 [~, ~, stats, residStats, predictions_single_abs, ...
560     residuals_single_abs] = linReg(doStandardize,kk_s,Y,X);
561
562 pred_glob = figure;
563 scatter(alltrees.x(kk_s), alltrees.y(kk_s), 3, ...
564     predictions_single_abs(kk_s), 'fill');
565 set(pred_glob,'Position',[0 0 900 600]);
566 swisstick;
567 axis equal;
568 caxis(colorRangeAbs);
569 colorbar;
570 if doStandardize
571     title('OLS Predictions for Single Trees, absolute growth - std');
572     print(pred_glob,'ols_single_abs_pred_std',outputFormatSingle);
573 else
```

```
574     title('OLS Predictions for Single Trees, absolute growth');
575     print(pred_glob,'ols_single_abs_pred',outputFormatSingle);
576 end;
577 %close(pred_glob);
578 
579 % Residual maps
580 res_glob = figure;
581 scatter(alltrees.x(kk_s), alltrees.y(kk_s), 3, ...
582     residuals_single_abs(kk_s), 'fill');
583 title('Residuals for absolute growth (single tree model); global model');
584 colorbar;
585 set(res_glob,'Position',[0 0 900 600]);
586 swisstick;
587 axis equal;
588 caxis(colorRangeAbs);
589 colorbar;
590 if doStandardize
591     title('OLS Residuals for Single Trees, absolute growth – std');
592     print(res_glob,'ols_single_abs_resid_std',outputFormatSingle);
593 else
594     title('OLS Residuals for Single Trees, absolute growth');
595     print(res_glob,'ols_single_abs_resid',outputFormatSingle);
596 end;
597 %close(res_glob);
598 
599 % Residual histogram
600 res_hist = figure;
601 hist(residuals_single_abs(kk_s), 20);
602 set(res_hist,'Position',[0 0 900 600]);
603 if doStandardize
604     title('Histogram of OLS Residuals for Single Trees, absolute growth –
    standardized');
605     print(res_hist,'hist_ols_single_abs_resid_std',outputFormatDCHM);
```

```
606 else
607     title('Histogram of OLS Residuals for Single Trees, absolute growth');
608     print(res_hist,'hist_ols_single_abs_resid',outputFormatDCHM);
609 end;
610 %close(res_hist);
611 
612 % Normal distribution test
613 if doStandardize
614     [h,p,ksstat,cv] = normDistTest(residuals_single_abs, ...
615         'absolute single tree growths (standardized)', ...
616         'Predicted growths (standardized)', ...
617         'normDist_abs_single_std', outputFormatSingle);
618 else
619     [h,p,ksstat,cv] = normDistTest(residuals_single_abs, ...
620         'absolute single tree growths', 'Predicted growths', ...
621         'normDist_abs_single', outputFormatSingle);
622 end;
623 
624 % Homoscedasticity test
625 pred_std = standardize(predictions_single_abs(kk_s));
626 res_std = standardize(residuals_single_abs(kk_s));
627 homosc = figure;
628 scatter(pred_std, res_std, '.b');
629 title('Standardized Residuals Plot for Single Trees, absolute growth');
630 xlabel('Standardized Predicted Values');
631 ylabel('Standardized Residuals');
632 print(homosc, 'resplot_ols_single_abs', '-depsc');
633 
634 %% ------------------------------------------------------------------------
635 
636 %% Single Trees, relative
637 X = [ones(length(alltrees.deltaH),1), alltrees.asp, alltrees.sr_s, ...
638     alltrees.z, alltrees.grad_smoothed, alltrees.twi];
```

```
639 Y = alltrees.dHrel;
640
641 [~, ~, stats, residStats, predictions_single_rel, ...
642     residuals_single_rel] = linReg(doStandardize,ll_s,Y,X);
643
644 pred_glob = figure;
645 scatter(alltrees.x(ll_s), alltrees.y(ll_s), 3, ...
646     predictions_single_rel(ll_s), 'fill');
647 set(pred_glob,'Position',[0 0 900 600]);
648 swisstick;
649 axis equal;
650 caxis([-1 1]);
651 colorbar;
652 if doStandardize
653     title('OLS Predictions for Single Trees, relative growth - std');
654     print(pred_glob,'ols_single_rel_pred_std',outputFormatSingle);
655 else
656     title('OLS Predictions for Single Trees, relative growth');
657     print(pred_glob,'ols_single_rel_pred',outputFormatSingle);
658 end;
659 %close(pred_glob);
660
661 % Residual maps
662 res_glob = figure;
663 scatter(alltrees.x(ll_s), alltrees.y(ll_s), 3, ...
664     residuals_single_rel(ll_s), 'fill');
665 title('Residuals for relative growth (single tree model); global model');
666 set(res_glob,'Position',[0 0 900 600]);
667 swisstick;
668 axis equal;
669 caxis([-1 1]);
670 colorbar;
671 if doStandardize
```

```
672     title('OLS Residuals for Single Trees, relative growth - std');
673     print(res_glob,'ols_single_rel_resid_std',outputFormatSingle);
674 else
675     title('OLS Residuals for Single Trees, relative growth');
676     print(res_glob,'ols_single_rel_resid',outputFormatSingle);
677 end;
678 %close(res_glob);
679 
680 % Residual histogram
681 res_hist = figure;
682 hist(residuals_single_rel(ll_s), 20);
683 set(res_hist,'Position',[0 0 900 600]);
684 if doStandardize
685     title('Histogram of OLS Residuals for Single Trees, relative growth -
        standardized');
686     print(res_hist,'hist_ols_single_rel_resid_std',outputFormatDCHM);
687 else
688     title('Histogram of OLS Residuals for Single Trees, relative growth');
689     print(res_hist,'hist_ols_single_rel_resid',outputFormatDCHM);
690 end;
691 %close(res_hist);
692 
693 % Normal distribution test
694 if doStandardize
695     [h,p,ksstat,cv] = normDistTest(residuals_single_rel, ...
696         'relative single tree growths (standardized)', ...
697         'Predicted growths (standardized)', ...
698         'normDist_rel_single_std', outputFormatSingle);
699 else
700     [h,p,ksstat,cv] = normDistTest(residuals_single_rel, ...
701         'relative single tree growths', 'Predicted growths', ...
702         'normDist_rel_single', outputFormatSingle);
703 end;
```

```
704
705 % Homoscedasticity test
706 pred_std = standardize(predictions_single_rel(ll_s));
707 res_std = standardize(residuals_single_rel(ll_s));
708 homosc = figure;
709 scatter(pred_std, res_std, '.b');
710 title('Standardized Residuals Plot for Single Trees, relative growth');
711 xlabel('Standardized Predicted Values');
712 ylabel('Standardized Residuals');
713 print(homosc, 'resplot_ols_single_rel', '-depsc');
714
715
716 %-------------------------------------------------------------------------
717 %-------------------------------------------------------------------------
718
719 %% OLS Revised (only with Solar Radiation and TWI)
720 X = [ones(length(alltrees.deltaH),1), alltrees.sr_s, alltrees.twi];
721 Y = alltrees.dHrel;
722
723 [~, ~, stats, residStats, predictions_single_rel, ...
724     residuals_single_rel] = linReg(doStandardize,ll_s,Y,X);
725
726 pred_glob = figure;
727 scatter(alltrees.x(ll_s), alltrees.y(ll_s), 3, ...
728     predictions_single_rel(ll_s), 'fill');
729 set(pred_glob,'Position',[0 0 900 600]);
730 swisstick;
731 axis equal;
732 caxis([-1 1]);
733 colorbar;
734 if doStandardize
735     title('OLS Revised Predictions for Single Trees, relative growth -
    standardized');
```

```
736     print(pred_glob,'ols_revised_single_rel_pred_std',outputFormatSingle);
737 else
738     title('OLS Revised Predictions for Single Trees, relative growth');
739     print(pred_glob,'ols_revised_single_rel_pred',outputFormatSingle);
740 end;
741 %close(pred_glob);
742
743 % Residual maps
744 res_glob = figure;
745 scatter(alltrees.x(ll_s), alltrees.y(ll_s), 3, ...
746     residuals_single_rel(ll_s), 'fill');
747 set(res_glob,'Position',[0 0 900 600]);
748 swisstick;
749 axis equal;
750 caxis([-1 1]);
751 colorbar;
752 if doStandardize
753     title('OLS Revised Residuals for Single Trees, relative growth -
    standardized');
754     print(res_glob,'ols_revised_single_rel_resid_std',outputFormatSingle);
755 else
756     title('OLS Revised Residuals for Single Trees, relative growth');
757     print(res_glob,'ols_revised_single_rel_resid',outputFormatSingle);
758 end;
759 %close(res_glob);
760
761 % Residual histogram
762 res_hist = figure;
763 hist(residuals_single_rel(ll_s), 20);
764 set(res_hist,'Position',[0 0 900 600]);
765 if doStandardize
766     title('Histogram of OLS Revised Residuals for Single Trees, relative
    growth - standardized');
```

```
767     print(res_hist,'hist_ols_revised_single_rel_resid_std',
        outputFormatDCHM);
768 else
769     title('Histogram of OLS Revised Residuals for Single Trees, relative
        growth');
770     print(res_hist,'hist_ols_revised_single_rel_resid',outputFormatDCHM);
771 end;
772 %close(res_hist);
773
774 % Normal distribution test
775 if doStandardize
776     [h,p,ksstat,cv] = normDistTest(residuals_single_rel, ...
777         'relative single tree growths (standardized)', ...
778         'Predicted growths (standardized)', ...
779         'normDist_rel_single_revised_std', outputFormatSingle);
780 else
781     [h,p,ksstat,cv] = normDistTest(residuals_single_rel, ...
782         'relative single tree growths', 'Predicted growths', ...
783         'normDist_rel_single_revised', outputFormatSingle);
784 end;
785
786 % Homoscedasticity test
787 pred_std = standardize(predictions_single_rel(ll_s));
788 res_std = standardize(residuals_single_rel(ll_s));
789 homosc = figure;
790 scatter(pred_std, res_std, '.b');
791 title('Standardized Residuals Plot for Single Trees, relative growth (
        revised model)');
792 xlabel('Standardized Predicted Values');
793 ylabel('Standardized Residuals');
794 print(homosc, 'resplot_ols_revised_single_rel', '-depsc');
```

Upon successful calculation of the SLR models (see B for the script), the following commands are executed for statistics and map retrieval of the SLR results:

```
% ------------------------------------------------------------------------
% 4. SLR Results Analysis
% ------------------------------------------------------------------------

% These commands take place after calculation of all SLR models as lis-
% ted in Script "slr.py".



load trees.mat;
load logicals_single.mat;

fileFormatDCHM = '-dpng';
fileFormatSingle = '-depsc';

doStandardize = 0;



if doStandardize
    colorRangeAbs = [-1 1];
else
    colorRangeAbs = [-4 4];
end;


%% Global; single trees; absolute
stats1 = analyzeSLRResults('slr_global_abs_03233_results.txt', ...
    alltrees.x, alltrees.y, kk_s, doStandardize, colorRangeAbs, ...
    'global SLR model on absolute single tree growths (kernel size 1km)',
    ...
```

```
31      'slr_global_abs_1km', fileFormatSingle);
32
33  stats2 = analyzeSLRResults('slr_global_abs_01617_results.txt', ...
34      alltrees.x, alltrees.y, kk_s, doStandardize, colorRangeAbs, ...
35      'global SLR model on absolute single tree growths (kernel size 500m)',
         ...
36      'slr_global_abs_500m', fileFormatSingle);
37
38  stats3 = analyzeSLRResults('slr_global_abs_00808_results.txt', ...
39      alltrees.x, alltrees.y, kk_s, doStandardize, colorRangeAbs, ...
40      'global SLR model on absolute single tree growths (kernel size 250m)',
         ...
41      'slr_global_abs_250m', fileFormatSingle);
42
43
44
45  %% Global; single trees; relative
46  stats4 = analyzeSLRResults('slr_global_rel_03233_results.txt', ...
47      alltrees.x, alltrees.y, ll_s, doStandardize, [-1 1], ...
48      'global SLR model on relative single tree growths (kernel size 1km)',
        ...
49      'slr_global_rel_1km', fileFormatSingle);
50
51  stats5 = analyzeSLRResults('slr_global_rel_01617_results.txt', ...
52      alltrees.x, alltrees.y, ll_s, doStandardize, [-1 1], ...
53      'global SLR model on relative single tree growths (kernel size 500m)',
         ...
54      'slr_global_rel_500m', fileFormatSingle);
55
56  stats6 = analyzeSLRResults('slr_global_rel_00808_results.txt', ...
57      alltrees.x, alltrees.y, ll_s, doStandardize, [-1 1], ...
58      'global SLR model on relative single tree growths (kernel size 250m)',
         ...
```

```
    'slr_global_rel_250m', fileFormatSingle);



% SLR Revised (relative growth; without altitude):
stats7 = analyzeSLRResults('slr_global_rel_01617_custom_results.txt', ...
    alltrees.x, alltrees.y, ll_s, doStandardize, [-1 1], ...
    'SLR revised model on relative single tree growths (kernel size 500m)'
    , ...
    'slr_global_rel_revised_500m', fileFormatSingle);
```

B.2 Custom Functions

This Section covers all custom functions used in the main workflow, in chronological order of invocation.

B.2.1 Function "ch1903ToWgs84"

```
function [lat lon] = ch1903ToWgs84(easting, northing)

    % Approximative Conversion from CH1903 Easting/Northing
    % to WGS84 Lat/Lon [degs] using the formulae described in
    % Marty (1999).
    % See http://www.swisstopo.admin.ch/internet/swisstopo/en/home/topics/
    survey/sys/refsys/switzerland.parsysrelated1.37696.downloadList.12749.
    DownloadFile.tmp/ch1903wgs84en.pdf

    eastC = (easting - 2E5) ./ 10E6;
    northC = (northing - 6E5) ./ 10E6;

    latC = 16.9023892 + (3.238272 .* eastC) - (0.270978 .* northC .^2) +
    (0.002528 .* eastC .^ 2) - (0.0447 .* northC .^ 2 .* eastC) - (0.0140
    .* eastC .^ 3);
```

```
    lonC = 2.6779094 + (4.728982 .* northC) + (0.791484 .* eastC .* northC
    ) + (0.1306 .* northC .* eastC .^2) - (0.0436 .* northC .^ 3);

    lat = latC .* 100 ./ 36;
    lon = lonC .* 100 ./ 36;

end
```

B.2.2 Function "smoothenMatrix"

```
function result = smoothenMatrix(input, kernelSize, varargin);

    filterType = 'gaussian';

    if nargin > 2
        filterType = varargin{1};
    end

    filter = fspecial(filterType,kernelSize);
    result = filter2(filter, input);

end
```

B.2.3 Function "solrad"

```
function srad = solrad(dem,lat,lon,r)
%
%
% Script follows the approach of Kumar et al 1997. Calculates clear sky
% radiation corrected for the incident angle (selfshading) plus
% diffuse and reflected radiation. Insolation is depending on
% time of year (and day), latitude, elevation, slope and aspect.
%
```

```
%
%
% Reference: Kumar et al., 1997; ESRI 2014a
%
%
% Felix Hebeler, Dept. of Geography, University Zurich, May 2008.
% Edited and adapted by Benjamin Kellenberger, Feb 2014.
%
%%%%%%%%%%%%%%%%%%%%%%%%%%%%%%%%%%%%%%%%%%%%%%%%%%%%%%%%%%%%%%%%%%%%%%%%%%%


%% parameters
%It ;               % total hours of daily sunshine (calculated inline)
%M ;                % air mass ratio parameter (calculated inline)
%r = 0.20;          % ground reflectance coefficient (more sensible to
    give as input)
n = 1;              % timestep of calculation over sunshine hours: 1=
    hourly, 0.5=30min, 2=2hours etc
tau_a    = 365;     %length of the year in days
S0 = 1367;          % solar constant W m^-2   default 1367

dr= 0.0174532925;   % degree to radians conversion factor

%%  convert factors
[slop,asp]=get_ders(dem,lat,lon);   % calculate slope and aspect in
    radians using given cellsize cs

lat=lat*dr;                     % convert to radians
fcirc = 360*dr; % 360 degrees in radians

%% some setup calculations
srad=0;
sinL=sin(lat);
```

```
39 cosL=cos(lat);
40 tanL=tan(lat);
41 sinSlop=sin(slop);
42 cosSlop=cos(slop);
43 cosSlop2=cosSlop.*cosSlop;
44 sinSlop2=sinSlop.*sinSlop;
45 sinAsp=sin(asp);
46 cosAsp=cos(asp);
47 term1 = ( sinL.*cosSlop - cosL.*sinSlop.*cosAsp);
48 term2 = ( cosL.*cosSlop + sinL.*sinSlop.*cosAsp);
49 term3 = sinSlop.*sinAsp;
50
51
52
53
54
55 %% calculating for the shortest and longest day (day nr. 172 and 355):
56 d = 172;
57 unfinished = 1;
58 while unfinished;
59     if d == 355
60         unfinished = 0;
61     end;
62
63     display(['Calculating solar radiation for day ',num2str(d)]);
64     % clear sky solar radiation
65     I0 = S0 * (1 + 0.0344*cos(fcirc*d/tau_a)); % extraterr rad per day
                                EQ. 7; solar flux outside atmosphere
66     % sun declination dS
67     dS = 23.45 * dr* sin(fcirc * ( (284+d)/tau_a ) ); %in radians, correct
       /verified                EQ. 4; solar declination
68     % angle at sunrise/sunset
69     % t = 1:It; % sun hour
```

```
70    hsr = real(acos(-tanL*tan(dS)));  % angle at sunrise
                              EQ. 6; angle at sunrise
71
72    It=round(12*(1+mean(hsr(:))/pi)-12*(1-mean(hsr(:))/pi)); % calc
      daylength
73    %%  daily loop
74    I=0;
75    for t=1:n:It % loop over sunshine hours
76
77        disp(['Calculating radiation for hour ', num2str(t)]);
78
79        % hourangle of sun hs
80        hs=hsr-(pi*t/It);                % hs(t)
81        %solar angle and azimuth
82        alpha = asin(sinL .* sin(dS)+cosL .* cos(dS) .* cos(hs));% solar
      altitude angle
83        sinAlpha = sinL.*sin(dS)+cosL.*cos(dS).*cos(hs);
84        alpha_s = asin(cos(dS) .* sin(hs) ./ cos(alpha)); % solar azimuth
      angle
85        % correction  using atmospheric transmittivity taub_b
86        M=sqrt(1229+((614.*sinAlpha)).^2)-614.*sinAlpha; % Air mass ratio
87        tau_b = 0.56 * (exp(-0.65*M) + exp(-0.095*M));
88        tau_d = 0.271-0.294*tau_b; % radiation diffusion coefficient for
      diffuse insolation
89        tau_r = 0.271+0.706*tau_b; % reflectance transmittivity
90        % correct for local incident angle
91        cos_i = (sin(dS).*term1) + (cos(dS).*cos(hs).*term2) + (cos(dS).*
      term3.*sin(hs));
92        Is = I0 * tau_b; % potential incoming shortwave radiation at
      surface normal (equator)
93        % R = potential clear sky solar radiation W m2
94        R = Is .* cos_i;
95        R(R<0)=0;  % kick out negative values
```

```
96
97
98          % Hillshading
99          azimuth = alpha_s;
100         azimuth = 360.0-azimuth+90; %convert to mathematic unit
101         azimuth(azimuth>=360)=azimuth-360;
102         azimuth = azimuth .* (pi ./ 180); %  convert to radians
103
104         altitude = alpha;
105         altitude = (90-altitude) .* (pi ./ 180); % convert to zenith angle
        in radians
106
107
108         % calculate hillshading
109         h = 255.0 .* ( (cos(altitude) .* cos(slop) ) + ( sin(altitude) .*
    sin(slop) .* cos(azimuth-asp_hs)) ); % ESRIs algorithm
110         h(h<0)=0; % set hillshade values to min of 0.
111
112         h=setborder(h,1,NaN); % set border cells to NaN
113
114         h = h ./ 255;
115         R = R .* h; % apply hillshading
116
117         Id = I0 .* tau_d .* cosSlop2./ 2.*sinAlpha; %diffuse radiation;
118         Ir = I0 .* r .* tau_r .* sinSlop2./ 2.* sinAlpha; % reflectance
119         R= R + Id + Ir;
120         R(R<0)=0;
121         I=I+R;% solar radiation per day (sunshine hours)
122     end % end of sun hours in day loop
123     %%  add up radiation part for every day
124     srad = srad + I;
125
126     d = 355;
```

```
127 end;
128
129
130
131 function [grad,asp] = get_ders(dem,lat,lon)
132 [asp, grad] = gradientm(lat, lon, dem);
133 asp = asp .* pi ./ 180;
134 grad = grad .* pi ./ 180;
135 asp=asp.*-1+pi; % convert asp 0 facing south
136
137
138
139
140
141 function grid = setborder(grid,bs,bvalue)
142 grid(1:bs,:)=bvalue; %toprows
143 grid(size(grid,1)-bs+1:size(grid,1),:)=bvalue; %bottom rows
144 grid(:,1:bs)=bvalue; %left cols
145 grid(:,size(grid,2)-bs+1:size(grid,2))=bvalue;
```

B.2.4 Function "linReg"

```
1  function [b, bint, stats, residStats, predictions, residuals, regCoeffs,
       dwp] = linReg(doStandardize, logicalVar, dependent, X)
2
3  logicalVar(logicalVar > 1) = 1;
4
5  Y = dependent(logicalVar(:));
6
7
8
9  % Extract valid data points only (according to logicalVar)
10 numDim = 1;
```

```
11 if size(X,3) > 1    % at least 2 dimensions
12     numDim = 2;
13 end;
14
15
16 X_input = zeros(sum(logicalVar(:)),size(X,numDim+1));
17
18 for i=1:size(X,numDim+1)
19     if numDim == 1
20         tempVar = X(:,i);   % 1D data
21     else
22         tempVar = X(:,:,i); % 2D data
23     end;
24
25     X_input(:,i) = tempVar(logicalVar);
26 end;
27
28
29
30 [b, bint, ~, ~, stats] = regress(Y, X_input);  % we don't  use the MATLAB
       provided residuals as they are transformed to be Student-t distributed.
31 disp('Regression results:');
32 disp('********************');
33 disp(strcat('R square: ',num2str(stats(1))));
34 disp(strcat('F value: ',num2str(stats(2))));
35 disp(strcat('p value: ',num2str(stats(3))));
36 disp(strcat('Error variance estimation: ',num2str(stats(4))));
37 disp(' ');
38
39
40 % Collinearity Diagnostics (by Brian Lau, 2011;
41 % http://www.subcortex.net/research/code/...
42 % collinearity-diagnostics-matlab-code ; accessed 10.07.2014)
```

```
43 disp('Collinearity diagnostics:');
44 disp('************************');
45 cd = colldiag(X_input);
46 disp(cd.str);
47 colldiag_tableplot(cd);
48 disp(' ');
49
50
51 % Regression Coefficients calculation
52 regCoeffs = zeros(size(X_input, 2), 1);
53 for i=1:size(X_input, 2)
54     tempVar = X_input(:,i);
55     tempVar = tempVar(:);
56     regCoeffs(i) = b(i) .* std(tempVar) ./ std(Y(:));
57 end;
58
59
60
61 % Prediction and Residual calculation
62 predictions = NaN(size(dependent,1), size(dependent,2));
63 predictions(:) = b(1);
64
65 for i=2:size(X,numDim+1)
66     if numDim == 1
67         tempVar = X(:,i);   % 1D data
68     else
69         tempVar = X(:,:,i); % 2D data
70     end;
71     predictions = predictions + b(i) .* tempVar;
72 end;
73
74 predictions(~logicalVar) = NaN;
75
```

```
76
77  residuals = predictions - dependent;
78  residuals(~logicalVar) = NaN;   % maybe unneccessary since all unwanted
        values are already "NaN"
79
80  if doStandardize
81      predictions = standardize(predictions);
82      residuals = standardize(residuals);
83  end;
84
85
86
87
88  % Residual statistics
89  disp('Residual statistics:');
90  disp('**********************');
91
92  residStats = NaN(6,1);
93
94  r_abs = abs(residuals(logicalVar));
95  residStats(1) = min(r_abs); disp(strcat('Min |r|: ',num2str(residStats(1))
        ));
96  residStats(2) = max(r_abs); disp(strcat('Max |r|: ',num2str(residStats(2))
        ));
97  residStats(3) = mean(residuals(logicalVar)); disp(strcat('Mean r: ',
        num2str(residStats(3))));
98  residStats(4) = median(residuals(logicalVar)); disp(strcat('Median r: ',
        num2str(residStats(4))));
99  residStats(5) = std(residuals(logicalVar)); disp(strcat('Std.Dev. r: ',
        num2str(residStats(5))));
100 residStats(6) = rmsError(Y, residuals(logicalVar)); disp(strcat('RMSE: ',
        num2str(residStats(6))));
101 disp(' ');
```

```
102
103 dwp = dwtest(residuals(logicalVar), X_input);
104 disp(strcat('Durbin-Watson p: ', num2str(dwp)));
105
106
107
108 end
```

B.2.5 Function "normDistTest"

```
1  function [h,p,ksstat,cv] = normDistTest(variable, titleString, x_label,
       outputPath, fileFormat)
2
3  % Provides a test for Normal distribution of data, using the following
4  % three evaluation methods:
5  %
6  % 1. Histogram of data
7  % 2. Q-Q-plot
8  % 3. K.S.-test
9  %
10 % 2014 Benjamin Kellenberger
11
12
13
14 %% 1. Histogram
15 if nargin > 1
16     hfig = figure;
17     hist(variable, 20);
18     title(['Histogram of residuals (', titleString, ')']); %,'FontSize
       ',18);
19     xlabel(x_label);
20     ylabel('Number of samples');
21     set(hfig,'Position',[0 0 900 600]);
```

```
    if nargin > 3
        print(hfig, strcat(outputPath, '_hist'), fileFormat);
    end;
    close(hfig);
end;




%% 2. Q-Q-plot
if nargin > 1
    qqfig = figure;
    qqplot(variable);
    title(['Quantile-Quantile plot of residuals (', titleString, ')']);
    set(qqfig,'Position',[0 0 900 600]);
    if nargin > 3
        print(qqfig, strcat(outputPath, '_qq'), fileFormat);
    end;
    close(qqfig);
end;



%% 3. K.S.-test
[h,p,ksstat,cv] = kstest(variable);

if p < 0.05
    disp(['Data are not Normal distributed at the 0.05 level (p=', num2str
    (p), ').']);
else
    disp(['Normal distribution present at 0.05 level (p=', num2str(p), ').
    ']);
end;
```

B.2.6 Function "analyzeSLRResults"

```
function [stats, data] = analyzeSLRResults(path, xcoord, ycoord, logicVar,
    doStandardize, cRange, titleString, outputFileName, fileFormat)

data = csvread(path);


data(:,1) = xcoord(logicVar);
data(:,2) = ycoord(logicVar);

residuals = data(:,4) - data(:,3);
if doStandardize
    data(:,4) = standardize(data(:,4));
    residuals = standardize(residuals);
end;


%% Statistics
stats = zeros(6,1);
residuals_abs = abs(residuals);

stats(1) = min(residuals_abs);
stats(2) = max(residuals_abs);
stats(3) = mean(residuals);
stats(4) = median(residuals);
stats(5) = std(residuals);
stats(6) = rmsError(data(:,3), data(:,4));


%% Figures
if nargin > 5

    % Predictions
```

```
32      pred = figure;
33      scatter(data(:,1), data(:,2), 3, data(:,4), 'fill');
34
35      set(pred,'Position',[0 0 900 600]);
36      swisstick;
37      axis equal;
38      colorbar;
39      caxis(cRange);
40      if doStandardize
41          title(['Predictions for ', titleString,' (standardized)']);
42          if nargin > 7
43              print(pred,strcat(outputFileName,'_pred_std'), fileFormat);
44          end;
45      else
46          title(['Predictions for ', titleString]);
47          if nargin > 7
48              print(pred,strcat(outputFileName,'_pred'), fileFormat);
49          end;
50      end;
51      %close(pred);
52
53
54      % Residuals
55      resid = figure;
56      scatter(data(:,1), data(:,2), 3, residuals, 'fill');
57
58      set(resid,'Position',[0 0 900 600]);
59      swisstick;
60      axis equal;
61      colorbar;
62      caxis(cRange);
63      if doStandardize
64          title(['Residuals of ', titleString,' (standardized)']);
```

```
65          if nargin > 7
66              print(resid,strcat(outputFileName,'_resid_std'), fileFormat);
67          end;
68      else
69          title(['Residuals of ', titleString]);
70          if nargin > 7
71              print(resid,strcat(outputFileName,'_resid'), fileFormat);
72          end;
73      end;
74      %close(resid);
75
76
77      residHist = figure;
78      hist(residuals(:));
79      set(residHist,'Position',[0 0 900 600]);
80      if doStandardize
81          title(['Histogram of standardized residuals of ', titleString]);
82          if nargin > 7
83              print(resid,strcat(outputFileName,'_residhist_std'),
    fileFormat);
84          end;
85      else
86          title(['Histogram of residuals of ', titleString]);
87          if nargin > 7
88              print(resid,strcat(outputFileName,'_residhist'), fileFormat);
89          end;
90      end;
91      %close(residHist);
92  end;
93
94  end
```

Appendix C

Python Scripts

```
#!/usr/bin/env python

"""
SLR Analysis Procedure

Script based on the work of Christian Kaiser
(christian.kaiser@nuim.ie)
and Alexei Pozdnoukhov (alexei.pozdnoukhov@nuim.ie);
adapted by Benjamin Kellenberger
(benjamin.kellenberger@geo.uzh.ch).

Note that the SLR method requires a Linux platform to run cor-
rectly. The Python distribution shipped with Mac OS X will not
work (reason: their implementation of the "Queue" data structu-
re has a maximum capacity of 32'767 entries, which is not enough
for the high number of samples examined here).

Furthermore, the original SLR method would not give a result if
the local VIF was over 10. This test was therefore bypassed.

2014 Benjamin Kellenberger

"""

"""
0. Initialization
"""

import numpy as np
from slr import SLR
from util import csv_to_ndarray


"""
N. Main Function Definition
"""

def calculateSLR(path, cr, sr, tr, wRange, nameOut):
```

```
39      # Read the data
40      data = (csv_to_ndarray(path,
41          sep=" ", header=False, dtype="float32"))
42      print "File read-in done."
43      coords = data[:, cr[0]:cr[1]]
44      samples = data[:, sr[0]:sr[1]]
45      targets = data[:, tr[0]:tr[1]]
46
47      # Initialize the SLR algorithm
48      print "Creating the SLR model"
49      slr = SLR(params = {
50          'w_range': wRange, 'dist_adapt': False, 'diag_only':
    True,
51          'meta': False, 'penalty': 1e-7
52      })
53
54      # Feed in the stream, one sample at a time
55      nsamples = samples.shape[0]
56      for i in range(nsamples):
57          slr.update(coords[i,:], targets[i], samples[i,:])
58          if not i % 1000:
59              print("Iter %d of %d, %d in dictionary"  % (i,
    nsamples, len(slr.rfs)))
60
61      # Prediction of all new points
62      results = {}
63      for i in range(nsamples):
64          job_id = slr.query(coords[i,:], samples[i,:])
65          results[job_id] = {
66              'coords': coords[i,:], 'samples': samples[i,:], '
    target': targets[i]
67          }
68          if not i % 1000:
69              print("Predicted %d of %d samples"  % (i, nsamples))
70
71      # Get all the results
72      slr.save_state(nameOut + "_state")
73      output = open(nameOut + "_results.txt", "w")
74
75      cnt = 0
76      for r in slr.results(nmax=nsamples):
77          results[r[0]]['prediction'] = r[1]
78          cnt += 1
79          tgt = str(results[r[0]]['target']).replace("[","").
    replace("]","").strip()
80          res = str(results[r[0]]['prediction']).replace("[","").
    replace("]","").strip()
81          crd = ",".join(map(str, results[r[0]]['coords'])).strip
    ()
82          output.write("%s,%s,%s\n" % (crd, tgt, res))
83
84          if not cnt % 1000:
85              print("%d of %d results retrieved." % (cnt, nsamples
    ))
86
87      output.close();
88
```

```
89      # Flush memory
90      del slr
91      del data
92      del coords
93      del samples
94      del targets
95
96      print("All done.")
97
98
99  """
100 1. Function Calls for all investigated Datasets
101 """
102 #
103 # Type, Kernel Size (1km = 0.3233, 500m = 0.1617, 250m = 0.0808)
104 #
105
106 # Absolute, 1km
107 calculateSLR('../datasets/slr_global_abs_single.csv', [0,2],
        [3,9], [2,3], 0.3233,
108      "../results/slr_global_abs_03233")
109
110 # Absolute, 500m
111 calculateSLR('../datasets/slr_global_abs_single.csv', [0,2],
        [3,9], [2,3], 0.1617,
112      "../results/slr_global_abs_01617")
113
114 # Absolute, 250m
115 calculateSLR('../datasets/slr_global_abs_single.csv', [0,2],
        [3,9], [2,3], 0.0808,
116      "../results/slr_global_abs_00808")
117
118
119 # Relative, 1km
120 calculateSLR('../datasets/slr_global_rel_single.csv', [0,2],
        [3,8], [2,3], 0.3233,
121      "../results/slr_global_rel_03233")
122
123 # Relative, 500m
124 calculateSLR('../datasets/slr_global_rel_single.csv', [0,2],
        [3,8], [2,3], 0.1617,
125      "../results/slr_global_rel_01617")
126
127 # Relative, 250m
128 calculateSLR('../datasets/slr_global_rel_single.csv', [0,2],
        [3,8], [2,3], 0.0808,
129      "../results/slr_global_rel_00808")
130
131
132 # SLR Revised (relative, 500m, only Solar Radiation & TWI)
133 calculateSLR('../datasets/slr_global_rel_single.csv', [0,2],
        [5:7], [2,3], 0.1617,
134      "../results/slr_global_rel_01617_custom")
```

Bibliography

Alvarez-Uria, P., Körner, C., 2007. Low temperature limits of root growth in deciduous and evergreen temperate tree species. Functional Ecology 21, 211–218.

Ampratwum, D.B., Dorvlo, A.S.S., 1999. Estimation of solar radiation from the number of sunshine hours. Applied Energy 63, 161–167.

Andersen, H.E., Reutebuch, S.E., McGaughey, R.J., 2006. A rigorous assessment of tree height measurements obtained using airborne lidar and conventional field methods. Canadian Journal of Remote Sensing 32, 355–366.

Avsar, M.D., 2004. The relationships between diameter at breast height, tree height and crown diameter in calabrian pints (*Pinus brutia* ten.) of baskonus mountain, kahramanmaras, turkey. Journal of Biological Sciences 4, 437–440.

Babst, F., Bouriaud, O., Frank, D., 2012. A new sampling strategy for tree-ring based forest productivity estimates. ATR TRACE Proceedings 10, 62–70.

Barber, V.A., Juday, G.P., Finney, B.P., 2000. Reduced growth of alaskan white spruce in the twentieth century from temperature-induced drought stress. Nature 405, 668–673.

Beck, P.S.A., Juday, G.P., Alix, C., Barber, V.A., Winslow, S.E., Sousa, E.E., Heiser, P., Herriges, J.D., Goetz, S.J., 2011. Changes in forest productivity across alaska consistent with biome shift. Ecology Letters 14, 373–379.

Becker, A., Bugmann, H., 2001. Global change and mountain regions: The mountain research initiative. IGBP Report 49.

Belsley, D.A., Kuh, E., Velsch, R.E., 2004. Regression Diagnostics: Identifying Influential Data and Sources of Collinearity. John Wiley & Sons.

Berryman, A.A., 1989. Forest insects: principles and practice of population management. Plenum Press, New York.

Bigler, C., Bräker, O.U., Bugmann, H., Dobbertin, M., Rigling, A., 2006. Drought as an inciting mortality factor in scots pine stands of the valais, switzerland. Ecosystems 9, 330–343.

Birmann, K., Körner, C., 2009. Nitrogen status of conifer needles at the alpine treeline. Plant Ecology & Diversity 2, 233–241.

Bonan, G.B., 2008. Forests and climate change: Forcings, feedbacks, and the climate benefits of forests. Science 320, 1444–1449.

Briffa, K.R., Jones, P.D., Schweingruber, F.H., Shiyatov, S.G., Cook, E.R., 1995. Unusual twentieth-century summer warmth in a 1000-year temperature record from siberia. Nature 376, 156–159.

Brunsdon, C., Fotheringham, S., Charlton, M., 1998. Geographically weighted regression—modelling spatial non-stationarity. Journal of the Royal Statistical Society. Series D (The Statistician) 47, 431–443.

Chalkias, C., 2004. Embedding time in gis educational applications. a greek paradigm. Fourth European GIS Education Seminar, Villach, Austria .

Chapin, F.S., 1974. Morphological and physiological mechanisms of temperature compensation in phosphate absorption along a latitudinal gradient. Ecology 55, 1180–1198.

Chapin, F.S.I., Zimov, S.A., Shaver, G.R., Hobbie, S.E., 1996. co_2 fluctuation at high latitudes. Nature 383, 585–586.

Chen, G., Zhao, K., McDermid, G.J., Hay, G.J., 2012. The influence of sampling density on geographically weighted regression: a case study using forest canopy height and optical data. International Journal of Remote Sensing 33, 2909–2924.

Chen, Q., Gong, P., Baldocchi, D., Xie, G., 2007. Filtering airborne laser scanning data with morphological methods. Photogrammetric Engineering & Remote Sensing 73, 175–185.

Ciais, P., Schelhaas, M.J., Zaehle, S., Piao, S.L., Cescatti, A., Liski, J., Luyssaert, S., Le-Maire, G., Schulze, E.D., Bouriaud, O., Freibauer, A., Valentini, R., Nabuurs, G.J., 2009. Carbon accumulation in european forests. Nature Geoscience 1, 425–429.

Corripio, J.G., 2003. Vectorial algebra algorithms for calculating terrain parameters from dems and solar radiation modelling in mountainous terrain. International Journal of Geographical Information Science 17, 1–23.

Danby, R.K., Hik, D.S., 2007. Responses of white spruce (*Picea glauca*) to experimental warming at a subarctic alpine treeline. Global Change Biology 13, 437–451.

Däniker, A., 1923. Biologische studien über baum- und waldgrenze, insbesondere über die klimatischen ursachen und deren zusammenhänge. Vierteljahresschrift der Naturforschenden Gesellschaft Zürich 68, 1–102.

Daubenmire, R.F., 1974. Plants and Environment: A Textbook of Plant Autecology. John Wiley & Sons.

Devi, N., Hagedorn, F., Moiseev, P., Bugmann, H., Shiyatov, S., Mazepa, V., Rigling, A., 2008. Expandecosystems and changing growth forms of siberian larch at the polar urals treeline during the 20th century. Global Change Biology 14, 1581–1591.

Dickinson, W.C., Cheremisinoff, P.N., 1980. Solar Energy Technology Handbook. Dekker, New York.

Dobbertin, M., Baltensweiler, A., Rigling, D., 2001. Tree mortality in an unmanaged mountain pine (*Pinus mugo var. uncinata*) stand in the swiss national park impacted by root rot fungi. Forest Ecology and Management 145, 79–89.

Dullinger, S., Dirnböck, T., Grabherr, G., 2004. Modelling climate change-driven treeline shifts: relative effects of temperature increase, dispersal and invasibility. Journal of Ecology 92, 241–252.

Erb, K., Kastner, T., Luyssaert, S., Houghton, R.A., Kuemmerle, T., Olofsson, P., Haberl, H., 2013. Bias in the attribution of forest carbon sinks. Nature Climate Change 3, 854–856.

ESRI, 2011a. How aspect works. URL: `http://webhelp.esri.com/arcgisdesktop/9.3/index.cfm?TopicName=How%20Aspect%20works`.

ESRI, 2011b. How slope works. URL: `http://webhelp.esri.com/arcgisdesktop/9.3/index.cfm?TopicName=How%20Slope%20works`.

ESRI, 2014a. How gwr works. URL: http://resources.arcgis.com/en/help/main/10.1/index.html#//005p00000031000000.

ESRI, 2014b. How hillshade works. URL: http://edndoc.esri.com/arcobjects/9.2/net/shared/geoprocessing/spatial_analyst_tools/how_hillshade_works.htm.

Fairchild, J., Leymarie, P., 1991. Drainage networks from grid digital elevation models. Water Resources Research 27, 29–61.

Farrar, D.E., Glauber, R.R., 1967. Multicollinearity in regression analysis: The problem revisited. The Review of Economics and Statistics 49, 92–107.

Fekedulegn, D., Jr., R.R.H., Colbert, J.J., 2002. Influence of topographic aspect, precipitation and drought on radial growth of four major tree species in an appalachian watewater. Forest Ecology and Management 6094, 1–17.

Friendly, M., Kwan, E., 2009. Where's waldo: Visualizing collinearity diagnostics. The American Statistician 63, 56–65.

Gamache, I., Payette, S., 2004. Height growth response of tree line black spruce to recent climate warming across the forest-tundra of eastern canada. Journal of Ecology 92, 835–845.

Gaveau, D.L.A., Hill, R.A., 2003. Quantifying canopy height underestimation by laser pulse penetration in small-footprint airborne laser scanning data. Canadian Journal of Remote Sensing 29, 650–657.

Gorsuch, D.M., Oberbauer, S.F., 2002. Effects of mid-season frost and elevated growing season temperature on stomatal conductance and specific xylem conductivity of the arctic shrub, *Salix pulchra*. Tree Physiology 22, 1027–1034.

Gower, S.T., McMurtrie, R.E., Murty, D., 1996. Aboveground net primary production decline with stand age: potential causes. Trends in Ecology & Evolution 11, 378–382.

Grace, J., Berninger, F., Nagy, L., 2002. Impacts of climate change on the tree line. Annals of Botany 90, 537–544.

Graumlich, L.J., Brubaker, L.B., 1986. Reconstruction of annual temperature (1590-1979) for longmire, washington, derived from tree rings. Quarternary Research 25, 223–234.

Harsch, M.A., Hulme, P.E., McGlone, M.S., Duncan, R.P., 2009. Are treelines advancing? a global meta-analysis of treeline response to climate warming. Ecology Letters 12, 1040–1049.

Hart, J.C., Baker, B., Michaelraj, J., 2003. Structural simulation of tree growth and response. The Visual Computer 19, 151–163.

Heinzel, J., Koch, B., 2011. Exploring full-waveform lidar parameters for tree species classification. International Journal of Applied Earth Observation and Geoinformation 13, 152–160.

Hopkinson, C., 2007. The influence of lidar acquisition settings on canopy penetration and laser pulse return characteristics. Canadian Journal of Remote Sensing 33, 312–324.

Huang, H., Li, Z., Gong, P., Cheng, X., Clinton, N., Cao, C., Ni, W., Wang, L., 2011. Automated methods for measuring dbh and tree heights with a commercial scanning lidar. American Society for Photogrammetry and Remote Sensing 77, 219–227.

Hubbard, R.M., Bond, B.J., Ryan, M.G., 1999. Evidence that hydraulic conductance limits photosynthesis in old *Pinus ponderosa* trees. Tree Physiology 19, 165–172.

Hughes, P., 2000. Direct solar radiation :a modelling technique, in: SIRC 2000 – The 12th Annual Colloquium of the Spatial Information Research Centre.

Iakovoglou, V., Thompson, J., Burras, L., Kipper, R., 2001. Factors related to tree growth across urban-rural gradients in the midwest, usa. Urban Ecosystems 5, 71–85.

Iverson, L.R., Dale, M.E., Scott, C.T., Prasad, A., 1997. A gis-derived integrated moisture index to predict forest composition and producitivity of ohio forests (u.s.a.). Landscape Ecology 12, 331–348.

Jacoby, G.C., Cook, E.R., Ulan, L.D., 1985. Reconstructed summer degree days in central alaska and northwestern canada since 1524. Quaternary Research 23, 18–26.

Jacovides, C.P., Tymvios, F.S., Asimakopoulos, D.N., Theofilou, K.M., Pashiardes, S., 2003. Global photosynthetically active radiation and its relationship with global solar radiation in the eastern mediterranean basin. Theoretical and Applied Climatology 74, 227–233.

Jones, R., 2002. Algorithms for using a dem for mapping catchment areas of stream sediment samples. Computers & Geosciences 28, 1051–1060.

Kalliovirta, J., Tokola, T., 2005. Functions for estimating stem diameter and tree age using tree height, crown width and existing stand database information. Silva Fennica 39, 227–248.

Kimmins, J.P., 2004. Forest Ecology. Pearson Prentice Hall.

Kittel, T.G.F., Steffen, W.L., Chapin, F.S., 2000. Global and regional modelling of arctic-boreal vegetation distribution and its sensitivity to altered forces. Global Change Biology 6, 1–18.

Koch, G.W., Sillett, S.C., Jennings, G.M., Davis, S.D., 2004. The limits to tree height. Nature 428, 851–854.

Körner, C., 1998. A re-assessment of high elevation treeline positions and their explanation. Oecologia 115, 445–459.

Körner, C., 2003. Alpine plant life – functional plant ecology of high mountain ecosystems. Springer-Verlag.

Körner, C., Paulsen, J., 2004. A world-wide study of high altitude treeline temperatures. Journal of Biogeography 31, 713–732.

Kumar, L., Skidmore, A.K., Knowles, E., 1997. Modelling topographic variation in solar radiation in a gis environment. International Journal of Geographical Information Science 11, 475–497.

Lefsky, M.A., Cohen, W.B., Harding, D.J., Parker, G.G., Acker, S.A., Gower, S.T., 2002a. Lidar remote sensing of above-ground biomass in three biomes. Global Ecology and Biogeography 11, 393–399.

Lefsky, M.A., Cohen, W.B., Parker, G.G., Harding, D.J., 2002b. Lidar remote sensing for ecosystem studies. BioScience 52, 19–30.

Legendre, P., 1993. Spatial autocorrelation: trouble or new paradigm? Ecology 74, 1659–1673.

Lloyd, A.H., Fastie, C.L., 2002. Spatial and temporal variability in the growth and climate response of treeline trees in alaska. Climatic Change 52, 481–509.

Loudermilk, E.L., Scheller, R.M., Weisberg, P.J., Yang, J., Dilts, T.E., Karam, S.L., Skinner, C., 2013. Carbon dynamics in the future forest: the importance of long-term successional legacy and climate-fire interactions. Global Change Biology 19, 3502–3515.

Ma, Z., Peng, C., Zhu, Q., Chen, H., Yu, G., Li, W., Zhou, X., Wang, W., Zhangq, W., 2012. Regional drought-induced reduction in the biomass carbon sink of canada's boreal forests. PNAS 109, 2423–2427.

Mallet, C., Bretar, F., 2009. Full-waveform topographic lidar: State-of-the-art. ISPRS Journal of Photogrammetry & Remote Sensing 64, 1–16.

Martínez-Vilalta, J., Vanderklein, D., Mencucchini, M., 2007. Tree height and age-related decline in growth in scots pine (*Pinus sylvestris* l.). Oecologia 150, 529–544.

Martz, L.W., Gabrecht, J., 1998. The treatment of flat areas and depressions in automated drainage analysis of raster digital elevation models. Hydrological Processes 12, 843–855.

Mattson, W.J., Haack, R.A., 1987. The role of drought in outbreaks of plant-eating insects. Bioscience 37, 110–118.

Mayr, S., Hacke, U., Schmid, P., Schwienbacher, F., Gruber, A., 2006. Frost drought in conifers ant the alpine timberline: Xylem dysfunction and adaptations. Ecology 87, 3175–3185.

Mayr, S., Rothart, B., Damon, B., 2003a. Hydraulic efficiency and safety of leader shoots and twigs in norway spruce growing at the alpine timberline. Journal of Experimental Botany 54, 2563–2568.

Mayr, S., Schwienbacher, F., Bauer, H., 2003b. Winter at the alpine timberline. why does embolism occur in norway spruce but not in stone pine? Plant Physiology 131, 780–792.

Mayr, S., Wolfschwenger, M., Bauer, H., 2002. Winter-drought induced embolism in norway spruce (picea abies) at the alpine timberline. Physiologia Plantarum 115, 74–80.

McCree, K.J., 1981. Photosynthetically Active Radiation. Springer Berlin Heidelberg. volume 12 / A of *Encyclopedia of Plant Physiology*. chapter 12. pp. 41–55.

Miehe, G., Miehe, S., 1994. Zur oberen waldgrenze in tropischen gebirgen. Phytocoenologia 24, 53–110.

Monteith, J.L., 1972. Solar radiation and producitivity in tropical ecosystems. The Journal of Applied Ecology 9, 747–766.

Morsdorf, F., Frey, O., Meier, E., Itten, K.I., Alllgöwer, B., 2006. Assessment on the influence of flying height and scan angle on biophysical vegetation products derived from airborne laser scanning. Workshop on 3D Remote Sensing in Forestry , 145–150.

Morsdorf, F., Kötz, B., Meier, E., Itten, K.I., Alllgöwer, B., 2005. The potential of discrete return, small footprint airborne laser scanning data for vegetation density estimation. ISPRS Workshop "Laser scanning 2005", Enschede, the Netherlands , 198–203.

Morsdorf, F., Leiterer, R., N., N., Schaepman, M.E., in revision. Measuring tree height change in a mountain forest using airborne laser scanning. Remote Sensing of Environment .

Morsdorf, F., Meier, E., Kötz, B., Itten, K.I., Dobbertin, M., Alllgöwer, B., 2004. Lidar-based geometric reconstruction of boreal type forest stands at single tree level for forest and wildland fire management. Remote Sensing of Environment 92, 353–362.

Nabuurs, G.J., Schelhaas, M.J., Mohren, G.M.J., Field, C.B., 2003. Temporal evolution of the european forest sector carbon sink from 1950 to 1999. Global Change Biology 9, 152–160.

Neter, J., Wasserman, W., Kutner, M.H., 1989. Applied Linear Regression Models. Irwin Homewood, Illinois.

Norton, D.A., 1984. Tree-growth-climate relationships in subalpine *Nothofagus* forests, south island, new zealand. New Zealand Journal of Botany 22, 471–481.

Pan, Y., Birdsey, R.A., Fang, J., Houghton, R., Kauppi, P.E., Kurz, W.A., Phillips, O.L., Shvidenko, A., Lewis, S.L., Canadell, J.G., Ciais, P., Jackson, R.B., Pacala, S.W., McGuire, A.D., Piao, S., Rautiainen, A., Sitch, S., Hayes, D., 2011. A large and persistent carbon sink in the world's forests. Science 333, 988–993.

Paulsen, J., Weber, U.M., Körner, C., 2000. Tree growth near treeline: Abrupt or gradual reduction with altitude? Arctic, Antarctic and Alpine Research 32, 14–20.

Petit, G., Anfodillo, T., Carraro, V., Grani, F., Carrer, M., 2011. Hydraulic constraints limit height growth in trees at high altitude. New Phytologist 189, 241–252.

Popescu, S.C., Wynne, R.H., Nelson, R.F., 2003. Measuring individual tree crown diameter with lidar and assessing its influence on estimating forest volume and biomass. Canadian Journal of Remote Sensing 29, 564–577.

Pozdnoukhov, A., Kaiser, C., 2011. Scalable local regression for spatial analytics, in: Proceedings of the 19th ACM SIGSPATIAL GIS'2011.

Pregitzer, K.S., King, J.S., Burton, A.J., Brown, S.E., 2000. Responses of tree fine roots to temperature. New Phytologist 147, 105–115.

Reichstein, M., Bahn, M., Frank, P.C.C., Mahecha, M.D., Seneviratne, S.I., Zscheischler, J., Beer, C., Buchmann, N., Frank, D.C., Papale, D., Rammig, A., Smith, P., Thonicke, K., van der Velde, M., Vicca, S., Walz, A., Wattenbach, M., 2013. Climate extremes and the carbon cycle. Nature 500, 287–295.

Richardson, A.D., Friedland, A.J., 2007. A review of the theories to explain arctic and alpine treelines around the world. Journal of Sustainable Forestry 25.

Rigling, A., Bräker, O.U., Schneiter, G., Schweingruber, F., 2002. Intra-annual tree-ring parameters indicating differences in drought stress of *Pinus sylvestris* forests within the erico-pinion in the valais (switzerland). Plant Ecology 163, 105–121.

Rivas, J.J.C., Álvarez González, J.G., Aguirre, O., Hernández, F.J., 2005. The effect of competition on individual tree basal area growth in mature stands of *Pinus cooperi* blanco in durango (mexico). European Journal of Forest Research 124, 133–142.

Rossi, S., Deslauriers, A., Anfodillo, T., Morin, H., Saracino, A., Motta, R., Borghetti, M., 2006. Conifers in cold environments synchronize maximum growth rate of tree-ring formation with day length. New Phytologist 170, 301–310.

Ryan, M.G., Yoder, B.J., 1997. Hydraulic limits to tree height and tree growth. BioScience 47, 235–242.

Schaal, S., Atkeson, C.G., 1998. Constructive incremental learning from only local information. Neural Computation 10, 2047–2084.

Schaepman, M.E., Kötz, B., Schaepman-Strub, G., Zimmermann, N.E., Itten, K.I., 2004. Quantitative retrieval of biogeophysical characteristics using imaging spectroscopy – a mountain forest case study. Community Ecology 5, 93–104.

Schimel, D., 2014. Challenges and Opportunities for the World's Forests in the 21st Century. Springer Verlag. chapter Forests in the Global Carbon Cycle. pp. 231–239.

Schubert, P., Lagergren, F., Aurela, M., Christensen, T., Grelle, A., Heliasz, M., Klemedtsson, L., Lindroth, A., Pilegaard, K., Vesala, T., 2012. Modeling gpp in the nordic forest landscape with modis time series data – comparison with the modis gpp product. Remote Sensing of Environment 126, 136–147.

Schwanghart, W., Kuhn, N.J., 2010. Topotoolbox: A set of matlab functions for topographic analysis. Environmental Modelling & Software 25, 770–781.

Shi, P., Körner, C., Hoch, G., 2008. A test of the growth-limitation theory for alpine tree line formation in evergreen and deciduous taxa of the eastern himalayas. Functional Ecology 22, 213–220.

Shiyatov, S.G., Mazepa, V.S., 2007. Climatogenic dynamics of forest-tundra vegetation at the polar urals. Lesovedenie 6, 37–48.

Smith, W.K., Germino, M.J., Hancock, T.E., Johnson, D.M., 2003. Another perspective on altitudinal limits of alpine timberlines. Tree Physiology 23, 1101–1112.

Sørensen, R., Zinko, U., Seibert, J., 2006. On the calculation of the topographic wetness index: evaluation of different methods based on field observations. Hydrology and Earth System Sciences 10, 101–112.

Suarez, M.L., Ghermandi, L., Kitzberger, T., 2004. Ffactor predisposing episodic drought-induced tree mortality in *Nothofagus* – site, climatic sensitivity and growth trends. Journal of Ecology 92, 954–966.

Szargut, J.T., 2003. Anthropogenic and natural exergy losses (exergy balance of the earth's surface and atmosphere). Energy 28, 1047–1054.

Tobler, W.R., 1970. A computer movie simulating urban growth in the detroit region. Economic Geography 46, 234–240.

Tranquillini, W., 1979. Physiological ecology of the alpine timberline. tree existence at high altitudes with special references to the european alps. Ecological Studies 31.

Tranquillini, W., 1980. Winter desiccation as the cause for alpine timberline. NZFS FRI Techn. Paper 70, 263–267.

Vaganov, E.A., Hughes, M.K., Kirdyanov, A.V., Schweingruber, F.H., Silkin, P.P., 1999. Influence of snowfall and melt timing on tree growth in subarctic eurasia. Nature 400, 149–151.

Vapaavuori, E.M., Rikala, R., Ryyppö, A., 1992. Effects of root temperature on growth and photosynthesis in conifer seedlings during shoot elongation. Tree Physiology 10, 217–230.

Verrelst, J., Schaepman, M.E., Malenovský, Z., 2010. Effects of woody elements on simulated canopy reflectance: Implications for forest chlorophyll content retrieval. Remote Sensing of Environment 114, 647–656.

Vicca, S., Luyssaert, S., nuelas, J.P., Campioli, M., Ciais, F.S.F.S.C., Heinemeyer, A., Högberg, P., Kutsch, W.L., Law, B.E., Malhi, Y., Papale, D., Piao, S.L., Reichstein, M., Schulze, E.D., Janssens, I.A., 2012. Fertile forests produce biomass more efficiently. Ecology Letters 15, 520–526.

Wardle, P., 1993. Forest development in cold climates. Plenum Press, New York. chapter Causes of alpine timberline: a review of the hypotheses. pp. 89–103.

Wehr, A., Lohr, U., 1999. Airborne laser scanning—an introduction and overview. ISPRS Journal of Photogrammetry & Remote Sensing 54, 68–82.

Whittaker, R.H., Bormann, F.H., Likens, G.E., Siccama, T.G., 1974. The hubbard brook ecosystem study: Forest biomass and production. Ecological Monographs 44, 233–254.

Wild, M., Gilgen, H., Roesch, A., Ohmura, A., Long, C.N., Dutton, E.G., Forgan, B., Kallis, A., Russak, V., Tsvetkov, A., 2005. From dimming to brightening: Decadal changes in solar radiation at earth's surface. Science 308, 847–850.

Yao, W., Krzystek, P., Heurich, M., 2012. Tree species classification and estimation of stem volume and dbh based on single tree extraction by exploiting airborne full-waveform lidar data. Remote Sensing of Environment 123, 368–380.

Personal Declaration

I hereby declare that the submitted thesis is the result of my own, independent work. All external sources are explicitly acknowledged in this thesis.

_____ _____

Place, Date Signature